The Impact Of Propofol On *Klebsiella* Lung Infection

By

DAVID MAINS

B.S. Microbiology

University of Minnesota, Minneapolis, MN 2007

THESIS

Submitted as a partial fulfillment of the requirement for the degree of Doctor of Philosophy in Microbiology and Immunology in the Graduate College of the University of Illinois at Chicago, 2017

Chicago, Illinois

Defense Committee:

Nancy Freitag, Advisor and Chair

Bin He

Alan McLachlan

William Walden

Michael Federle, Medicinal Chemistry and Pharmacognosy

Alexander Mankin, Medicinal Chemistry and Pharmacognosy

ACKNOWLEDGEMENTS

I would like to first thank my parents, Jeff and Cindy, for their unwavering and unconditional love and support of me and my academic career spanning some twenty years now. Without you, I would be paying down college loans and wondering "What If" about a life with a Ph.D. I need to thank my wife and best friend Kristin, for her steadfast support and love for these last ten years, for making me a better person, and for giving me the greatest gift yet, a beautiful baby boy, Jackson. The sleepless nights and associated delirium drove me to work harder than I ever have to be a better scientist.

I would like to thank Steven Juhn at the University of Minnesota, for taking me on board in his lab over a decade ago. While best described as an unconventional experience, it gave me perspective and taught me both perseverance and patience that I have found valuable in my graduate career. I need to thank the researchers at Cargill for supporting me in my first bid for graduate school and the researchers at 3M, specifically Tonya, Neil, and Jesse, for supporting my second (successful) bid.

Of course, none of the following work would have been possible without my mentor, Nancy Freitag. Her reputation as a kind-hearted, savvy bacteriologist preceded her but failed to adequately convey how great she is. Thanks to her relentless positivity, constructive criticisms, and eagerness to share her knowledge, I am a far better scientist than I would have been anywhere else. I'd like to thank Lavanya Visvabharathy for all the time and effort she poured into investigating propofol. These studies were critical and the foundation of almost everything I did these last three years. I would like to thank Ben Gantner for his invaluable contributions to my understanding of the *Klebsiella* model and immunity in general in his short time here in the lab. I would like to thank Bobbi Xayarath and Laty Cahoon for their invaluable advice, technical support, and friendship, and I thank all my fellow lab members, rotation students, and visiting researchers for being great people and making this experience better than graduate school is supposed to be.

TABLE OF CONTENTS

LIST OF TABLES

LIST OF FIGURES

LIST OF FIGURES (Continued)

LIST OF ABBREVIATIONS

$5\text{-}HT_3$	5-Hydroxytryptamine type 3 receptor
AA	Arachidonic acid
ALT	Alanine aminotransferase
AMP	Antimicrobial peptide
AST	Aspartate aminotransferase
BAL	Bronchoalveolar lavage
BBB	Blood-brain barrier
BUN	Blood urea nitrogen
CAR	Constitutive androstane recepton
CBC	Complete blood count
CFU	Colony forming unit
cgMLST	Core gene multi-locus sequence type
CLP	Cecal ligation and puncture
CNS	Central nervous system
COX	Cyclooxygenase
CPM	Counts per million
DAPI	4',6-diamidino-2-phenylindole
DC	Dendritic cell
DNA	Deoxyribonucleic acid
ELISA	Enzyme-linked immunosorbent assay
FACS	Fluorescence-activated cell sorting
fMLP	N-Formylmethionyl-leucyl-phenylalanine
FPR1	Formyl peptide receptor 1
GABA	Gamma aminobutyric acid
$GABA_AR$	Gamma aminobutyric acid A receptor
G-CSF	Granulocyte colony-stimulating factor
GM-CSF	Granulocyte macrophage colony-stimulating factor
GPCR	G protein-coupled receptor

H&E	Hematoxylin and eosin
HAI	Healthcare-acquired infection
HIF	Hypoxia inducible factor
HSC	Hematopoietic stem cell
HV	Hypervirulent
ICAM	Intracellular adhesion molecule
IF	Immunofluorescence
IFN	Interferon
IKK	IκB kinase
IL	Interleukin
IN	Intranasal
IRF	Interferon regulatory factor
IT	Intratracheal
LB	Lysogeny broth
LPS	Lipopolysaccharide
LT	Leukotriene
MAPK	Mitogen-activated protein kinase
M-CSF	Macrophage colony-stimulating factor
MLST	Multi-locus sequence type
MRSA	Methicillin-resistant *Staphylococcus aureus*
MyD88	Myeloid differentiation primary response gene 88
MZM	Marginal zone macrophage
NF-κB	nuclear factor kappa-light-chain-enhancer of activated B cells
NK	Natural killer (cell)
NGS	Next generation sequencing
NMDA	N-methyl-D-aspartate
NOS	Nitric oxide synthase
NR	Nuclear receptor
PAM	Positive allosteric modulator

PAMP	Pathogen-associated molecular pattern
PBS	Phosphate buffered saline
PG	Prostaglandin
PLA_2	Phospholipase A_2
PXR	Pregnane X receptor
qRT-PCR	Quantitative reverse transcription polymerase chain reaction
RNA	Ribonucleic acid
RNS	Reactive nitrogen species
ROS	Reactive oxygen species
SIRS	Systemic inflammatory response syndrome
ST	Sequence type
TBS	Tris-buffered saline
TLR	Toll-like receptor
TIR	Toll/interleukin-1 receptor
TNF	Tumor necrosis factor
TRIF	TIR-domain-containing adapter-inducing interferon-β
UGT	UDP- glucuronosyltransferase
WT	Wild type

Chapter 1: Introduction

1.1. *Klebsiella* characteristics and diversity

The genus of Klebsiella was originally identified and named in 1885 by Trevisan (1) and is a member of the family Enterobacteriacea. Currently, there are five species of *Klebsiella: K. oxytoca, K. ornithinolytica, K. planticola, K. terrigena,* and *K. pneumoniae*, the last of whom is further divided into three subspecies: subsp *pneumoniae*, subsp. *ozaenae,* and subsp. *rhinoscleromatis* (2). For the remainder of this work, references to *K. pneumoniae* will specifically refer to subsp. *pneumoniae* as this is the dominant clinical species globally. *Klebsiella* spp. are found in a wide variety of environments, including water, vegetation, and soil, and may also colonize human and other mammalian hosts (3). *Klebsiella* are Gram negative, facultative anaerobic, non-motile rod-shaped bacteria approximately six microns in length (2,4). *K. pneumoniae* grows readily on lysogeny broth (LB) agar plates and in liquid culture may have a doubling time as quick as 18 minutes, although there is fair strain-to-strain variance (2).

To identify strain diversity, a multi-locus sequence typing (MLST) strategy was implemented in 2005 that compared the sequences of seven housekeeping genes to estimate population phylogeny (5,6). This strategy led to the identification of clinically important sequence types (ST) conferring exceptional virulence and/or antimicrobial resistance. With the advent of affordable next-generation sequencing (NGS) platforms, a high resolution approach to MLST was introduced in 2014 that analyzes the sequences of 694 core genes, cgMLST (7). cgMLST has identified almost 200 unique lineages and it is estimated that the actual number may be in the thousands (8,9). *K. pneumoniae* features a genome of approximately 5,500 genes with a total size of 5.5 mega-base pairs, but sequencing analyses suggest that fewer than 2,000 of these genes are common to all strains (7,8). The other 3,500 genes are assembled from a pool of more than 30,000 potential protein-encoding genes that tend to cluster by

lineage (8). In addition to this chromosomal genetic diversity, *K. pneumoniae* also features a diverse array of highly-mobile genetic elements often encoding virulence determinants and antibiotic resistance cassettes, discussed further in section 1.4 (10). This exceptional genetic diversity suggests that virulence strategies may be equally diverse and thus high-throughput analyses are required to efficiently identify these factors.

1.2. Routes of infection, clinical manifestations, and treatment modalities

K. pneumoniae is capable of colonizing humans in a variety of niches, including the nasopharynx, oropharynx, gastrointestinal tract, and skin (11). These commensal populations seldom lead to invasive disease in healthy individuals; *K. pneumoniae* infections largely impact neonates, the elderly, and immunocompromised individuals (2,6,11). *K. pneumoniae* is recognized as a significant source of community-acquired pneumonias in the Asia/Western Pacific regions that typically present as sudden onset fever and a cough producing sputum (12). Alcoholism is a common comorbidity in these individuals and leads to an alarmingly high mortality rate despite treatment (12). Another clinical presentation far more common in the Asia and Western Pacific regions is the manifestation of invasive disease as pyogenic liver abscesses, typically in the absence of other previously diagnosed hepatic dysfunction (13–15), however, upwards of 70% of these patients also have a previous diagnosis of diabetes mellitus.

Typical treatment for invasive *K. pneumoniae* infection is intravenous and/or oral antibiotics – aminoglycosides, fluoroquinolones, cephalosporins, and carbapenems are the primary classes with the most efficacy in treating this pathogen and may be used singularly or in combination as warranted (8,10,16). Extensive work has been given to determining the most efficacious antibiotic regiment in response to *K. pneumoniae* infection, but of highest importance is determining a given strain's antibiotic susceptibility profile due to widespread multi-drug resistance (8,11,17–19), which will be further

discussed in Section 1.4. Ventilation, mechanical or otherwise, may be necessary based on the severity of a pneumonia, and chest X-rays or computed tomographic scans may be utilized to assess recovery and monitor for abscess or gangrene (20). Resolution of pneumonia or bacteremia is determined by traditional culture methods as well as white blood cell counts.

1.3. Host defenses against *K. pneumoniae* infection

The human respiratory tract is exposed to a large amount of potentially infectious or non-infectious particles every day. Its primary defense is the mucociliary escalator, whereby mucus is secreted continuously by the epithelial lining, forming a thin layer that serves to trap unwanted particles and organisms (21). Ciliary action moves this layer of mucus upwards and out of the respiratory tract. Gastrointestinal colonization is hampered by several host strategies, again including a mucus layer that blocks bacterial adherence and moves non-adherent bacteria out. Bile from the gall bladder and other enzymes create a hostile chemical environment and peristalsis continually advances luminal contents out (22). If *K. pneumoniae* is able to overcome these barriers, it must still face the host's humoral and innate defenses.

Alveolar spaces are lined with surfactant proteins that serve to enhance *K. pneumoniae* killing and neutrophil recruitment (22,23). The complement cascades serve to form membrane attack complexes which create pores in bacterial membranes, while also recruiting professional phagocytes and opsonizing the bacteria (24). The epithelial cells lining the mucosal surfaces of the lung also secrete a variety of antimicrobial peptides, a trait shared by the resident immune cells in the lungs. Alveolar macrophages serve as critical sentinel cells in the lung and will phagocytose *K. pneumoniae* while simultaneously releasing a variety of pro-inflammatory cytokines and chemokines to recruit neutrophils and inflammatory monocytes to the site(s) of infection (25,26). These responding immune populations are critical for clearance of *K. pneumoniae,* employing multiple strategies to enhance killing (27–30).

Resident dendritic cells have also been shown to contribute to the optimization of phagocytic killing in a toll-like receptor 9 (TLR9)-dependent manner (31). Finally, while T cells are traditionally a part of the adaptive immune system, the lungs contain a circulating pool of naïve $CD4^+$ αβ-T cells and a smaller subset of γδ-T cells (32,33). Moore et al found that when mice lacking either αβ-T cells or γδ-T cells were infected with *K. pneumoniae*, there were no detectable differences in lung burdens, but γδ-T cell-deficient mice displayed increased dissemination from the lungs and increased mortality compared to αβ-T cell-deficient mice and wild type mice (32). They further identified that γδ-T cell-deficient mice had delayed induction of tumor necrosis factor alpha (TNFα) and interferon gamma (IFNγ) in the lungs at both the transcript and protein levels compared to controls, while αβ-T cell-deficient mice actually displayed greater expression of these factors both at 24 and 48 hours post-infection (32).

Other cytokines have been shown to be critical for the clearance of *K. pneumoniae.* Interleukin (IL)-17A has been shown to be a critical cytokine during pulmonary infection with *K. pneumoniae,* and mice lacking the IL-17 receptor (IL-17R) displayed higher lung burdens, increased dissemination to secondary organs, and greater mortality compared to WT controls (27). IL-23p19-deficient mice were also found to be highly susceptible to *K. pneumoniae* lung infections as they failed to induce IL-17 production in response to infection, demonstrating that IL-23 signaling is a critical trigger for IL-17 production and the immune response to extracellular bacterial infections in the lungs (34). Fate mapping IL-17A-producing cells during *K. pneumoniae* lung infection has identified γδ-T cells as a primary source of innate IL-17A at two days post-infection, as well as a smaller subset of invariant natural killer (iNK) T cells and other undefined $CD3\varepsilon^+$ T cells. These populations, along with type 3 innate lymphoid cells (ILCs), are collectively referred to as "type 17" cells, the innate counterparts of T helper (Th)-17 cells in the adaptive immune system (35). IL-17 strongly induces the expression of antimicrobial peptides (AMPs), particularly beta defensins and lipocalin-2, at mucosal sites such as in the lung (35–37).

Downstream signaling through IL-17R induces the expression of additional pro-inflammatory cytokines and chemokines essential for neutrophil accumulation (38).

Neutrophil recruitment to the lungs has been shown to be critical for successful defense against intrapulmonary *K. pneumoniae* and this trafficking is mediated by several key chemotactic proteins. CCL2 (monocyte chemoattractant protein-1; MCP-1) deficient mice display increased lung burdens and dissemination following lung infection as well as reduced circulating neutrophils, lower levels of pro-inflammatory cytokines, and increased mortality (39). This deficient immune response was corrected by intra-tracheal administration of recombinant MCP-1 or granulocyte colony-stimulating factor (G-CSF), a growth factor and potent neutrophil activator. G-CSF is critical for neutrophil function and maturation by signaling to release precursors from bone marrow pools during inflammation (29,40). G-CSF additionally drives pro-survival and pro-inflammatory functionality in neutrophils (29) and is highly expressed following treatment with IL-17A and IL-22 (41).

Finally, interleukin 22 is an IL-10 family cytokine that, in the context of *K. pneumoniae* lung infection, is produced by $CD90^+$ T cells at early time points (41). While Aujla et al did not further characterize this population, it is highly likely that a major fraction of these $CD90^+IL\text{-}22^+$ cells are γδ-T cells as neutralizing IL-22 led to increased dissemination and mortality in a mouse model, highly similar to data reported by Moore et al (32). While considerable effort has gone toward elucidating host cytokines and chemokines critical during *K. pneumoniae* lung infection, a greater understanding how these regulatory networks cross talk needs to be investigated.

1.4. *K. pneumoniae* virulence determinants and antibiotic resistance

As an extracellular bacterium, *K. pneumoniae* is subject to all the aforementioned clearance mechanisms, however, it is interesting to note that *K. pneumoniae* foregoes many of the overt virulence strategies employed by other common nosocomial pathogens. Instead *K. pneumoniae* employs a

paradigm of evasion to hide itself from the host immune system. *K. pneumoniae* is an encapsulated bacterium and the strain-specific capsular polysaccharides are termed K antigens (K1-K78). Capsule is critical for *K. pneumoniae* virulence as acapsular strains have been shown to be far less virulent than isogenic encapsulated strains and are unable to disseminate systemically (42,43). Strains overexpressing capsule (hypercapsule) tend to display increased virulence in the clinic, suggesting a correlation between virulence and the amount of capsule a strain produces (16,44,45).

Like all Gram-negative bacteria, *K. pneumoniae* expresses lipopolysaccharide (LPS) as a major component of the outer membrane. LPS is comprised of three components: lipid A, an oligosaccharide core, and the O-antigen. Lipid A serves as the membrane anchor for LPS and is well regarded as a major ligand of TLR4, stimulation of which leads to secretion of cytokines and chemokines. Despite this immunogenicity, Lipid A has also been shown to benefit *K. pneumoniae* in mouse models of infection through secondary acylation that confers resistance to cationic antimicrobial peptides (46,47). There are now twelve distinct O antigens (O1-O12) identified in *K. pneumoniae* (48). The O antigen comprises the distal end of the LPS molecule and has been shown to mediate complement resistance in *K. pneumoniae*. While all strains activate the complement pathway, full length O antigens are critical determinants in resisting complement-mediated killing (49,50) by binding C3b and physically separating it from the bacterial surface (51).

A third major virulence feature is *K. pneumoniae's* siderophore repertoire. Siderophores are iron scavenging proteins secreted by *K. pneumoniae* to acquire iron from the surrounding environment. During infection, iron is sequestered and serum iron levels can fall by up to 90%, creating a state of anemia in the host (52). Four siderophores have been identified in *K. pneumoniae* strains: enterobactin, salmochelin, yersiniabactin, and aerobactin. Enterobactin features the highest affinity for iron, however the host is able to counter this siderophore with the protein lipocalin-2, which binds and effectively disables enterobactin. To bypass this defense, enterobactin can be glucosylated to salmochelin, which is

no longer antagonized by lipocalin-2 (53,54). Yersiniabactin was originally identified in *Yersinia pestis*, but has since been found in other Gram negative bacteria (55). Aerobactin has the lowest affinity of the four siderophores and is found in just 6% of environmental isolates, however, both aerobactin and yersiniabactin are expressed by ≥90% of hypervirulent (HV) clinical isolates (56–60).

K. pneumoniae expresses both types I and III fimbriae, key adhesive molecules that it utilizes to bind to host cells. Type I fimbriae are common amongst Enterobacteriaceae and bind D-mannosylated glycoproteins, while type III fimbriae may bind to extracellular matrix proteins (61–63). Although mutants lacking either or both fimbriae types display no virulence defects in the lungs, both are thought to be important for biofilm formation and adhesion to abiotic surfaces (64). With 5,500 protein-encoding genes, the virulence determinant repertoire continues to expand. Multiple groups have turned to high-throughput methods to mine the *K. pneumoniae* genome for genes of interest, which has resulted in an exponential increase in the identification of genes likely involved in virulence, however many of these proteins remain to be characterized to better understand the strategies *K. pneumoniae* employs in the host.

Finally, in addition to these virulence strategies, *K. pneumoniae* infections have become a serious threat to patient health due to the rapid acquisition of antibiotic resistance. Clinical isolates with extended spectrum resistance are increasing globally, with recent data from the Center for Disease Control and Prevention (CDC) estimating that 29% of *K. pneumoniae* isolates are resistant to the third generation cephalosporin antibiotic ceftazidime and 13% are resistant to imipenem, a carbapenem-class antibiotic representing the last line of antibiotic therapy available. Data from outside the United States is even more dire, with HAIs in general at least five times more common and the rates of resistance for ceftazidime and imipenem at 73% and 43%, respectively (65,66). Less than a year ago, the first bacterial isolate (so far) that was resistant to all available antibiotics was a strain of *K. pneumoniae* likely acquired in India and that resulted in the death of the patient (19).

K. pneumoniae carries the SHV beta-lactamase in its core genome, thus all strains are resistant to ampicillin. There are dozens of other core genes associated with intrinsic or mutational resistance to aminoglycosides, fluoroquinolones, colistin, macrolides, etc., but the vast majority of antimicrobial resistance determinants are disseminated via horizontal gene transfer on plasmids to other *Klebsiella* spp. and related Enterobacteriaceae (9). Arguably of the greatest concerns are multiple plasmids conferring cephalosporinase activity, extended spectrum beta-lactamase activity, and carbapenemase activity. These isolates with extended or pan-resistance profiles are much more difficult to treat in the clinic, can carry mortality rates upwards of 38%, and have disseminated globally in just a few years (67). It is therefore critical that host immunity be as effective as possible in fighting infections if supportive therapies will be of limited or no use due to resistance. One underappreciated factor that may be affecting host responses is sedation with certain general anesthetics, which will now be described.

1.5. General anesthetics and their clinical use

Hospital-centered outbreaks caused by bacteria have been a persistent issue and are more frequently associated with strains that carry exceptional antibiotic resistance. These outbreaks tend to affect critically ill patient populations with already weakened immune systems, so for years the increased morbidity and mortality was taken for granted. More recently, digitalized hospital record management platforms have enabled comprehensive views of individual patient care, while simultaneously assembling enormous datasets on the care and outcomes of thousands of patients that can then be data mined for multivariate risk analyses. Previous to this “big data” approach, research had identified that all anesthetics feature a spectrum of immune altering secondary effects (68–70) and it was the responsibility of the clinician to take these into account for each patient. Now reports have been published specifically analyzing anesthetic exposure as a variable with regards to patient outcomes and infection risks and have identified that not all anesthetics are created equal (71,72).

Nonetheless, sedation is an essential aspect of clinical care today, primarily for pain management. The ability to render a patient unconscious and unable to perceive pain makes general anesthesia one of the most valuable components in modern medicine. While attempts at general anesthesia have been pursued for millennia, it was not until the 1840s when diethyl ether and nitrous oxide were first practically applied for surgical anesthesia. Since that time, the field of anesthesia has expanded and matured to what we see today. General anesthetics in clinical use today can be broadly separated by route of administration, inhaled or intravenous. While nitrous oxide remains in use as an adjuvant to the following drugs, inhaled anesthetics are often halogenated ethers: halothane, enflurane, isoflurane, methoxyflurane, sevoflurane, and desflurane are all highly-fluorinated, structurally related small molecules with relatively similar pharmacokinetic properties (Fig. 1.1)(69). They are typically used for the maintenance of anesthesia as opposed to induction due to the potential for airway irritation. Their mechanisms of action for inducing anesthesia centers on several key neurotransmitter receptors in the central nervous system (CNS), principally the gamma aminobutyric acid (GABA) A receptor (68,73).

The GABA A receptor ($GABA_AR$) is a heteropentameric, ligand-gated chloride channel that opens in response to binding GABA, the major inhibitory neurotransmitter (Fig. 1.2)(74). Opening normally results in transient hyperpolarization of the neuronal membrane and blocking of action potential propagation (75–77). The aforementioned inhalational anesthetics induce a loss of consciousness by positive allosteric modulation of the $GABA_AR$, meaning the molecules bind the receptor at sites separate from GABA and keep the channel open longer than it would be in the absence of drug, thus prolonging GABA's inhibitory effects (68). Due to structural similarities, these anesthetics have also been shown to likely bind a subclass of the glutamate receptors as well as the glycine receptor (78,79). Glutamate is the major excitatory neurotransmitter in the CNS and several anesthetics may bind to and inhibit the function of the ionotropic N-methyl-D-aspartate (NMDA) receptor subclass, a non-selective cationic

channel (80). Glycine is another inhibitory amino acid neurotransmitter and its cognate receptor is an anion-selective ligand-gated ion channel (81).

Intravenous, non-opioid anesthetic agents include the barbiturates, such as thiopental, benzodiazepines, such as midazolam, etomidate, ketamine, and propofol (Fig. 1.1). Barbiturates were the first class of intravenous anesthetics developed and have a wide range of therapeutic uses beyond general anesthesia. Lower doses produce sedation and can also have anxiolytic, anticonvulsant, and hypnotic effects in patients. Barbiturates work by positive allosteric modulation of the $GABA_AR$ (82). The class of barbiturates is still in limited use today, but has largely been displaced by benzodiazepines (83,84). The first benzodiazepine came on the market in 1960 and since then a number of derivatives have been approved. This class of drug retains the sedative, anxiolytic, anticonvulsant, and hypnotic effects that barbiturates produce, but with increased potency and a comparatively lower risk of overdose (85). In the clinic, benzodiazepines are commonly administered as a sedative prior to surgery or any procedure requiring general anesthesia (85). Benzodiazepines have a well-defined binding site on the $GABA_AR$, situated in the cleft between an alpha and gamma subunit, thus it is also a positive allosteric modulator (86).

Etomidate is a rapid-acting, imidazole-based, intravenous agent first developed in 1964 is the anesthetic of choice for conscious sedation in emergency settings due to rapid onset, typically within one minute (Fig. 1.2)(87,88). Etomidate is a positive allosteric modulator of $GABA_AR$, with an identified binding site on beta 2 or 3 subunits (89). While etomidate can be used for continuous sedation, drug levels need to be carefully monitored as etomidate also binds and reversibly inhibits 11β-hydroxylase, the enzyme catalyzing 11-deoxycortisol to cortisol in the adrenal cortex, thus leading to primary adrenal suppression (90,91).

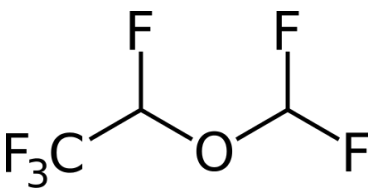

Desflurane

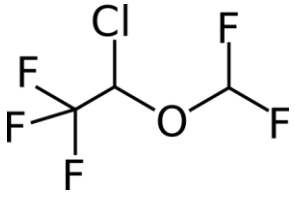

Isoflurane

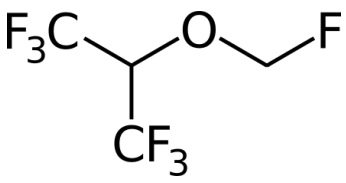

Sevoflurane

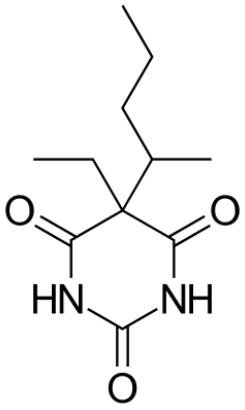

Pentobarbital

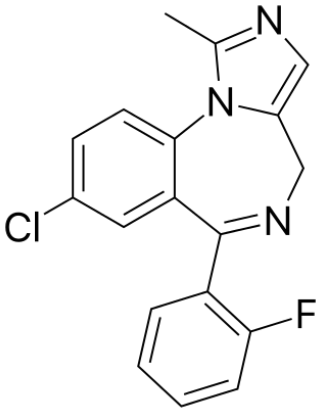

Midazolam

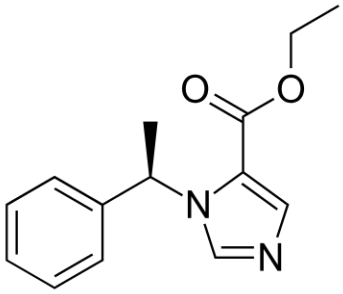

R-Etomidate

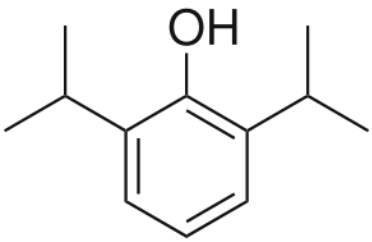

Propofol

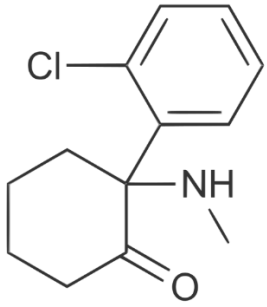

Ketamine

Figure 1.1. Structure of selected current generation general anesthetics. Fluorinated inhalation anesthetics are highly structurally related (desflurane, isoflurane, sevoflurane). Pentobarbital is a representative barbiturate. Midazolam is a representative benzodiazepine.

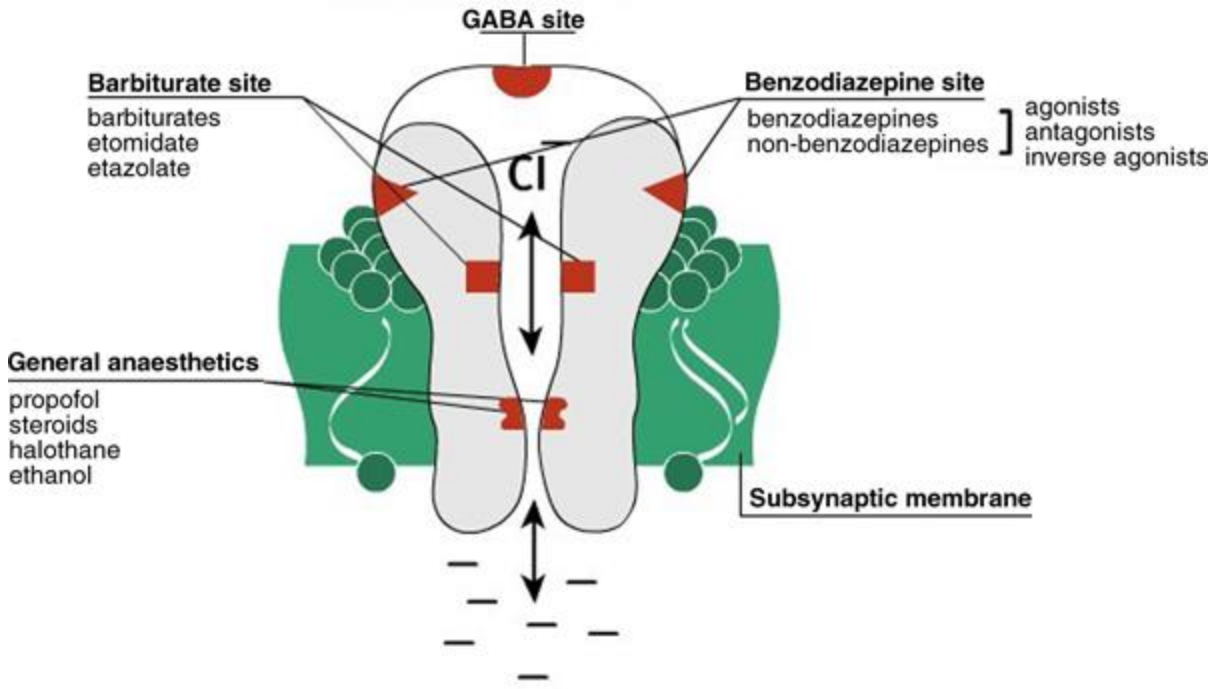

246

247 **Figure 1.2. The GABA A receptor with common drug binding sites.** The GABA A receptor is a

248 heteropentameric, ligand gated chloride channel. The GABA and benzodiazepine binding sites are

249 extracellular, while barbiturates and several general anesthetics bind sites in the transmembrane region

250 of the channel itself. Figure adapted from (92) Richards G, Schock P, Haefely W. 1991. Benzodiazepine

251 receptors: new vistas. Semin Neurosci. Jun 1;3(3):191–203.

Ketamine is a slower acting sedative than drugs discussed thus far, taking approximately five minutes to anesthetize a patient, but also causes less respiratory suppression than other anesthetics (Fig. 1.2)(93). It is also notable in that it possesses significant analgesic properties, unlike many other anesthetics, and remarkably fast-acting anti-depressant properties, which were recently attributed to the metabolite (2R,6R)-hydroxynorketamine (93,94). Ketamine's primary mechanism of action is attributed to antagonism of the NMDA receptor (93). Finally, there is the intravenous anesthetic propofol, described in the following section.

1.6. Propofol: Effects, pharmacokinetics, and mechanism of action

The anesthetic propofol (2,6-diisopropylphenol) is a small molecule phenol derivative that is one of the most commonly used intravenous anesthetics in the world today. It was first identified in 1976 at Imperial Chemical Industries (now Astra Zeneca Pharmaceutical). Since 1986, it has been sold as an emulsion containing 100 mg/ml soybean oil, 22.5 mg/ml glycerol, 0.6 mg/ml oleic acid, 12 mg/ml egg lecithin with sodium hydroxide to adjust the pH. After multiple bacterial outbreaks in hospitals were traced back to contaminated vials of propofol, benzyl alcohol was added to certain formulations to prevent bacterial growth (95).

Propofol is a highly lipophilic molecule with an approximate volume of distribution of 60 L/kg, meaning that propofol rapidly redistributes from the blood into peripheral tissues (70,96). In the blood, propofol is highly (95-99%) protein bound to serum albumin and other protein components (97). Upon injection, it features tri-phasic pharmacokinetic profile: a rapid distribution phase lasting two to four minutes, whereby the drug moves from the circulation across the blood brain barrier (BBB) into the CNS and other well vascularized tissues, followed by a slow distribution phase of thirty to sixty minutes representing propofol's initial elimination as well as diffusion into poorly vascularized and fatty tissues, and finally a slow elimination phase as propofol returns from poorly vascularized tissues (96). Propofol

is readily metabolized in liver microsomes, with a high hepatic extraction coefficient (≥0.7), meaning approximately 70% of propofol in the blood is metabolized each pass. In phase I metabolism, the cytochrome P450 enzymes, principally CYP2B6 in humans and CYP2B10 in mice (98), are responsible for hydroxylation of propofol to its 1,4-quinol form, although this step is not necessary (99,100). Phase II metabolism may take place in the liver or kidneys and involves conjugation to glucuronidate via the enzyme UDP-glucuronosyltransferase 1-9 (UGT1A9)(100). A minor fraction of propofol may undergo sulfate conjugation as well, but in total these modifications serve to increase propofol's water solubility and lead to it finally being excreted in the urine (100,101). The overall half-life of propofol in humans has been estimated at between three and eight hours with no discernable differences between sexes (96).

While propofol is dissimilar to other general anesthetics structurally (Fig. 1.1), its primary mechanism of action is still that of positive allosteric modulation of the $GABA_AR$. Photolabeling studies have identified multiple putative binding sites on the $GABA_AR$ that may be common to other anesthetics on both the alpha and beta subunits, plus an additional pocket created at the interface of adjacent alpha/beta or beta/beta subunits (102–105). In humans and mice, there are six alpha subunits and three beta subunits and it has been shown that propofol binds each with a spectrum of affinities due to amino acid polymorphisms (102).

Propofol's popularity in the clinical setting is driven by a variety of considerations. Propofol has a rapid on- and off-set, especially when given as a bolus dose, meaning patients wake up faster from anesthesia and regain cognitive and motor function more quickly, leading to a shorter recovery time (96). Propofol also has antiemetic effects, meaning patients are less likely to experience nausea and vomiting (106). This may be attributable to an indirect inhibition of the limbic system (107) or alternatively, through interaction with the serotonergic system. 5-Hydroxytryptamine type 3 receptors

(5-HT_3) are ligand-gated ion channels that have been associated with modulation of nausea and it has been shown that propofol has dose-dependent, non-competitive effects on these receptors (108,109).

Propofol may feature anxiolytic properties, similar to other anesthetics, although scientific literature regarding this does not reach a clear consensus (110–112). As a phenol derivative, propofol has demonstrable antioxidant capabilities, including increasing the plasma antioxidant capacity in humans, inhibiting lipid peroxidation, scavenging reactive oxygen species (ROS), and inhibiting protein nitration (113–117).

It is important to state that no drug is specific to a single target and that there will invariably be off-target effects, both direct and indirect. General anesthetics are no different, as has been discussed in the last two sections. Interactions with GABA A receptors, glycine receptors, and 5-HT_3 receptors have all been observed and implicated in the constellation of *in vivo* therapeutic effects that are leveraged every day in the clinic.

1.7. *In vitro* evidence of propofol immunomodulation

All anesthetics have been found to alter immune responses in one aspect or another and clinicians must take this into account for every patient. Decades of randomized, controlled trials have broadly illustrated many of these changes, yet the devils may remain in the details. Standard procedural sedation in a surgical patient may utilize four or five separate sedatives, analgesics, and anesthetics in order to achieve the desired level of anesthesia and clinical outcome. Thus *in vitro* studies have been extensively utilized to greatly simplify models and investigate specific mechanisms of action and studies focused on propofol are no exception. The following studies are summarized in figure 1.3.

Mikawa et al (118) used primary human neutrophils treated *ex vivo* with propofol and then stimulated responses with the formyl peptide N-formylmethionine-leucyl-phenylalanine (fMLP). Propofol was found to inhibit neutrophil reactive oxygen species (ROS) production, chemotaxis, and

phagocytosis in a dose-dependent manner, while simultaneously attenuating increases in intracellular calcium concentrations [Ca^{2+}]. Yang et al (119) used a similar approach with human neutrophils and again found that propofol could attenuate superoxide production, chemotaxis, and elastase release, but further observed that superoxide production was not affected in a cell-free system, indicating that propofol did not directly act on that molecular machinery. They also demonstrated that this mechanism was independent of the $GABA_AR$, as channel blockers did not inhibit propofol's mechanism. Instead, the authors were able to attribute these effects to competitive inhibition of fMLP binding the formyl peptide receptor FPR1. While the authors were confident that this represented a major mechanism for attenuating neutrophil activation, they still noted minor inhibition in FPR1-independent responses, strongly suggesting that propofol is acting through multiple mechanisms to achieve the observed inhibition.

Dendritic cells (DCs) have also been utilized in several studies. Dendritic cells are an antigen-presenting population critical in bridging the innate and adaptive immune systems by presenting pathogen-derived peptides to naïve T cells while producing pro-inflammatory cytokines and chemokines (120). Inada et al (121) observed that propofol could dose-dependently inhibit prostaglandin E_2 (PGE2) production, an eicosanoid lipid inflammatory mediator, in murine bone marrow-derived DCs stimulated with zymosan. The eicosanoid signaling network functions in parallel with cytokine signaling during inflammation and works to mediate the immune responses *in vivo* (122). Two cyclooxygenase enzymes, COX1 and COX2, convert arachidonic acid into PGE_2, with the former being an inducible form. The authors found that propofol appeared to be directly inhibiting COX function, but otherwise found no significant changes in cytokine expression or in the ability of propofol-treated DCs to stimulate T cell proliferation *in vitro*. This same group also later observed that propofol could inhibit leukotriene B_4 (LTB_4) production following zymosan stimulation (121). Leukotrienes are also eicosanoids derived from arachidonic acid via the enzyme 5-LOX in the lipoxygenase pathway and act as pro-inflammatory signals.

It was here proposed that propofol was suppressing LTB_4 synthesis through direct competitive inhibition of the enzyme 5-LOX as well. Thus, this group proposes that the anti-inflammatory effects of propofol may be at least in part explained by its inhibitory effect on inflammatory lipid signaling in DCs. Very recently, Okuno et al reported that propofol also reduced LTB_4 detected in a mouse model of polymicrobial sepsis at six hours post-infection, but not at later time points. This group photolabeled 5-LOX with propofol and identified two putative binding sites, including one near the 5-LOX active site. *In silico* docking simulations suggest that this could be the mechanism by which propofol competitively inhibits LTB_4 (and related eicosanoid) production. It is critical to note that the 50% inhibitory concentration (IC_{50}) was calculated at 1.37 μM, below the minimum concentration required for its hypnotic effect (123). Lastly, a second group described primary human platelet aggregation was dose-dependently inhibited by propofol during stimulation by three separate inducing molecules, including another COX1-dependent lipid mediator, thromboxane A_2 (TXA_2), without affecting intracellular calcium concentrations (124). This again suggests that propofol could be modulating these lipid signaling pathways.

The majority of *in vitro* work with propofol has utilized macrophage-like cell lines or primary elicited macrophages. Chen et al (125) observed that in the murine macrophage line RAW 264.7, propofol suppressed both chemotactic and oxidative functions after one hour of treatment, but that inhibition lessened as the experiment progressed to 24 hours. Exposure suppressed the expression of interferon gamma at the transcriptional level in response to LPS stimulation and transiently increased mitochondrial membrane potential, however this inhibition also decreased with time. In an interesting twist, Shiratsuchi et al (126) found that propofol actually increased phagocytic uptake in both human monocytes and the monocyte cell line THP-1, a phenotype that was independent of $GABA_AR$ activation. This clearly suggests that propofol is acting through multiple pathways to alter immune responses in this cell type.

LPS is a classic pathogen-associated molecular pattern (PAMP) for the stimulation of macrophages *in vitro*. LPS is recognized by toll-like receptor 4 (TLR4) and has been show to induce multiple pro-inflammatory programs through the adaptor proteins TIR-domain-containing adapter-inducing interferon-β (TRIF) and myeloid differentiation primary response gene 88 (MyD88)(120). Wu et al (127) investigated the TLR4-MyD88-dependent induction of the pro-inflammatory cytokine tumor necrosis factor alpha (TNFα) and found that not only did propofol suppress upregulation of TNFα, it suppressed TLR4 expression at both the transcript and protein levels. Furthermore, they observed that nuclear factor kappa-light-chain-enhancer of activated B cells (NF-κB), a critical transcription factor controlling the expression of multiple cytokines, had reduced translocation from the cytosol to the nucleus of propofol-exposed cells, which could explain reduced expression of both TLR4 and TNFα, although these observations were not empirically connected.

Other groups have also demonstrated that propofol can inhibit pro-inflammatory gene expression (128,129) in mono-cellular culture models, but other effects have been noted. In response to LPS stimulation, macrophages shift from a resting phenotype into the so-called M1 (pro-inflammatory) activated state. Among the alterations described is metabolic reprogramming away from oxidative phosphorylation toward increased glycolysis (130). Tanaka et al (131) demonstrated that propofol pretreatment prior to LPS stimulation inhibited genes downstream of hypoxia inducible factor (HIF)-1. HIF-1 is a hypoxia-responsive transcription factor that is constitutively expressed, however its alpha subunit is rapidly degraded under normoxic conditions. In response to hypoxia or PAMP stimulation, degradation is blocked and the protein may upregulate expression of its downstream target genes (132). Interestingly, Tanaka et al reported that propofol inhibited *de novo* HIF-1α protein synthesis only in response to LPS stimulation and not following hypoxia. The HIF-1 pathway has been known to cross-talk with the NF-κB pathway, demonstrating functional overlap between these regulatory mechanisms that may be especially relevant to propofol's mechanism of action (132,133).

1.8. *In vivo* evidence of propofol immunomodulation

As mentioned earlier, virtually all human studies investigating propofol's immunomodulatory effects have necessarily been in comparison to one or more anesthetic strategies in response to non-infectious stimuli, e.g. surgical stress. Only recently have large retrospective studies begun to identify risk associated with anesthetic exposure (71). Therefore, it is critical to establish experimental models to assess risk in highly controlled settings that are relevant to human health, such as infection. While there have been several studies reporting propofol's effects during the reaction to purified LPS (endotoxemia), little data is available using actual infection.

The first infection-based model was reported by Schläpfer et al (134) in 2015 which used the cecal ligation and puncture (CLP) method to induce a polymicrobial sepsis. Under continual anesthesia for the duration of the experiment, propofol-treated rats had a mean survival time of just twelve hours compared to a 56% survival rate at 24 hours post-infection for rats sedated with volatile anesthetics. Propofol-sedated rats demonstrated double the plasma endotoxin concentration at twelve hours compared to isoflurane-sedated rats and, interestingly, significantly higher plasma levels of the inflammatory mediators IL-1α, IL-1β, IL-10, TNFα, IFNγ, and CXCL2 (MIP-2α) at the same time point. This study clearly demonstrated a highly dysregulated immune response under continuous propofol sedation that rapidly resulted in morbidity and mortality, however it should be said that sepsis is seldom the result of multiple bacterial infections in the clinic, limiting the translatability of this model.

To identify the impact of propofol sedation on a single bacterial infection, Visvabharathy et al established a mouse model of bloodstream (systemic) infection with the Gram positive, intracellular bacterium *Listeria (L.) monocytogenes* (135). It is critical to note that this model involved only brief (≤5 minutes) sedation with propofol or controls and not a continuous infusion, therefore total exposure was

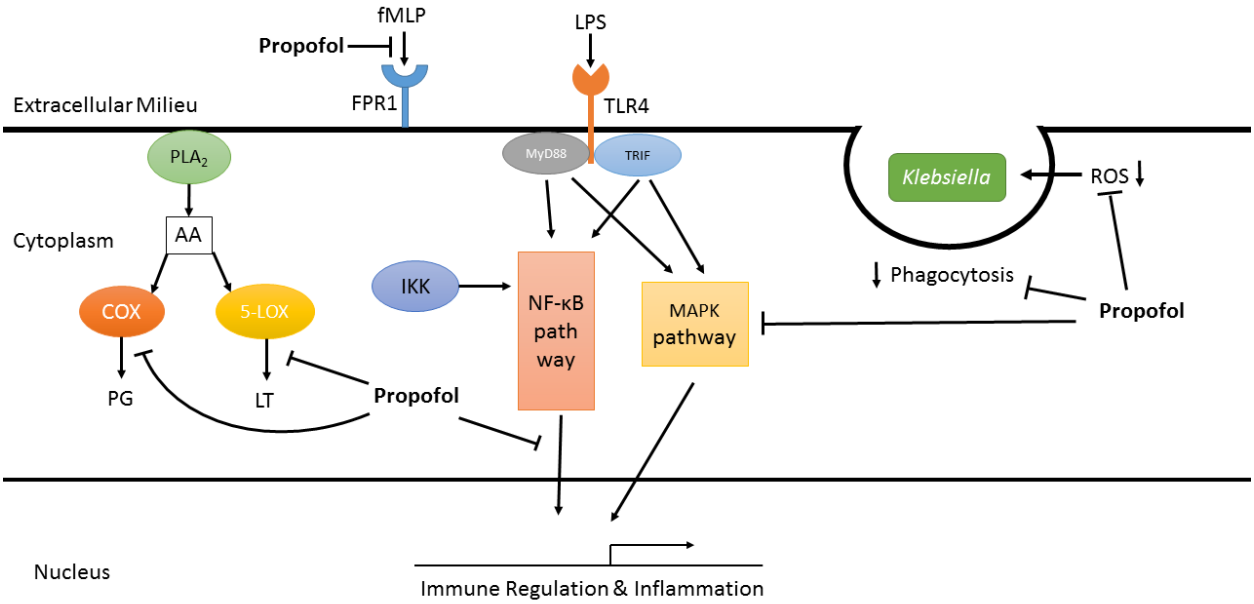

Figure 1.3. The pleotropic inhibitory effects of propofol. Extracellularly, propofol may competitively inhibit fMLP binding to its receptor, FPR1, on neutrophils. Propofol may additionally be suppressing production of reactive oxygen species (ROS) and phagocytic capacity of professional phagocytes. Intracellularly, propofol may antagonize NF-κB and MAPK pathway signaling downstream of lipopolysaccharide (LPS)-induced toll-like receptor (TLR)-4 activation, disrupting the activation of transcription. Finally, propofol may be binding directly and inhibiting both cyclooxygenase (COX) and lipoxygenase (5-LOX) enzymes, decreasing the production of prostaglandins (PG) and leukotrienes (LT), respectively. LPS, lipopolysaccharide; PLA2, phospholipase A2; AA, arachidonic acid; MyD88, myeloid differentiation primary response gene 88; TRIF, TIR-domain-containing adapter-inducing interferon-β; IKK, IκB kinase.

significantly less. Propofol, but not pentobarbital or ketamine/xylazine, was found to significantly increase bacterial burdens in infected mice compared with non-sedated controls. Unexpectedly, this immune defect was detectable even when mice were infected 96 hours after propofol or control sedation, demonstrating that the risk window for an altered immune response following propofol sedation is much longer than expected. While propofol-sedated mice demonstrated higher liver and spleen burdens and a reduced ability to resolve infection, even more striking was the organ pathology Visvabharathy reported, including extensive dissemination of *L. monocytogenes* into the white pulp of the spleen and overall disruption of splenic architecture. Serum cytokine levels were differentially affected, with significant elevations observed at 24 hours in interferon gamma and IL-10 at 72 hours post-infection. Serum chemokines KC, MCP-1, and CCL11 (eotaxin), were uniformly elevated throughout the time course compared to controls. These observations were then applied to the more common nosocomial pathogen *Staphylococcus (S.) aureus*, again using a bloodstream infection model. While differences in burdens appeared transiently during the time course of infection, mice once again were unable to effectively clear *S. aureus* from the kidneys, resulting in dramatic increases in abscess size. Visvabharathy continued to explore this model of *S. aureus* infection and found that in addition to exacerbating kidney pathology, propofol-sedated mice remained unable to clear *S. aureus* even 32 days post-infection, indicating a significant defect extending into the adaptive immune response (136). These mice displayed increased neutrophil infiltration into infected kidneys, but a decrease in other effector phagocytic populations and mature DCs. It was also observed that vancomycin prophylaxis, a common pre-treatment strategy to prevent infections prior to invasive procedures, only compounded the pathophysiological severity of *S. aureus* infection. Taken together, recent propofol sedation would appear to be a significant risk factor in patients with suspected or confirmed bloodstream infections caused by Gram positive bacteria. It is therefore prudent to investigate whether this susceptibility extends to Gram negative bacterial infections and other routes of infection.

1.9. Summary

Klebsiella pneumoniae is a Gram negative facultative anaerobic bacterium commonly found in environmental reservoirs and is capable of colonizing the human upper respiratory tract, skin, and gastrointestinal tract asymptomatically. In neonates, the elderly, and generally immunodeficient persons, *K. pneumoniae* is capable of causing invasive disease. This is of clinical significance due to the general distress caused by a variety of procedures in the healthcare setting that can increase the risk of infection. As a direct result, *K. pneumoniae* is the cause of approximately 12,000 HAIs every year in the United States. These infections are often complicated by extensive antibiotic resistance in clinical isolates, making these strains refractory to standard treatment modalities.

Our bodies have evolved multiple lines of defense for opportunistic pathogens like *K. pneumoniae*. To prevent foreign particulates and pathogens from reaching the lungs, the epithelial lining secretes mucus to capture airborne particles while cilia act in concert to move this mucus out of the trachea and into the digestive tract where the low pH environment can degrade bacteria. Even if bacteria can survive the stomach and advance to the intestinal lumen, they encounter a harsh chemical environment, competition with our microbiota, and another layer of mucus being moved distally by peristalsis. Recent research has identified at least some of the roles that alveolar macrophages, resident dendritic cells, neutrophils, and γδ-T cells play in the innate response, plus several cytokines and chemokines have been identified as critical for successful clearance *in vivo*. Invasive disease is thus rare in healthy individuals and requires one or more comorbidities to gain a foothold and cause infection. It is becoming clearer, however, that sedative exposure may be an underappreciated risk factor for the development of infection and may actually contribute to poorer prognoses in these critically ill patients. The specific deficiencies caused by sedation and their durations remain undefined in all manner of patient populations and *in vivo* modeling is required to investigate these effects.

Propofol is one of very small group of clinically important general anesthetics in use throughout the world today. Since its discovery and commercialization some thirty years ago, propofol has become an industry standard, lauded for its favorable anti-emetic, anti-inflammatory, and anxiolytic effects, as well as its rapid on- and off-set. Despite their ubiquity in the clinic, it is widely recognized that all general anesthetics have off target effects, including targets involved in the immune response, and as a result clinicians must take these into account to maximize positive patient outcomes. *In vitro* evidence suggests that propofol can have anti-inflammatory properties, particularly in non-infectious inflammatory responses, when examining key phagocytic cell populations such as macrophages and neutrophils. Conversely, *in vivo* models of infection are suggesting that propofol could be decreasing the efficacy of the immune response, yet amplifying pro-inflammatory signaling, resulting in exacerbated pathology at primary sites of infection. With no clear mechanistic insights into propofol's modulation of the immune response during clinically relevant infections, it is important to continue to phenotype and characterize these immune alterations and expand the scope of the available experimental models to better understand both the underlying mechanism(s) of action and the consequences of exposure.

1.10. Goals of this study

The studies detailed herein aim to not only better characterize the host immune response to *Klebsiella pneumoniae* lung infection in the presence and absence of acute exposure to the anesthetic propofol, but to also probe how this altered host immune response may lead to a shift in the virulence determinant repertoire required for successful lung colonization. In Chapter Two, propofol sedation as a risk factor for the development of sepsis will be investigated in a mouse model of lung infection, and in Chapter Three, several hypotheses will be explored regarding possible immunosuppressive mechanisms caused by propofol *in vivo*. Finally, while previous studies have used high throughput sequencing approaches to identify new virulence determinants in various organs, Chapter Four will describe how we

497 employed this strategy with unprecedented resolution to identify new virulence determinants for lung
498 pathogenesis while simultaneously taking into account sedation as a variable.

499 As previous infectious models used Gram positive bacteria or an artificial polymicrobial sepsis,
500 we sought to demonstrate that infection with a Gram negative bacterium is also affected by propofol
501 sedation. Previous infectious models also used systemic bloodstream models of infection, thus
502 bypassing the many layers of mucosal immunity. The studies described in this thesis used a non-invasive
503 intranasal route of infection to mimic microaspirations into the lungs that could be a significant source
504 of pneumonias. These investigations aimed to ascertain the extent to which acute propofol exposure
505 may render the host more susceptible (or resistant) to infection with the clinically relevant pathogen
506 *Klebsiella pneumoniae*.

507

Chapter 2: Propofol sedation promotes septic progression during *Klebsiella pneumoniae* lung infection

2.1. Summary

The general anesthetic propofol is widely used in clinical settings worldwide. However, a growing body of evidence suggests that propofol can suppress appropriate immune responses to infectious insults, potentially leading to greater susceptibility. The Gram-negative bacterium *Klebsiella (K.) pneumoniae* is a common cause of healthcare-acquired pneumonia and the second most common cause of Gram negative sepsis in the world. We investigated the impact brief propofol anesthesia had on *K. pneumoniae* lung infections in outbred Swiss Webster mice. Propofol had little effect on lung burdens and dissemination out to 48 hours post-infection, however, mice sedated with propofol demonstrated greatly increased transcription of pro-inflammatory cytokines, chemokines, and colony stimulating factors in the lung at 24 hours post-infection, suggesting a cytokine storm. The discrepancies in gene expression were largely resolved by 48 hours, yet propofol-sedated mice lost weight more rapidly than control animals. Serum cytokine and chemokine levels reflected this hyper-expressive phenotype and continued to rise throughout the course of infection in propofol-sedated mice. Histological analysis revealed that propofol-sedated mouse lungs contained significantly larger infectious foci, likely as a result of the increased gene expression. This study demonstrates that brief propofol anesthesia is capable of recapitulating clinical characteristics of sepsis in a mouse model of *K. pneumoniae* lung infection.

2.2. Introduction

Healthcare-associated infections (HAIs) are a persistent and pervasive complication in the global, modern healthcare setting (137). Patients undergoing surgery or extended stays in intensive care units (ICUs) are at an increased risk of acquiring bacterial infections, resulting in increased morbidity and mortality (138). While ongoing surveillance and management campaigns have resulted in significant

reductions in frequency over the past several decades (137,139), the Centers for Disease Control and Prevention (CDC) recorded more than 365,000 HAIs in the United States between 2011 and 2014 alone (140). These infections frequently progress to septicemia, further stressing already critically ill patients and often resulting in death despite supportive care (65,141–143). Compounding this issue is the alarming increase in multi-drug resistant isolates of *K. pneumoniae* globally, which further results in poor prognoses and increased mortality (138,140,9,7,10,8,16).

Critically ill patients often require sedation and the anesthetic propofol (2,6-diisopropylphenol) is one of the most commonly used agents for anesthesia. Propofol can be given as a single bolus for the induction of anesthesia or can be given continuously to maintain sedation for days or weeks. Despite the ubiquity of propofol in the clinical setting, recent research on propofol *in vitro* has identified a variety of potential immunomodulatory effects that may ultimately result in impaired pathogen clearance (118,125,124,144,126,127,145,131,146,121,128,147–149,129,123). More recently, work in our lab has demonstrated that in mouse models of bloodstream infections with the Gram-positive bacteria *Listeria monocytogenes* and *Staphylococcus aureus*, acute propofol sedation resulted in increased bacterial burdens in target organs, increased dissemination, more severe organ pathology, and impaired bacterial clearance (135,136). Propofol infusion anesthesia has also been shown to increase mortality in a rat model of polymicrobial sepsis (134). In human patients presenting with sepsis, propofol-sedated patients had significantly higher pro-inflammatory serum cytokines compared to dexmedetomidine-sedated patients (150). Furthermore, a large retrospective study of mechanically ventilated patients found that the use of propofol significantly increased the risk of developing infection compared to patients not receiving propofol sedation (71).

Given the breadth of applications for which propofol is used, it is necessary to apply these new *in vivo* models of infection to new pathogens and new routes of infection. Of the HAIs reported from 2011 to 2014, approximately 8% were caused by *Klebsiella* species (140). *Klebsiella pneumoniae* is an

opportunistic, Gram-negative bacterial pathogen of global concern for its ability to rapidly acquire antibiotic resistance (151,152). Clinical isolates with extended-spectrum beta-lactamase (ESBL) and carbapenemase activity have increased to 24% and 10%, respectively, in the United States in 2014 (140). Considering the clinical severity of *Klebsiella* infections and septicemia in critically ill patients, we sought to determine the impact of propofol sedation on acute *K. pneumoniae* lung infections and the host response in a mouse model of pneumonia.

2.3. Materials and Methods

Bacteria and culture conditions

K. pneumoniae strain KPPR1 (a rifampicin-resistant derivative of ATCC 43816) was used for this study. KPPR1 was cultured overnight, shaking (37°C, 180 rpm) in LB broth. The following morning, the strain was sub-cultured 1:50 in fresh LB and incubated at 37°C with shaking for one hour to mid-log phase growth. Optical density (OD 600nm) was adjusted to 0.2 with LB broth and diluted to the desired density in sterile 1X PBS for infection.

Animal infections

All animal procedures were approved by the University of Illinois at Chicago Animal Care Committee and were conducted in the Biological Resources Laboratory. Bacteria suspensions in PBS were kept on ice until immediately before infection. Animals were sedated via tail vein injection with either ketamine (25 mg/kg) and xylazine (4 mg/kg) or propofol (20 mg/kg; Zoetis, Kalamazoo, MI). Twenty microliters of bacterial suspension, containing approximately $1x10^3$ colony forming units of KPPR1 was administered via intranasal route into 6- to 8-week old Swiss Webster mice (Harlan, Madison, WI, USA) or 7- to 9-week old female C57BL/6 mice (Harlan). After 10 to 48 hours, mice were sacrificed, blood was collected, and lungs, livers, and spleens isolated, homogenized, and plated on LB agar containing 30 µg/ml rifampicin for enumeration of bacterial burdens in each organ.

RNA Extraction and cDNA Synthesis

The left lung lobe of each mouse was removed following PBS + 50U/ml heparin perfusion, snap frozen in liquid nitrogen, and stored at -80°C until processing. One milliliter TRIzol (Invitrogen, Carlsbad, CA) was added to each lung before mechanical homogenization (TH, Omni International, Kennesaw, GA). RNA was isolated as per the manufacturer's protocol and dissolved in 100 µl Tris-EDTA buffer, pH 8.0 (Millipore-Sigma). RNA was treated with Turbo DNase kit (Ambion, Carlsbad, CA) and quantified on a NanoDrop OneC spectrophotometer (Thermo Scientific, Waltham, MA). cDNA was synthesized with the High Capacity cDNA Reverse Transcription kit (Applied Biosystems, Carlsbad, CA) and diluted in DEPC-treated water.

Quantitative RT-PCR

Primers for quantitative reverse transcription PCR were designed using PrimerBLAST (NCBI), synthesized by Millipore-Sigma, and are listed in Table 2.1. Samples were prepared using Fast SYBR Green master mix (Applied Biosystems) with 200 nM final primer concentrations in 10 µl reaction volumes and run in 384-well plates on a ViiA 7 quantitative PCR machine (Applied Biosystems). Gene expression was assessed in triplicate for each sample and normalized to *Gapdh*. Baseline calls were set equivalent for each gene across all runs.

Serum Protein Quantitation

Blood was drawn from the inferior vena cava immediately following euthanasia and allowed to clot at room temperature for up to two hours. The clotted samples were spun at 2,000g for 15 minutes and serum was transferred into sterile 1.5 ml microcentrifuge tubes and stored at -20°C. A BioPlex Pro assay (Bio-Rad) was customized from the mouse cytokine group I targets for the following proteins: IL-1β, IL-6, IL-10, IL-12p70, IL-17A, IL-22, IFNγ, G-CSF, KC (CXCL1), MCP-1 (CCL2), MIP-1α (CCL3), MIP-1β (CCL4), and

TNFα. Samples were processed according to the manufacturer's protocol, run on a Bio-Plex 200 (Bio-Rad), and analyzed with Bio-Plex Manager 5.0 (Bio-Rad) software.

Histology

For histological analysis, infected mice were sacrificed via isoflurane overdose (Henry Schein, Dublin, OH). The lung vasculature was perfused with 10 ml ice cold PBS containing 50U/ml heparin to remove blood and lungs were re-inflated with one milliliter of Z-FIx solution (Anatech, Battle Creek, MI). Lungs, livers, and spleens were placed in 20 ml of Z-Fix solution for 48 hours, then transferred into 70% ethanol. Paraffin-embedded 5 µm thick sections were prepared by the UIC Research Histology and Tissue Imaging core facility. Digital scans of H&E stained lung sections were captured on a ScanScope CS (Aperio, Buffalo Grove, IL) and analyzed using ImageScope software (Aperio). Total area of lung tissue is defined as all alveolar and bronchiolar spaces, plus vascular endothelium found within lobular boundaries. An infectious focus is defined as an area of increased local cellular concentration with a minimum 10,000 μm^2 area. Adjacent foci must have been a minimum of 100 µm apart to be quantified separately.

Statistical Analyses

All statistical analyses were performed with Prism (GraphPad, La Jolla, CA). Organ burdens were analyzed using the Mann Whitney U test. Changes in gene expression were analyzed using a two-tailed, unpaired Student's T test with a correction for multiple comparisons using the Holm-Sidak method. Lung pathology area analyses used a two-tailed, unpaired Student's T test with Welch's correction.

Table 2.1: qRT-PCR primers used in this study

Gene	Accession	Forward	Reverse	Amplicon (bp)
Ccl2	NM_011333.3	5′-AGC TGT AGT TTT GTT CAC CAA GC-3′	5′-GAC CTT AGG GCA GAT GCA GT-3′	147
Ccl3	NM_011337.2	5′-ACT GCC TGC TGC TTC TCC TAC A-3′	5′-AGG AAA ATG ACA CCT GGC TGG-3′	100
Ccl4	NM_013652.2	5′-CCC AGC TCT GTG CAA ACC TA-3′	5′-CCA TTG GTG CTG AGA ACC CT-3′	114
Ccl11	NM_011330.3	5′-ACC AAC AAC AGA TGC ACC CT-3′	5′-GGA CCC ACT TCT TCT TGG GG-3′	88
Ccl20	NM_016960.2	5′-AAT CTG TGT GCG CTG ATC CA-3′	5′-TTG ACT CTT AGG CTG AGG AGG T-3′	70
Cxcl1	NM_008176.3	5′-AAC CGA AGT CAT AGC CAC AC-3′	5′-CAG ACG GTG CCA TCA GAG-3′	147
Cxcl2	NM_009140.2	5′-CCC CCT GGT TCA GAA AAT CAT C-3′	5′-AAC TCT CAG ACA GCG AGG CAC ATC-3′	172
Cxcl3	NM_203320.3	5′-CCA GAC AGA AGT CAT AGC CAC-3′	5′-CTT CAT CAT GGT GAG GGG CTT-3′	150
Cxcl5	NM_009141.3	5′-TGC CCT ACG GTG GAA GTC AT-3′	5′-AGC TTT CTT TTT GTC ACT GCC C-3′	120
Cxcl10	NM_021274.2	5′-ATG ACG GGC CAG TGA GAA TG-3′	5′-TCA ACA CGT GGG CAG GAT AG-3′	76
Gapdh	NM_008084	5′-CTT TGT CAA GCT CAT TTC CTG G-3′	5′-TCT TGC TCA GTG TCC TTG C-3′	133
Gcsf (Csf3)	NM_009971.1	5′-CAG CCC AGA TCA CCC AGA ATC-3′	5′-CTG CAG GGC CAT TAG CTT CAT-3′	70
Gmcsf (Csf2)	NM_009969.4	5′-GAT ATT CGA GCA GGG TCT ACG-3′	5′-AGG CTG TCT ATG AAA TCC GC-3′	150
Ifnb	NM_010510.1	5′-TGG GAG ATG TCC TCA ACT GC-3′	5′-CCA GGC GTA GCT GTT GTA CT-3′	93
Ifng	NM_008337.4	5′-GAA CTG GCA AAA GGA TGG TGA-3′	5′-TGT GGG TTG TTG ACC TCA AAC-3′	209
Il1b	NM_008361.4	5'-CTC ATC TGG GAT CCT CTC CA-3'	5'-TGT CAA AAG GTG GCA TTT CA-3'	99
Il6	NM_031168.2	5′-CAA AGC CAG AGT CCT TCA GAG-3′	5′-GTC CTT AGC CAC TCC TTC TG-3′	150
Il10	NM_010548.2	5′-GCC GGG AAG ACA ATA ACT G-3′	5′-GGA GTC GGT TAG CAG TAT GTT G-3′	138
Il12b	NM_001303244.1	5′-GGA AGC ACG GCA GCA GAA TA-3′	5′-AAC TTG AGG GAG AAG TAG GAA TGG-3′	177
Il17a	NM_010552.3	5′-TTT AAC TCC CTT GGC GCA AAA-3′	5′-CTT TCC CTC CGC ATT GAC AC-3′	164
Il17f	NM_145856.2	5′-TGG AGA AAC CAG CAT GAA GTG-3′	5′-AGT CCC AAC ATC AAC AGT AGC-3′	62
Il22	NM_016971.2	5′-GCT CAG CTC CTG TCA CAT CA-3′	5′-CAG TTC CCC AAT CGC CTT GA-3′	118
Il23a	NM_031252.2	5′-CCA GTG TGA AGA TGG TTG TGA CC-3′	5′-GGT GCT TAT AAA AAG CCA GAC CTT G-3′	94
Mcsf (Csf1)	NM_007778.4	5′-TGG CTT GGC TTG GGA TGA TT-3′	5′-TAT GCG AAG GGG AAG CTC AC-3′	73
Nos2	NM_010927.4	5′-GCA AAC ATC ACA TTC AGA TCC C-3′	5′-TCA GCC TCA TGG TAA ACA CG-3′	150
Tnfa	NM_013693.3	5′-CTT CTG TCT ACT GAA CTT CGG G-3′	5′-CAG GCT TGT CAC TCG AAT TTT G-3′	134

2.4. Results

The Swiss Webster mouse as a model of *Klebsiella pneumoniae* sepsis. The Swiss Webster (SW) mouse strain is commonly utilized for toxicological and pharmacological studies as it is outbred and thus provides a more heterogeneous output more accurately reflecting a spectrum of immune responses, thus we felt it most appropriate to use to investigate the anesthetic propofol in a *K. pneumoniae* lung infection model. We first sought to establish *in vivo* growth kinetics of *K. pneumoniae* strain KPPR1. Mice were anesthetized for approximately five minutes using a clinically relevant dose of propofol delivered intravenously (IV) or with ketamine and xylazine combination as control. While unconscious, mice were given a 20 µl bolus of *K. pneumoniae* intranasally, then allowed to recover. At multiple time points out to 48 hours, we sacrificed mice and quantified organ burdens. At the earliest time point, propofol-sedated mice had approximately twice as the bacterial burden in their lungs compared to controls (Fig. 2.1A), suggesting a potential underlying immune defect, while dissemination to distal organs was largely undetectable in both groups (Figs. 2.1BC).

Lung burdens rapidly increased between ten and 24 hours, however no significant differences between groups were detected out to 48 hours post-infection. Dissemination to the liver and spleen increased in both groups, with all animals having detectable burdens by 48 hours, however no significant differences were noted between treatment groups again. Despite these comparable burdens, propofol-sedated mice experienced significantly increased weight loss at both 32 and 48 hours post-infection (Fig. 2.1D), suggesting that *K. pneumoniae* burdens were not indicative of the true severity of infection.

Propofol sedation potentiates a transient hyper-inflammatory lung environment. To assess the immune response in the lungs of infected animals, we utilized quantitative reverse transcription PCR (qRT-PCR) to analyze gene expression for a variety of cytokines and chemokines in the mouse lung.

Following a 10^3 CFU intranasal inoculum, little change was detectable by ten hours post-infection with the notable exception of *Il23a*, encoding the IL-23p19 subunit. Propofol-sedated animals demonstrated a five-fold increase in *Il23a* transcript levels, while control-sedated mice had increased transcription 36-fold at 10 hours (Fig. 2.2K). After 24 hours, expression of nearly every gene assessed was significantly higher in propofol-sedated mice with expression levels being on average 4.6-fold higher (3.9-5.3 95% CI) than controls (Figs. 2.2 and 2.3). This expression was dependent on ongoing infection as mice sedated with propofol and mock infected with sterile phosphate-buffered saline (PBS) did not display any changes in gene expression compared to naïve mice at 24 hours (data not shown). Transcript levels continued to remain significantly elevated in the lungs of propofol-sedated mice at 32 hours post-infection, with an average of 3.2-fold higher (2.6-3.8 95% CI). Hyper-expression appeared transient in this time course and by 48 hours post-infection expression of most genes was comparable, with the exception of inducible nitric oxide synthase (*Nos2*) and *Cxcl5,* both of which remained significantly elevated above controls (Figs. 2.2E and 2.3). In addition to this pro-inflammatory response, anti-inflammatory interleukin (IL)-10 was also significantly upregulated earlier during infection in propofol-sedated mice (Fig 2.3). It must be noted that propofol did not universally induce gene expression, as demonstrated by the chemokine eotaxin (*Ccl11*, Fig. 2.3). The data clearly demonstrate broad changes in genes critical to the immune response and that toll-like receptor (TLR) 4 signaling through both the TRIF-dependent pathway (Figs. 2.2A-C) and the MyD88-dependent pathway (Figs. 2.2F-H) are both similarly impacted.

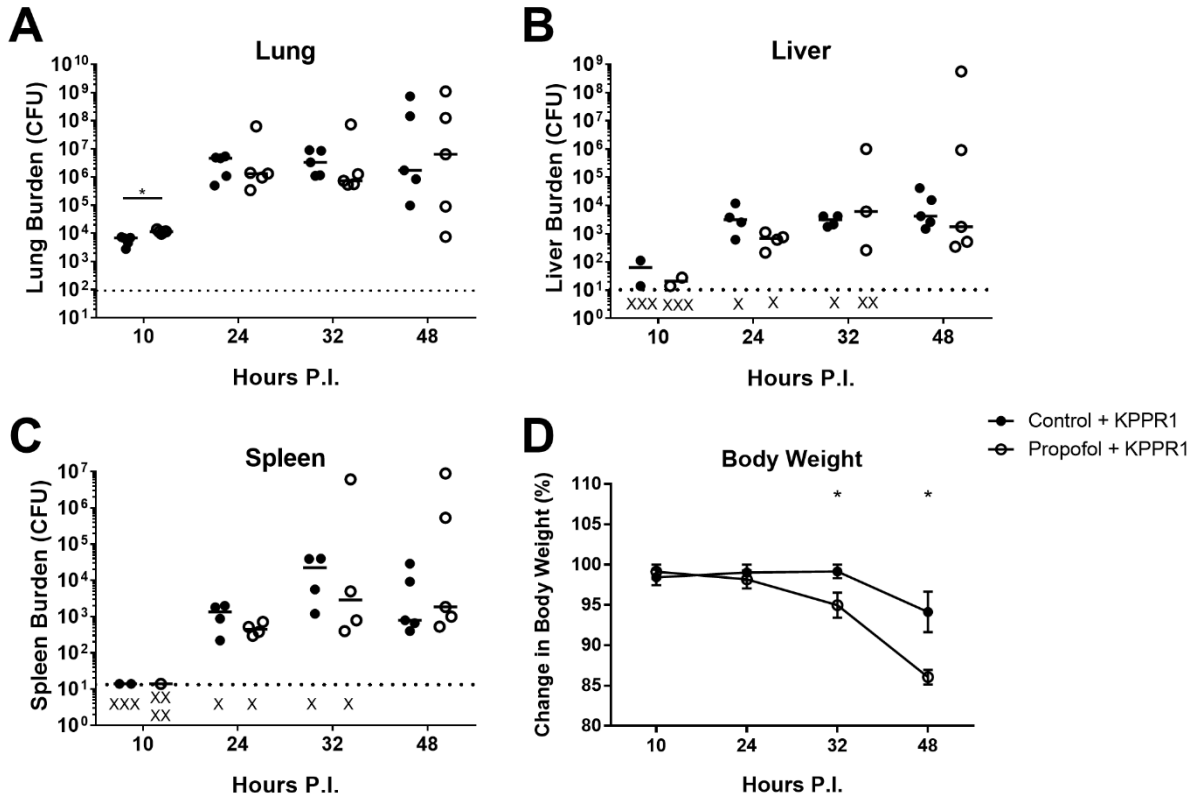

Figure 2.1. *K. pneumoniae* infection progression in the Swiss Webster mouse model. Female Swiss Webster mice were anesthetized intravenously with either ketamine/xylazine (control) or propofol and inoculated via intranasal route with $1x10^3$ CFU KPPR1. Organ burdens were assessed at the indicated time points in (A) lungs, (B) livers, and (C) spleens. (D) Average body weight percent lost during infection. N=5 per group, per time point. Data is representative of two independent experiments. *$p < 0.05$

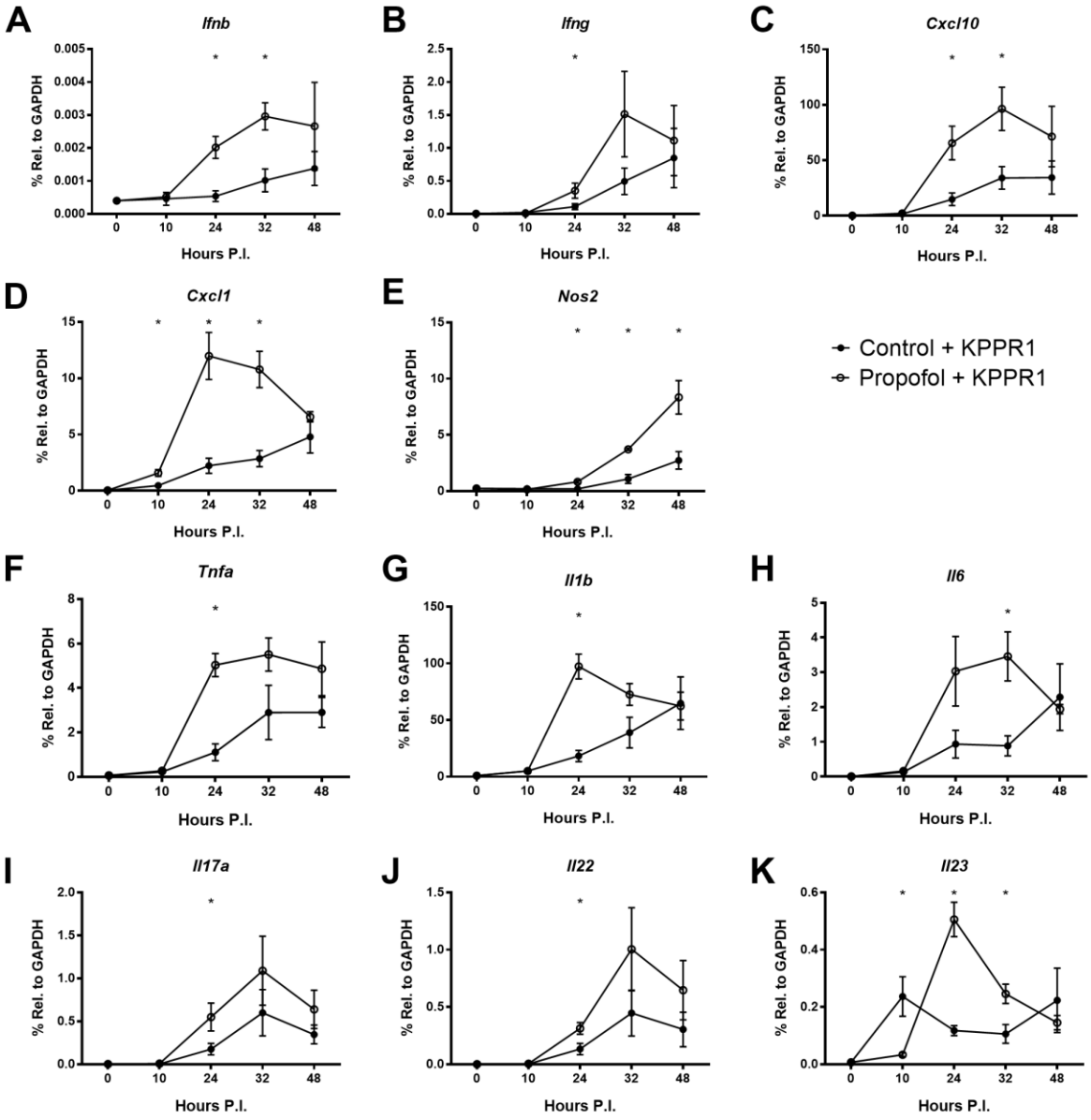

Figure 2.2. Mouse lung gene expression profiles during *K. pneumoniae* infection are significantly altered by propofol sedation. Female Swiss Webster mice were anesthetized intravenously with either ketamine/xylazine (control) or propofol and inoculated via intranasal route with $1x10^3$ CFU KPPR1. Quantitative RT-PCR analysis was performed on cDNA generated from total lung RNA collected at the indicated time points. Data were normalized to *Gapdh*. N=5 per group, per time point. Data is representative of two independent experiments. *$p < 0.05$

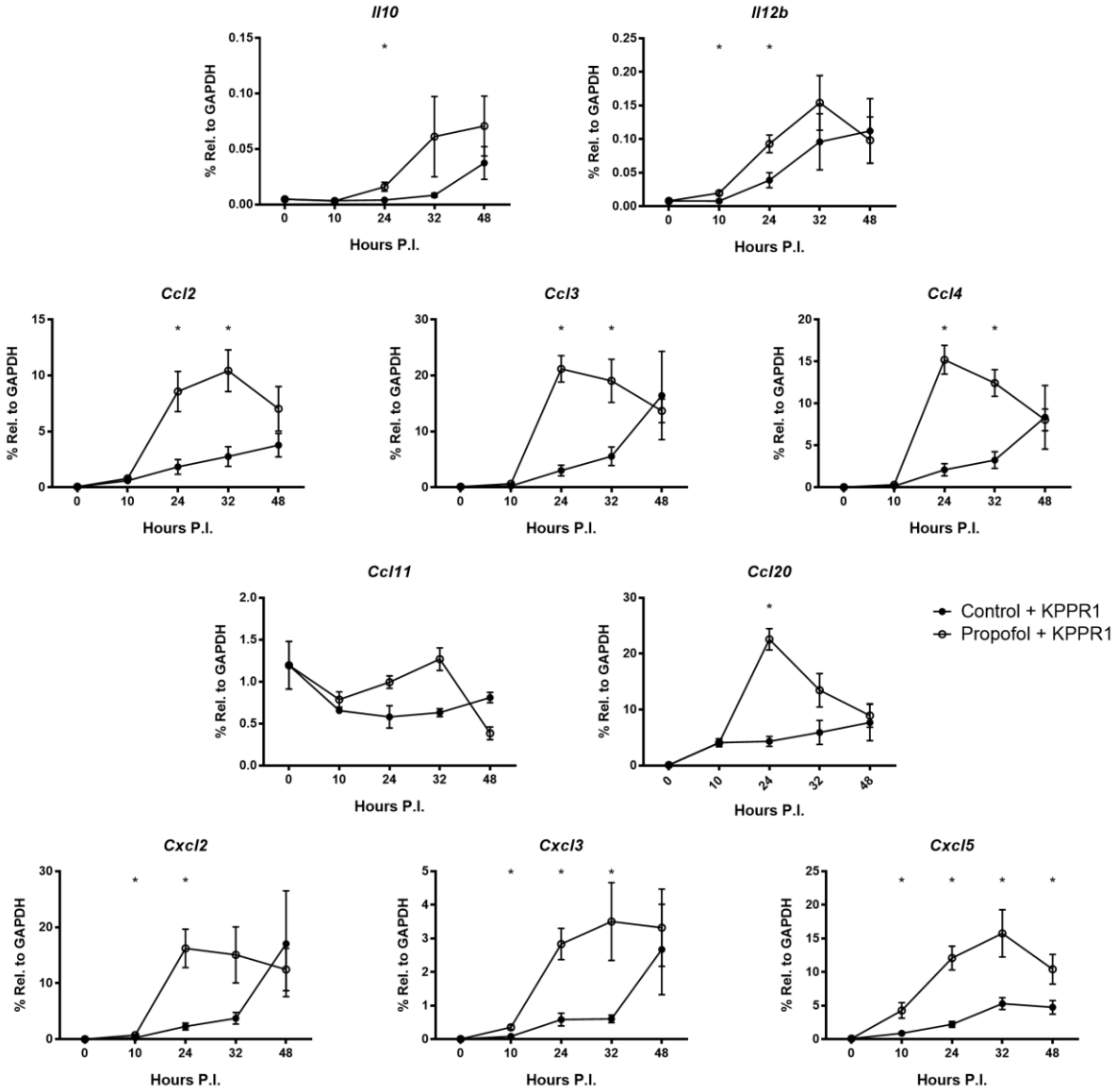

681

682 **Figure 2.3. Propofol increases expression of *Il10* and many different chemokines.** Female Swiss
683 Webster mice were anesthetized intravenously with either ketamine/xylazine (control) or propofol and
684 inoculated via intranasal route with $1x10^3$ CFU KPPR1. Quantitative RT-PCR analysis was performed on
685 cDNA generated from total lung RNA collected at the indicated time points. Data were normalized to
686 *Gapdh*. N=5 per group, per time point. Data is representative of two independent experiments. *p <
687 0.05

Propofol increases colony stimulating factor expression. In addition to cytokines and chemokines, colony stimulation factors (CSFs) are important signals for the recruitment and maturation of myeloid-lineage immune cells. Transcript analysis of these three factors in the lungs of infected mice also demonstrated significantly increased expression of granulocyte-macrophage (GM)-CSF and granulocyte (G)-CSF at 10 hours post-infection and of all three factors at 24 and 32 hours post-infection (Fig. 2.4). G-CSF, a potent neutrophil recruiter and activator, was clearly the dominant factor with 24 hour control-sedated mice demonstrating an average 245-fold increase over basal transcription levels versus 1,545-fold increase in propofol-sedated mice (Fig. 2.4C). Both macrophage (M)-CSF and GM-CSF appear to play minor roles in this infectious model with propofol increasing M-CSF expression 3-fold and GM-CSF 4-fold over naïve mice, however no induction in either gene was observed in control mice. These results suggest that propofol, in addition to potentiating a hyper-inflammatory state, may also be increasing recruitment of monocytes and granulocytes from the bone marrow, placing increased strain on the hematopoietic compartment.

To ensure that these findings were not the result of an idiosyncrasy of Swiss Webster mice, the infection was replicated in female C57BL/6 mice with 10^3 CFU KPPR1. Lung gene expression was found to follow highly similar induction profiles in both magnitude of induction and temporal characteristics, with expression levels 4.0-fold higher (3.3-4.7 95% CI) at 24 hours and 3.0-fold higher (2.2-3.8 95% CI) after 32 hours in propofol-sedated mice (Fig. 2.5). These data led us to conclude that propofol is radically altering expression levels of multiple pro-inflammatory cytokines, chemokines, and colony stimulating factors during the innate response to *K. pneumoniae* lung infection.

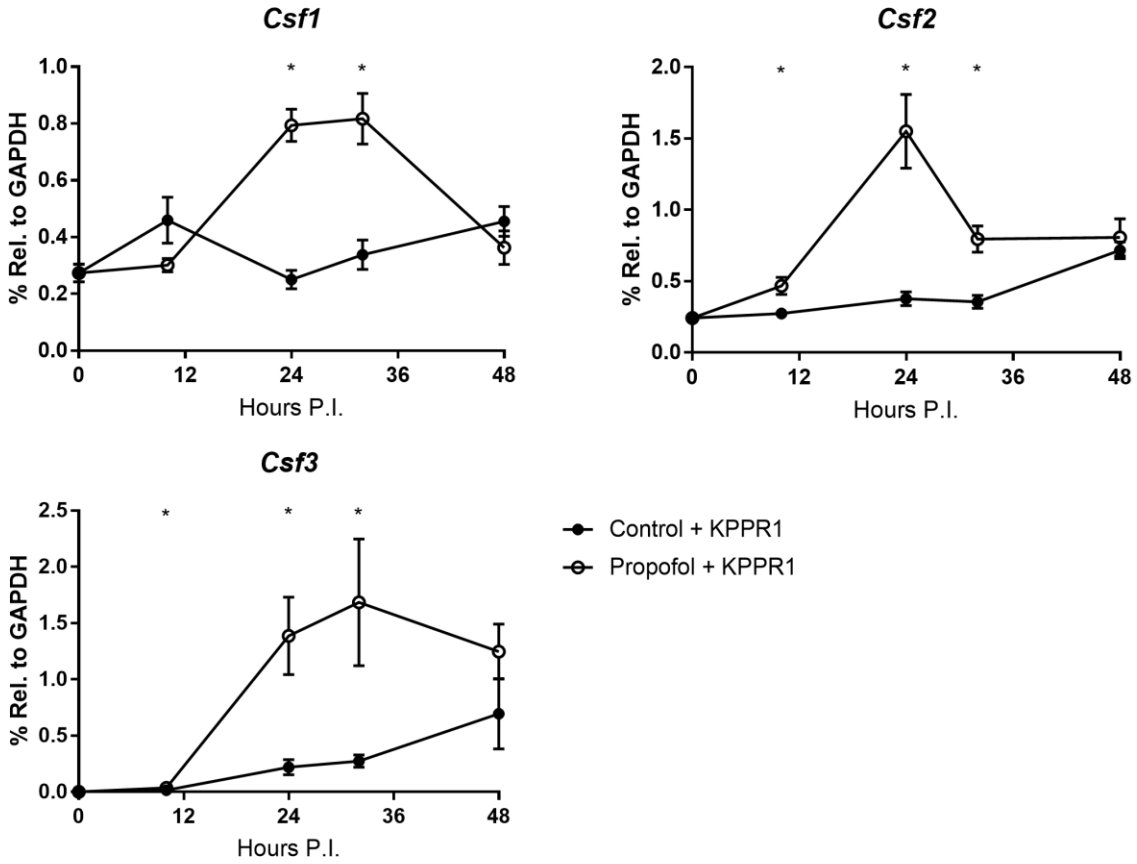

709

710 **Figure 2.4. Colony stimulating factor transcription is elevated in propofol-sedated animals.**

711 Quantitative RT-PCR of M-CSF (*Csf1*, A), GM-CSF (*Csf2*, B), and G-CSF (*Csf3*, C) in mouse lungs during *K.*

712 *pneumoniae* infection. Data were normalized to GAPDH. N=5 per group, per time point. Data is

713 representative of two independent experiments. *$p < 0.05$

714

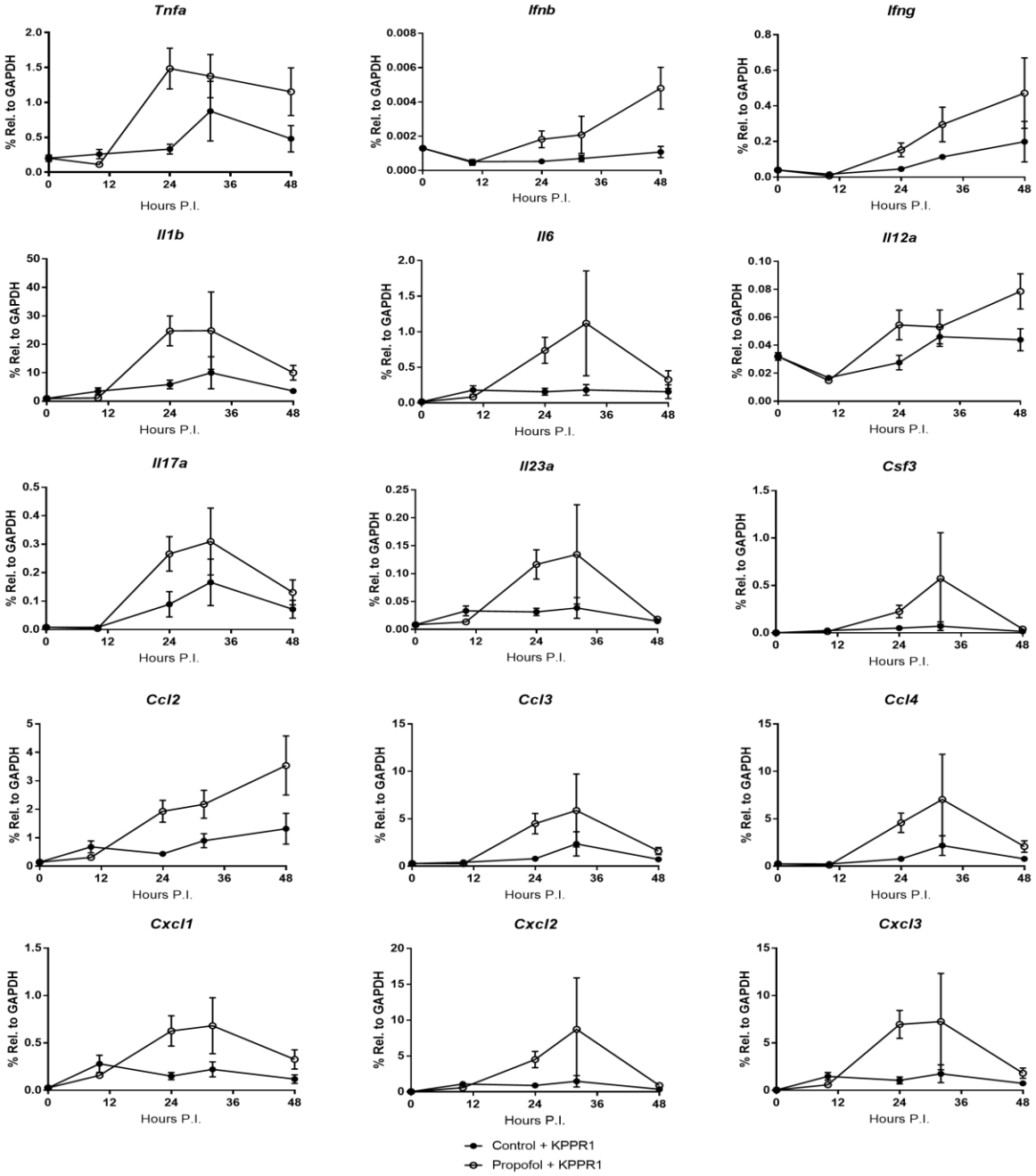

715

716 **Figure 2.5. Propofol leads to a hyper-inflammatory phenotype in C57BL/6 lungs.** C57BL/6 mice were

717 infected with 10^3 CFU. Total RNA was extracted from infected lungs and assayed for expression of

718 cytokines and chemokines at 10, 24, 32, and 48 hours post-infection. Significance was determined with

719 an unpaired, two-tailed Student's T-test. *, $p < 0.05$

Serum protein expression reflects heightened gene expression in propofol-sedated mice. Pro-inflammatory protein expression is controlled by multiple layers of post-transcriptional, translational, and post-translational control, so we sought to profile key cytokines and chemokines in the serum to assess if and how the observed increase in pro-inflammatory gene expression translated to bioactive protein. Serum from infected mice was obtained at 10, 24, 32, and 48 hours post-infection. At ten hours, small but statistically significant increases in chemokines CCL2 and CCL4 were detected in control mice, while propofol-sedated mice demonstrated no detectable changes (Figs. 2.2H and 2.7). Surprisingly, control mice also demonstrated a large increase in early serum G-CSF levels (Fig. 2.6F), despite having little induction of *Csf3* (Fig. 2.4C). This is in sharp contrast to propofol-sedated mice that had almost no increase in serum G-CSF at ten hours post-infection. This relationship then inverted for the remainder of the time course, with average serum G-CSF elevated well above control mice, consistent with lung *Csf3* expression. Pro-inflammatory cytokines TNFα, IL-1β, and IL-6 only experienced small increases in control infected mice, but followed a clear trend upward in propofol-sedated mice (Figs. 2.6A-C). Polarizing cytokines IL-10, IL-12p70, IL-17A, and interferon gamma displayed similar expression profiles with increases found at 32 and 48 hours post-infection (Figs. 2.6DE, 2.7). Lastly, neutrophil chemoattractant CXCL1 protein levels demonstrated steady increases as infection progressed and was again found in higher concentration in the serum of propofol-sedated mice. These results demonstrate that increases in lung gene expression are reflective of protein expression on a systemic level and that propofol-sedated mice are experiencing a systemic hyper-inflammatory response.

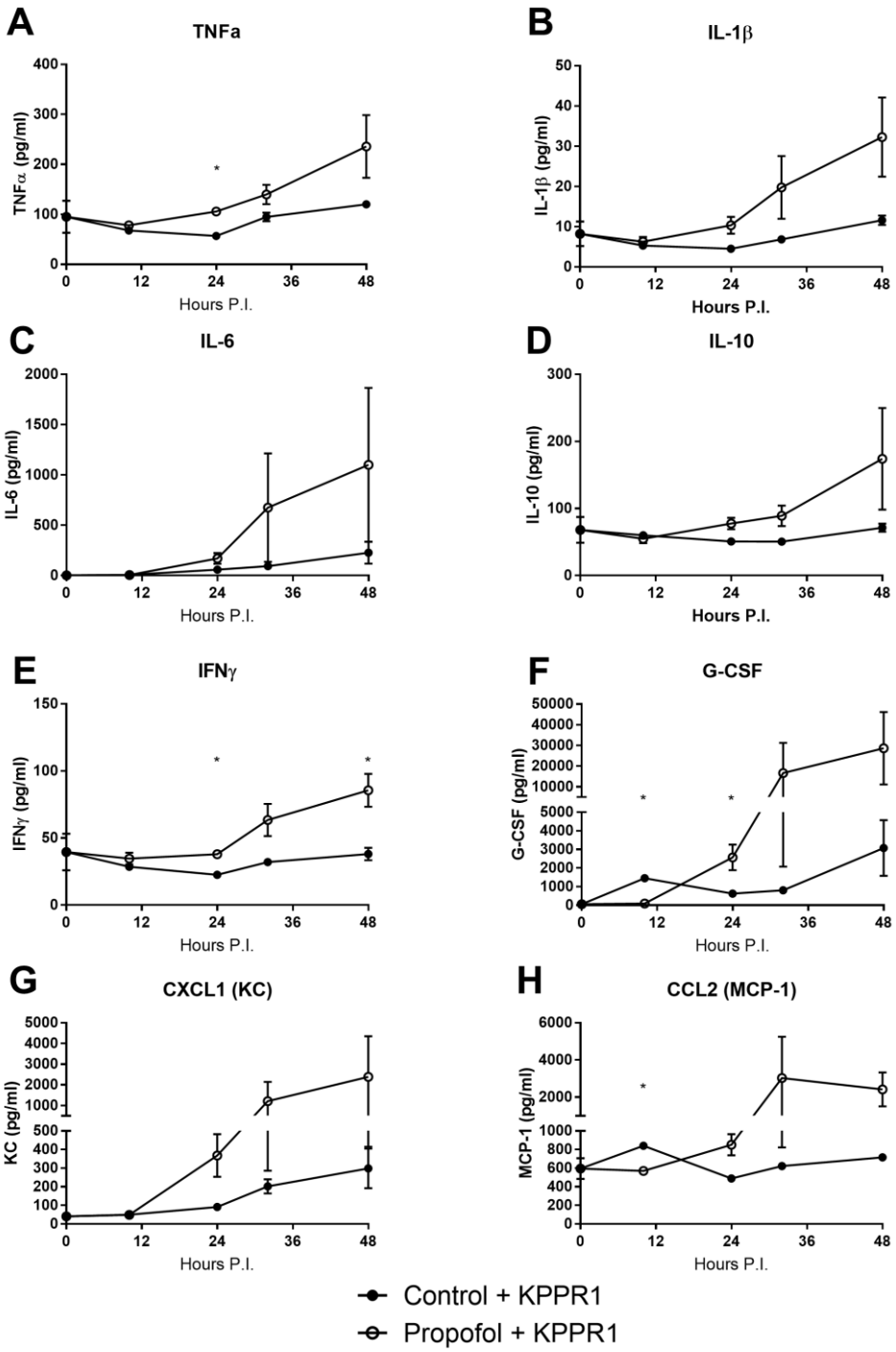

740

741 **Figure 2.6. Propofol increases serum cytokine and chemokines levels during *K. pneumoniae* lung**

742 **infection.** Serum protein levels were compared between control- and propofol-anesthetized Swiss

743 Webster mice (n≥4 per group, per time point) using a custom Bio-Plex protein panel. Data is

744 representative of two independent experiments. *$p < 0.05$

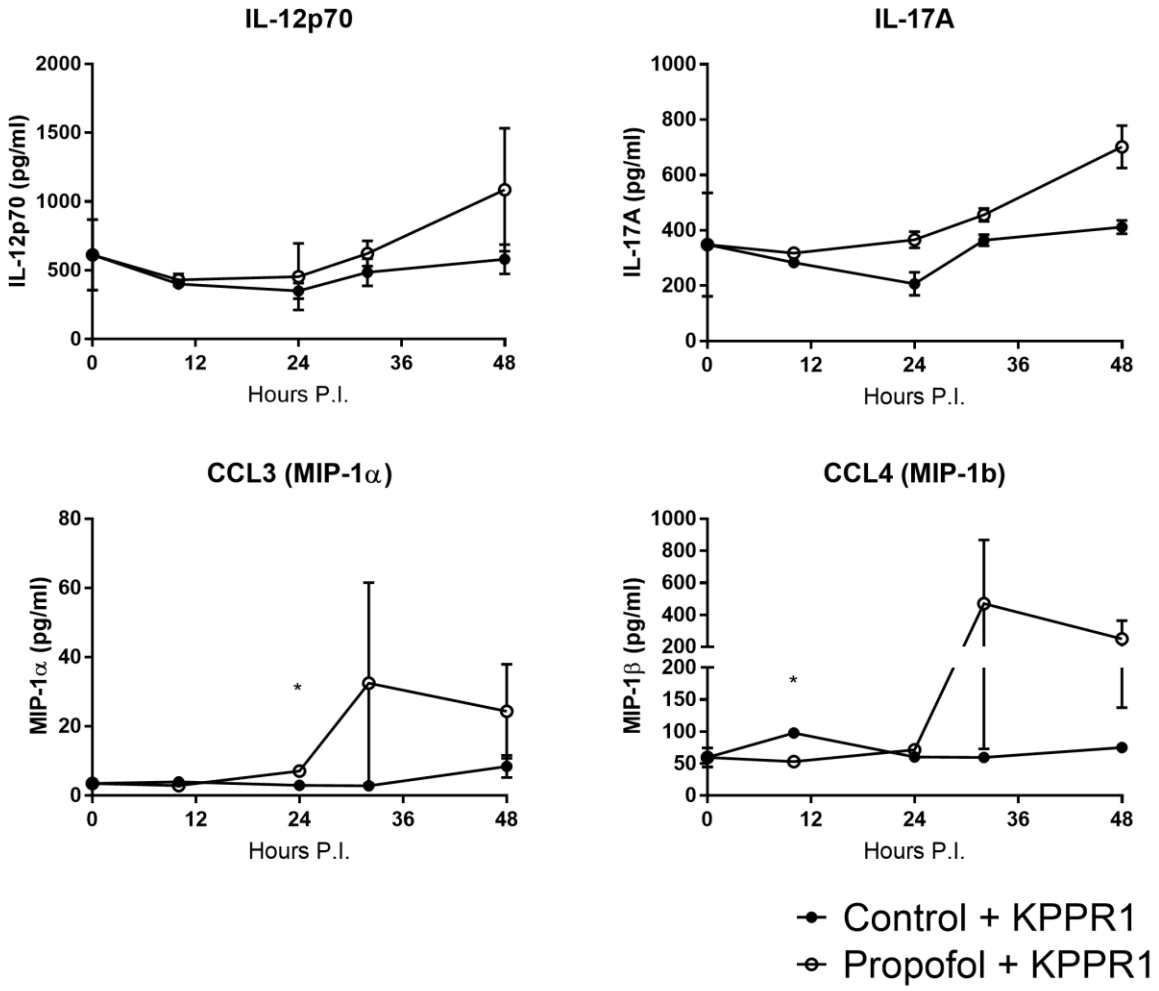

745

746 **Figure 2.7. Additional Swiss Webster serum protein levels.** Serum protein levels were analyzed as part

747 of the custom Bio-Plex protein panel at the indicated time points. *$p < 0.05$

748

Propofol increases infectious foci in the lungs. Having found that propofol dramatically increased pro-inflammatory gene expression in the lungs in response to *K. pneumoniae* infection, we hypothesized that these increases should result in increased immune cell infiltration into the lungs of propofol-anesthetized animals compared to controls. Using the same infection strategy as before, we collected hematoxylin and eosin (H&E)-stained lung sections from mice 24 hours post-infection and digitally analyzed the areas of infection (Fig. 2.8). In propofol-sedated mice, an increased average infectious focus size (Figs. 2.8B & C) and a trend toward increased frequency (Fig. 2.8D) was observed. This resulted in a five-fold increase in the overall percentage of total lung area infected per animal compared to control-sedated mice (Fig. 2.8E). This clearly demonstrates a hyper-recruitment immune phenotype as a result of significant over-expression of multiple cytokines, chemokines, and growth factors and furthermore demonstrates the clear potential for host-mediated tissue damage following propofol sedation.

2.5. Discussion

Propofol's effects on the host response to bacterial infection are multifaceted and warrant further elucidation. Previous studies from our lab found that propofol exposure exacerbated bacterial burdens and organ pathology in both *Listeria monocytogenes* and *Staphylococcus aureus* bloodstream infections. Now, this study confirms that propofol affects multiple routes of infection caused by Gram negative bacteria as well. While Swiss Webster mice have been used for decades in a variety of infection models, very few studies have investigated *K. pneumoniae* pathogenesis using this strain (153,154). The data presented here demonstrate that the Swiss Webster mouse is an exceptional model for septic progression with *K. pneumoniae* and we sought to utilize this to investigate how propofol impacts host innate immune responses during lung infection.

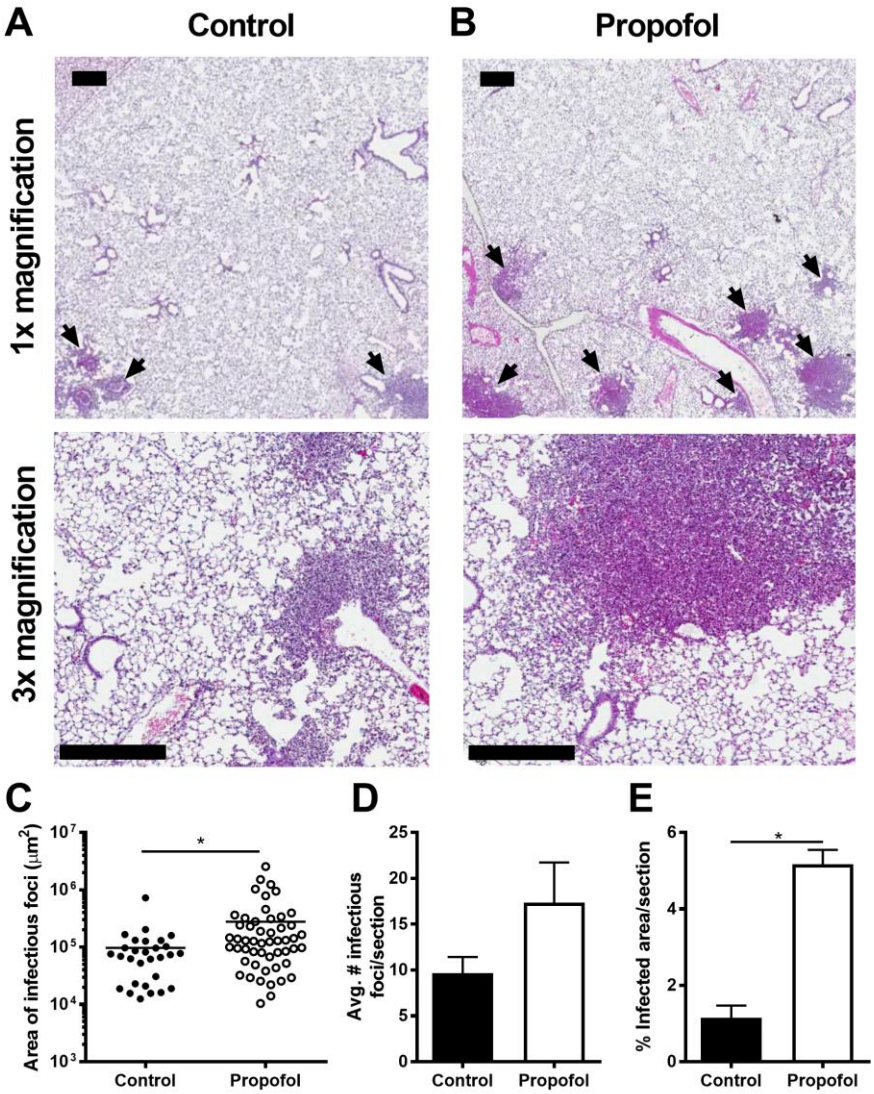

771

772 **Figure 2.8. Propofol increases lung immune cell recruitment.** Infected mouse lungs were formalin-

773 fixed, embedded in paraffin, sectioned in 5 µm thickness, and stained with hematoxylin and eosin. (A)

774 Representative control-sedated mouse lung 24 hours post-infection. (B) Representative propofol-

775 sedated lung 24 hours post-infection. Arrows are separate infectious foci. Black bars = 300 µm. (C)

776 Quantification of the area of individual infectious foci. (D) Average number of infectious foci per mouse;

777 n=3 mice per group. (E) Total infectious foci area per section, one section per mouse, n=3 mice per

778 group. Statistical significance determined with a two-tailed Student's T test with Welch's correction. *p

779 < 0.05

Upon entering the lower respiratory tract, the first immune cells *K. pneumoniae* encounters are alveolar macrophages, capable of phagocytosing *K. pneumoniae* and initiating the pro-inflammatory response. Propofol-sedated mice had a modest, but consistent, two-fold increase in viable bacteria in the lung at ten hours post-infection, suggesting that these alveolar macrophages may be moderately deficient in function. *In vitro* investigations of propofol in macrophage models supports this hypothesis by showing dose-dependent inhibition of both pro-inflammatory cytokine production and inflammatory lipid signaling in response to LPS stimulation (125,144,126,127,145,128,148). This inhibition was likely not detectable in our gene expression analysis because alveolar macrophages comprise a small percentage of total lung cellularity, thus this approach lacked the required resolution to discern these suppressive effects.

Consistent with a previous report (153), Swiss Webster mice failed to contain *K. pneumoniae* inoculated into the lung and dissemination was detectable in a minority of animals as early as 10 hours post-infection. By 32 hours, burdens were detectable in livers and spleens in a majority of mice and by 48 hours post-infection, all mice had detectable dissemination. Of particular interest to us was that a subset of propofol-sedated mice with the highest lung burdens ($\geq 10^8$ CFU) across our three independent time course experiments demonstrated liver and spleen burdens on the order of 1,000-fold higher than control-sedated mice with similar lung burdens (Figs. 2A-C). This suggests that propofol may be increasing the probability of developing severe sepsis following lung infection and further analysis of this trend is warranted.

A robust neutrophil response has been shown to be critical for the resolution of *K. pneumoniae* lung infection (26). Similar to the *in vitro* reports with macrophages, propofol attenuated reactive oxygen species (ROS) generation, elastase release, and chemotaxis in a dose dependent manner (118,119,155), suggesting that these neutrophils could have a reduced capacity for killing extracellular bacteria. G-CSF (*Csf3*) expression is essential for neutrophil differentiation, survival, and maturation and

804 the chemokines CXCL1, CXCL2, CXCL3, and CXCL5 are important neutrophil chemoattractants. All of
805 these genes were induced significantly more in propofol-sedated mice from ten to 32 hours post-
806 infection, suggesting that neutrophil recruitment should likewise be increased, dramatically so by 24
807 hours, yet propofol-sedated mice are unable to control *K. pneumoniae* any more effectively than control
808 mice. An interesting finding was the delayed increase in serum G-CSF, despite increased induction of
809 *Csf3* in the lung. It is possible that this is due to basal *Csf3* transcript levels being near the limit of
810 detection and thus by comparison the increase noted at ten hours post-infection were still insignificant,
811 however this also suggests an extra-pulmonary source of G-CSF production in control mice.

812 It is clear from lung pathology that more immune cells are trafficking to sites of infection in
813 propofol-sedated mouse lungs by 24 hours post-infection. That these swarms form distinct foci and do
814 not appear scattered throughout the lungs suggest that chemotaxis is largely intact in these immune
815 responders. However, the systemic increase in circulating cytokines and chemokines suggests
816 significant immune dysregulation. These systemic changes mirror multiple clinical aspects of acute
817 sepsis, including elevated pro- and anti-inflammatory gene expression and hyper-mobilization of
818 immune populations to sites of infection, and as such, further analysis of clinically relevant septic
819 biomarkers in this model is strongly needed.

820 These data support a hypothetical model in which brief propofol anesthesia may suppress early
821 immune functionality in macrophage and neutrophil populations in response to bacterial pneumonia.
822 As the severity of the infection progresses, the propofol-altered immune system fails to appropriately
823 ramp up its response, suddenly resulting in hyper-expression of the entire pro-inflammatory
824 compartment. This results in a massive mobilization of immature monocytes and neutrophil progenitors
825 from the hematopoietic compartment that are not as effective as their mature counterparts in
826 combating increasing bacterial burdens. These mobilized responders traffic to sites of infection but may
827 themselves display reduced functionality caused by residual propofol being slowly released from fatty

828 bodily tissues. Thus, infection control following propofol sedation is the result of increased numbers of
829 immune responders that mask individual functional deficiencies, while likely depleting the
830 hematopoietic compartment progenitor pools. If the increased numbers still fail to resolve infection,
831 dissemination increases with little host resistance. More work is necessary to characterize this model of
832 septic progression following acute lung infection, but the data herein suggest that propofol is increasing
833 the incidence of sepsis following a low infectious dose of *K. pneumoniae*.

Chapter 3: Further investigation of the impact of propofol on host immune responses in the context of *Klebsiella* infection

3.1. Summary

The discovery that the propofol phenotype could be obfuscated at higher initial infectious doses cast new light on the interpretation of previous infection data. As mentioned in Chapter Three, it was found that when mice were inoculated with a dose of 10^4 CFU instead of 10^3 CFU, the changes in gene expression profiles were no longer readily detectable, strongly suggesting that in the Swiss Webster mouse, danger signals quickly saturate receptors and the pro-inflammatory response is maximized, regardless of sedative exposure.

In an effort to characterize and compare the immune response to *K. pneumoniae* lung infection in the presence and absence of propofol sedation, multiple approaches were undertaken, including extensive titration of the initial bacterial inoculum size. Time course infections were performed at multiple doses while assessing whether propofol could overtly affect bacterial lung burdens and septic progression in the Swiss Webster mouse model. As later demonstrated in Chapter 4.3, $3x10^4$ CFU was found to result in increased lung, liver, and spleen burdens at 48 hours post-infection (Fig. 4.1). Analysis of aggregate data suggests that higher lung burdens precipitate increased bacterial burdens in distal tissues and organs versus increased dissemination purely resulting from propofol exposure. In an attempt to uncover manifestations of propofol's altered responses, several hypotheses were investigated. Several biomarkers of organ injury and sepsis were quantified, but interestingly did not reveal any differences in propofol-sedated mice. Propofol did significantly reduce the numbers of multiple splenic immune cell populations throughout infection, suggesting that these mice should have a reduced capacity to control disseminated bacteria. Propofol was also found to alter some, but not all, of

the liver's acute phase reactants, without significantly altering the liver's pro-inflammatory gene expression. These data suggest that immune alterations are truly systemic following propofol sedation.

3.2. Materials and Methods

Animal infections

Animals were anesthetized intravenously via tail vein injection with a combination of ketamine (25 mg/kg) and xylazine (4 mg/kg) or propofol (20 mg/kg; Zoetis, Kalamazoo, MI). Twenty microliters of bacterial suspension containing KPPR1 was administered via intranasal route into 6- to 8-week old Swiss Webster mice (Harlan, Madison, WI, USA). After 24, 48, or 72 hours, mice were sacrificed, blood was collected, and lungs, livers, and spleens isolated, homogenized, and plated on LB agar containing 30 µg/ml rifampicin for enumeration of bacterial burdens in each organ.

RNA Extraction and cDNA Synthesis

The left lung lobe of each mouse was removed following PBS + 50U/ml heparin perfusion, snap frozen in liquid nitrogen, and stored at -80°C until processing. One milliliter TRIzol (Invitrogen, Carlsbad, CA) was added to each lung before mechanical homogenization (TH, Omni International, Kennesaw, GA). RNA was isolated as per the manufacturer's protocol and dissolved in 100 µl Tris-EDTA buffer, pH 8.0 (Millipore-Sigma). RNA was treated with Turbo DNase kit (Ambion, Carlsbad, CA) and quantified on a NanoDrop OneC spectrophotometer (Thermo Scientific, Waltham, MA). cDNA was synthesized with the High Capacity cDNA Reverse Transcription kit (Applied Biosystems, Carlsbad, CA) and diluted in DEPC-treated water.

Quantitative RT-PCR

Primers for quantitative reverse transcription PCR were designed using PrimerBLAST (NCBI), synthesized by Millipore-Sigma, and are listed in Table 3.1. Samples were prepared using Fast SYBR

Green master mix (Applied Biosystems) with 200 nM final primer concentrations in 10 µl reaction volumes and run in 384-well plates on a ViiA 7 quantitative PCR machine (Applied Biosystems). Gene expression was assessed in triplicate for each sample. Average Ct values were linearized ($L=1/2^{Ct}$) and normalized to linearized *Gapdh*. Baseline calls were set equivalent for each gene across all runs.

Immunofluorescence

For immunofluorescent analysis, mice were sacrificed via isoflurane (Henry Schein, Dublin, OH). The lung vasculature was perfused with 10 ml ice cold PBS containing 50U/ml heparin to remove blood and lungs were infused with one milliliter of neutral buffered formalin solution (Sigma). Lungs, livers, and spleens were placed in 20 ml of neutral buffered formalin for 48 hours, then transferred into 70% ethanol. Unstained, paraffin-embedded sections of 5µm thickness were prepared by the UIC Research Histology and Tissue Imaging core facility. Paraffin was dissolved in xylenes and sections were rehydrated in graded ethanol washes, followed by washing in tris-buffered saline (TBS, pH 7.6). Antigen retrieval was carried out in 10mM sodium citrate buffer with 0.05% Tween-20 (pH 6.0) in a pressure cooker on high temperature for fifteen minutes. Slides were blocked with Background Buster (Innovex, Richmond, CA). Primary antibodies were *K. pneumoniae* rabbit polyclonal (ThermoFisher, Waltham, MA), rat SIGN-R1 (Bio-Rad), rat F4/80 (Tonbo Biosciences, San Diego, CA), rat Ly-6C (BioLegend, San Diego, CA), or rat Ly-6G (BD Biosciences, San Jose, CA). Secondary antibodies were goat anti-rabbit-FITC (Invitrogen, Carlsbad, CA) and goat anti-rat DyLight 594 (Abcam, San Francisco, CA). Slides were mounted with ProLong Gold antifade with DAPI (ThermoFisher), imaged using a Zeiss Axio Imager A2 upright microscope (Carl Zeiss, Thornwood, NY), and analyzed on Zen 2012 (Carl Zeiss) imaging software.

Protein Quantitation

Il-6Rα, Angiopoietin-2, and sICAM-1 were measured in serum using Quantikine ELISA (R&D Systems, Minneapolis, MN) per the manufacturer's directions and measured on a Synergy2 plate reader (BioTek, Winooski, VT).

Statistical Analyses

All statistical analyses were performed with Prism (GraphPad, La Jolla, CA). Organ burdens were analyzed using the Mann Whitney U test. Changes in gene expression were analyzed using a two-tailed, unpaired Student's T test with a correction for multiple comparisons using the Holm-Sidak method. Lung pathology area analyses used a two-tailed, unpaired Student's T test with Welch's correction.

Gene	Accession	Forward	Reverse
Apcs	NM_011318.2	5’-AGC CTT TTG TCA GAC AGA CCT-3’	5’-GAG AGC GGG AAA GGT CAC TG-3’
Lbp	NM_008489.2	5’-TGG AGC TCC TTG GAA CAG TG-3’	5’-TTA GTG ACC ACG CCA AGC C-3’
Hamp	NM_032541.2	5’-AGG GCA GAC ATT GCG ATA CC-3’	5’-GCA ACA GAT ACC ACA CTG GGA-3’
Saa1	NM_009117.3	5’-GAC ACC AGG ATG AAG CTA CTC A-3’	5’-CCC TTG GAA AGC CTC GTG AAC-3’
Saa2	NM_011314.2	5’-CTT TCC AAG GGG CTG GAG AC-3’	5’-TCC CCC GAG CAT GGA AGT AT-3’
Il6	NM_031168.2	5’-CAA AGC CAG AGT CCT TCA GAG-3’	5’-GTC CTT AGC CAC TCC TTC TG-3’
Il6ra	NM_010559	5’-CAA GAA TCC TCG TCC ATG TCC-3’	5’-TCG TCT TGC TTT CCT TCT CAG-3’
Il1b	NM_008361.4	5'-CTC ATC TGG GAT CCT CTC CA-3'	5'-TGT CAA AAG GTG GCA TTT CA-3'
Tnfa	NM_013693.3	5’-CTT CTG TCT ACT GAA CTT CGG G-3’	5’-CAG GCT TGT CAC TCG AAT TTT G-3’

Table 3.1. Quantitative RT-PCR primers used. Primers were designed with NCBI PrimerBLAST software and synthesized through Millipore-Sigma. Final concentrations were 200 nM.

Results

3.3. Propofol sedation does not appear to alter septic progression at higher initial infectious doses

Time course burdens were assessed following a variety of initial *K. pneumoniae* doses ranging from $5x10^3$ to $7.5x10^4$ CFU. To assess whether propofol was altering the dissemination kinetics of *K. pneumoniae* from the lungs, animal matched lung, liver, and spleen burdens at all times were aggregated and assessed as a single data set. Plotting lung burdens against liver or spleen burdens in the same animal revealed that lung burden is a strong predictor of secondary organ burden (Table 3.2) and this is not significantly altered by sedation with propofol (Fig. 3.1). This demonstrates that instead of potentiating increased dissemination at lower lung burdens, propofol must be decreasing the efficacy of the immune response in the lung, leading to higher burdens at earlier time points and this is responsible for the increased distal organ burdens compared to control-sedated mice (Fig. 2.1).

3.4. Propofol alters immune cell populations in the spleen during dissemination

Using immunofluorescent staining of unstained FFPE histological sections, we sought to assess immune cell markers in lungs, liver, and spleens of infected Swiss Webster mice at 24, 48, and 72 hours post-infection. Immunologists have identified profiles of protein expression that can collectively be used to identify and segregate individual cell types for further analysis. This approach is the basis for flow cytometric analyses of immune cell populations. However, this approach can also be applied to fixed tissues to assess the structure and spatial distribution of proteins using fluorescently-labeled antibodies. Due to technical limitations, both lung and liver tissues were recalcitrant to successful probing, however, splenic tissue was successfully analyzed.

The spleen is the largest secondary lymphoid organ in the body and can be divided into two distinct regions. The red pulp acts as a filter, removing senescent erythrocytes and foreign particulates

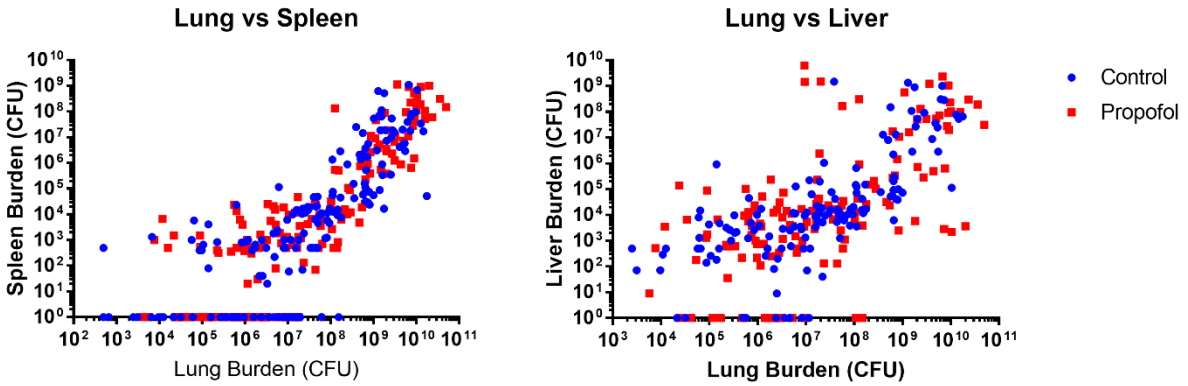

935

936

937

938 **Figure 3.1. Propofol does not alter septic progression at higher initial *K. pneumoniae* dosages.** Swiss

939 Webster mice sedated with either propofol or controls and infected at a range of infectious doses from

940 $5x10^3$ to $7.5x10^4$ CFU via intranasal route. Mice were sacrificed at 24, 48, and 72 hours post-infection

941 and burdens were enumerated. Plots are animal-matched lung and liver or lung and spleen burdens to

942 demonstrate dissemination from the lungs (primary) to secondary organs (liver or spleen) in each

943 individual animal, n≥128. Animals with no detectable burdens in secondary organs were assigned a

944 value of one.

945

Organs	Treatment	Spearman correlation	P value
Lung vs. Spleen	Control	r = 0.84	$<1x10^{-10}$
	Propofol	r = 0.83	$<1x10^{-10}$
Lung vs. Liver	Control	r = 0.78	$<1x10^{-10}$
	Propofol	r = 0.62	$<1x10^{-10}$

Table 3.2. Lung burdens are correlated with distal organ burdens during infection. Lung burdens in each animal were plotted against spleen or liver burdens as shown in figure 4.1. Correlation coefficients were calculated using the nonparametric Spearman test, demonstrating highly significant correlative relationships in dissemination. An r value of 0 means no relationship, while a value of 1 means a perfect relationship. N≥128.

and contains, among other cell types, roughly half of the body's monocyte pool. The white pulp contains a large pool of B and T cells and is thus highly important for adaptive immunity. Dividing the red and white pulp is the marginal zone, containing sentinel macrophages (marginal zone macrophages, MZM) and dendritic cells that prevent dissemination of bacteria into the white pulp while also facilitating antigen presentation and activation of the B and T cells within the white pulp. In the *L. monocytogenes* infection model, Visvabharathy et al (135) observed that propofol-sedated mice had fewer numbers of both MZMs and $CD3^+$ T cells in the spleen compared to control mice and that this led to significant dissemination of *L. monocytogenes* into the white pulp. While the spleen and liver are the primary organs for infection and replication for systemic *L. monocytogenes* infection, they are secondary organs in a lung infection model. Nonetheless, because the spleen is a reservoir for multiple relevant immune cell populations and because burden data consistently demonstrates significant dissemination from the lungs to the spleen during *K. pneumoniae* infection, immune cell populations in the spleen were investigated.

Staining for *K. pneumoniae* and for the MZM marker SIGN-R1 revealed that both propofol- and control-sedated mice demonstrated increased numbers of this cell type 24 hours post-infection compared to naïve mice. Despite this increase, propofol-sedated mice still had significantly fewer MZMs at 24, 48, and 72 hours post-infection compared to control-sedated mice. Figure 3.2 is a representative field demonstrating reduced SIGN-$R1^+$ cells (red) in propofol-sedated mice despite abundant staining for *K. pneumoniae* (green). It was also found that propofol in the absence of infection had no discernable effect on all populations assessed compared to naïve mice (Fig. 3.3). Another murine macrophage marker is F4/80, an adhesive G protein-coupled receptor (GPCR), which is strongly expressed on red pulp macrophages (156). While propofol-sedated, infected mice had similar counts to control infected mice at 24 hours post-infection, ketamine-sedated control numbers continued to increase as infection

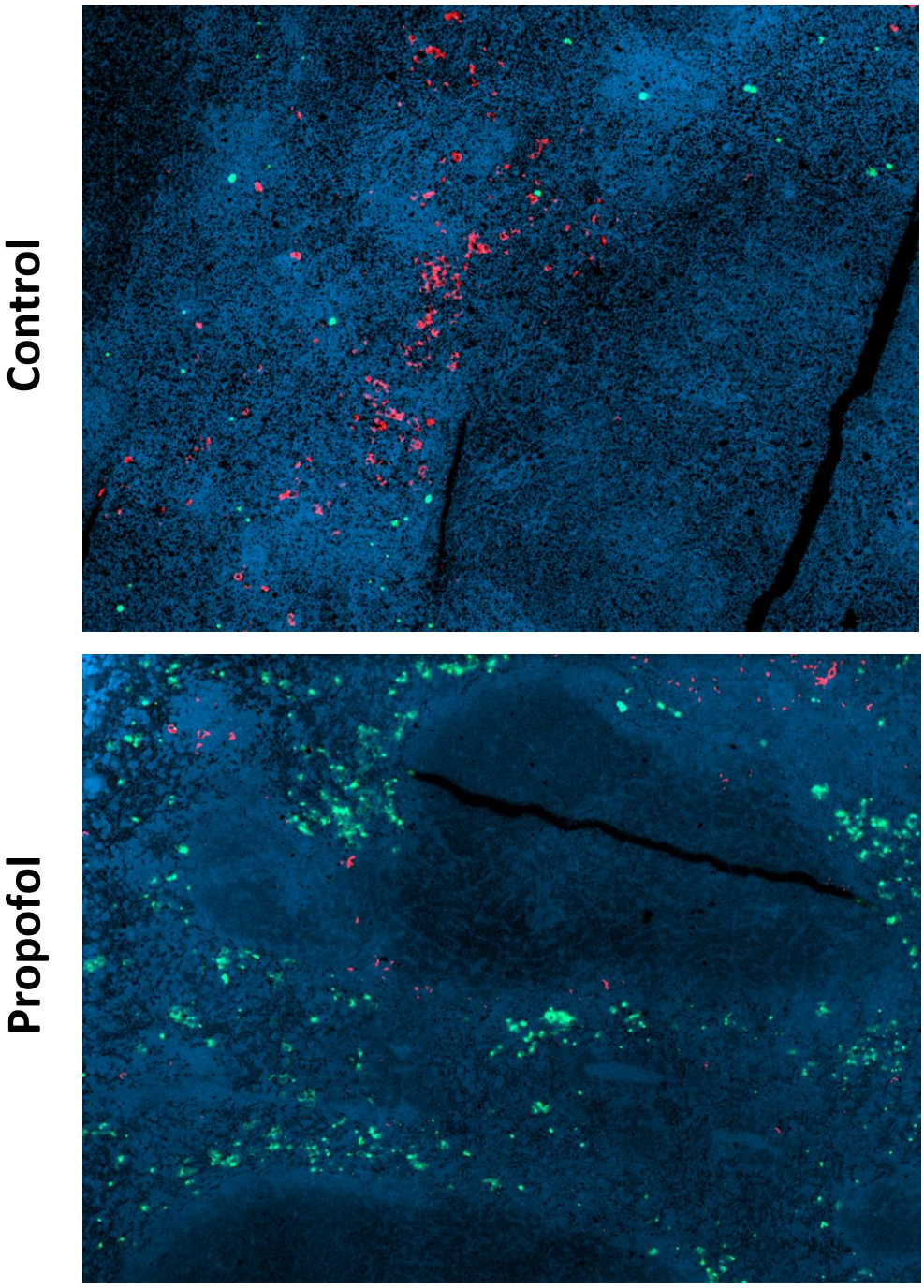

Figure 3.2. Propofol sedation decreases SIGN-R1^{+} marginal zone macrophages in the spleen.

Representative immunofluorescent images of infected spleens at 72 hours post-infection. SIGN-R1 staining is red, *K. pnuemoniae* is green, and nuclei stained with DAPI are blue. 100x magnification.

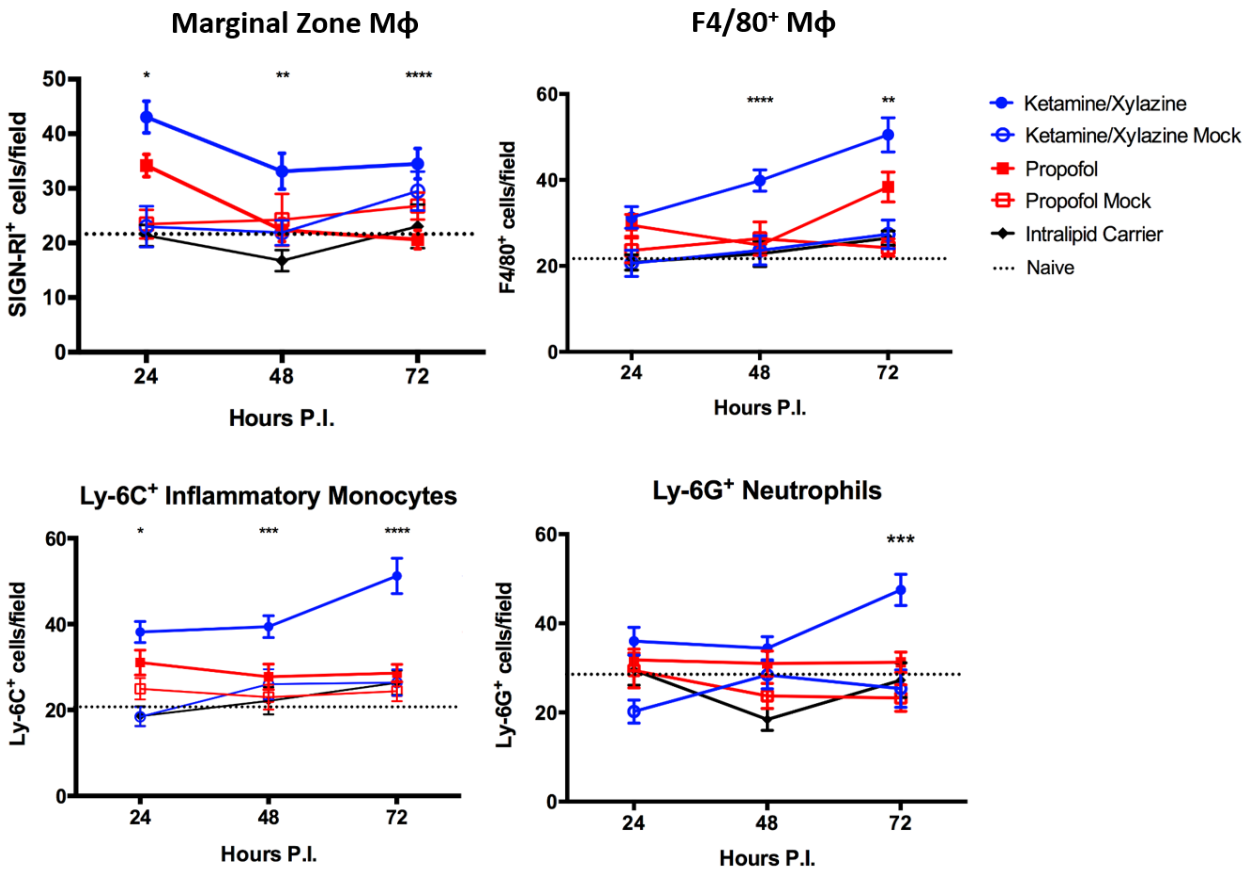

983

984

985

986 **Figure 3.3. Propofol decreases multiple immune cell populations in infected spleens.** Swiss Webster

987 mice infected with 10^4 CFU *K. pneumoniae* were sacrificed and spleens examined with

988 immunofluorescent staining for immune cell markers. Mϕ = macrophage. Data is average number of

989 positively-stained cells per field at 40x magnification, ≥20 fields per treatment, per time point.

990 Significance was calculated comparing ketamine/xylazine and propofol (infected) mice using a two-tailed

991 Student's t test with Welch's correction. * p <0.05; ** p<0.01; *** p<0.001; **** p<0.0001

992

progressed with propofol-sedated mice exhibiting a small decrease at 48 hours followed by a small increase in numbers at 72 hours post-infection (Fig 3.3).

Further investigation of cell populations focused on cells types shown to be critical for the resolution of *K. pneumoniae* in the lung, inflammatory monocytes and neutrophils (26,157). Both markers analyzed were found to follow similar kinetics in control mice, with increased numbers at 24 and 48 hours post-infection over naïve mice, then an additional increase at 72 hours. Despite propofol-sedated mice having higher spleen burdens at earlier time points, no increase in either population was observed out to 72 hours (Fig 3.3).

3.5. Propofol does not appear to increase endothelial permeability during severe lung infection.

To better understand propofol's apparent ability to enhance dissemination from the lungs, it was hypothesized that propofol could be increasing vascular permeability in the lung to allow *K. pneumoniae* out into circulation, thus a literature search for biomarkers of sepsis and organ injury was performed. Dozens of plasma proteins and microRNAs (miRNA) have been investigated with varying degrees of prognostic and diagnostic utility in septic patients (158–161). Two markers were investigated in the Swiss Webster mouse lung infection model: Angiopoietin (Ang)-2 and soluble intracellular adhesion molecule (sICAM)-1. Angiopoietins 1 and 2 are vascular growth factors important for angiogenesis. While Ang-1 is constitutively expressed and important for the maturation, adhesion, and survival of vascular endothelial cells, Ang-2 is inducible and associated with an inflammatory stimulus. Ang-2 is released by the endothelium itself and potentiates pro-inflammatory and pro-thrombotic signals, as well as vascular leakage (158). In Swiss Webster mice infected with 10^4 CFU into the lung, serum levels of Ang-2 was assessed at 24 and 48 hours post-infection. Neither propofol nor control animals demonstrated elevated levels of Ang-2 at either time point, suggesting that this protein is not a viable biomarker for vascular permeability in the Swiss Webster model (Fig. 3.4).

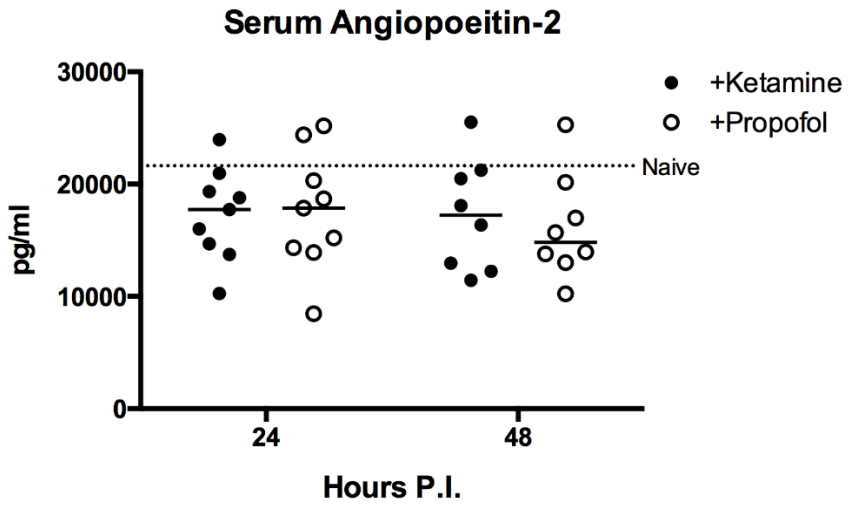

1016

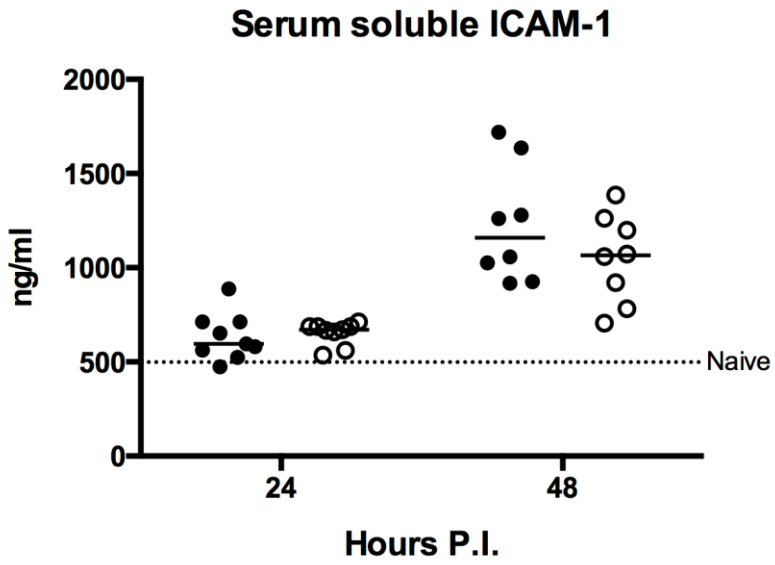

1017

1018 **Figure 3.4. Propofol does not alter markers of vascular permeability.** Swiss Webster mice infected with

1019 10^4 CFU K. pneumoniae were sacrificed 24 or 48 hours post-infection. Serum was analyzed by ELISA for

1020 the indicated targets.

1021

Next, soluble ICAM-1 was assessed in the serum of the same mouse cohort as Ang-2. ICAM-1 is a surface expressed glycoprotein found on endothelial cells that binds several integrins (which are expressed on many immune cells). Its expression is very low during quiescent periods and is highly upregulated during inflammation to facilitate capture of said immune cells for rolling cell adhesion and extravasation from the vasculature and into inflamed tissue (162). ICAM-1 is shed frequently into the circulation during inflammation and has been found to correlate with disease severity and as a diagnostic marker for sepsis (158,163–165). Again, when Swiss Webster mice were infected with 10^4 CFU, propofol-sedated mice demonstrated increases commensurate with control infected animals (Fig. 3.4). While this data suggests significant increases in vascular endothelium permeability, the results for Ang-2 and sICAM-1 levels in the serum of infected mice suggests that propofol does not enhance permeability as a mechanism for increased dissemination in this model.

3.6. Propofol does not increase soluble IL-6 receptor levels in serum.

Interleukin 6 is a pleiotropic cytokine with context dependent anti- or pro-inflammatory properties (166). It is produced by most immune cells in the body and while expression may be primarily driven by IL-1β and TNFα during inflammation, a multitude of other inducing pathways have been identified. Expression of its cognate receptor (IL-6Rα) is restricted to megakaryocytes, leukocytes, and hepatocytes, however the adaptor gp130 is required for signal transduction, which is expressed widely. Soluble IL-6R may be produced either by proteolytic cleavage or alternative messenger (m)RNA splicing and can bind free IL-6. This complex may then bind any surface expressed gp130 and trigger *trans*-IL-6R signaling. This *trans*-signaling is thought to primarily drive the pro-inflammatory aspects of IL-6, while classical IL-6 receptor signaling (with IL-6Rα and gp130 both membrane-bound) is thought to drive anti-inflammatory IL-6 activity (166). Soluble IL-6R primarily is shed by monocytes, neutrophils, and activated $CD4^+$ T cells (167–171).

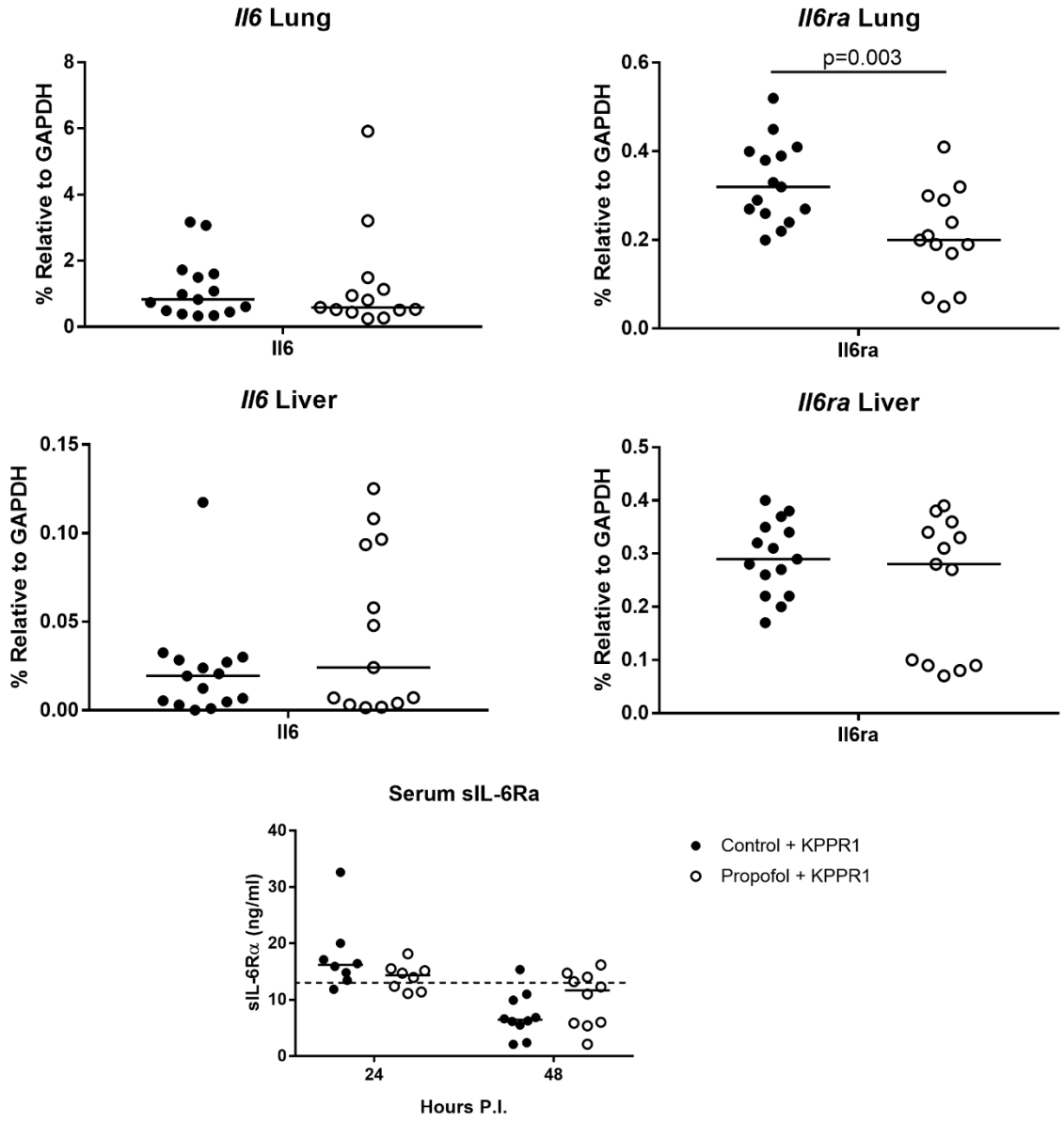

Figure 3.5. Propofol does not affect serum soluble IL-6 receptor. Swiss Webster mice were infected with 10^4 CFU *K. pneumoniae* and sacrificed at 24 or 48 hours post-infection. *Il6* and *Il6ra* transcripts were analyzed by qRT-PCR at 48 hours post-infection. Serum was analyzed for soluble IL-6Rα by ELISA. Dotted line represents average naïve mouse serum protein level. Solid lines represent median values. Gene expression was analyzed for statistical significance with a two-tailed Student's T test with Welch's correction.

As it was postulated that propofol was suppressing a pro-inflammatory response, it was hypothesized that one mechanism for this suppression could be reducing the shedding of IL-6R from immune cells, thus suppressing the pro-inflammatory properties of IL-6 signaling *in vivo*. To assess this, quantitative reverse transcription polymerase chain reaction (qRT-PCR) was used to assess gene expression of IL-6 and IL-6Rα in the lungs of mice infected with 10^4 CFU *K. pneumoniae* (Fig 3.5). At 48 hours post-infection, no significant differences were noted in the expression *Il6* transcripts, however, there was a small but significant decrease in *Il6ra* expression in propofol-sedated, infected lungs ($n \geq 13$, Fig. 3.5). As hepatocytes were identified as a major non-immune cell type expressing IL-6Rα, expression was also gauged in infected livers, but no changes in expression were noted for either *Il6ra* or *Il6* mRNA. Finally, serum IL-6Rα protein levels were assayed by ELISA and no significant differences were found at 48 hours post-infection. Thus modulation of IL-6 signaling through manipulation of sIL-6R shedding does not appear to play a role in the immunomodulation by propofol.

3.7. Propofol may impact part of the acute phase response

The acute phase response is a systemic response to inflammation and/or infection that involves widespread changes in the body. Part of this is a subset of proteins, primarily of hepatic origin, that are increased or decreased in response to a number of signals, including pro-inflammatory cytokines IL-1β, IL-6, and TNFα (172). These proteins include protease inhibitors, such as the Serpin family, hepcidin, an antimicrobial peptide that is a master regulator of iron homeostasis, opsonins, such as C reactive protein, and the complement system (172). Downstream of these mediators, anti-inflammatory aspects are to be found, such as increasing glucocorticoid synthesis. Having found that propofol-sedated mice infected with 10^4 CFU did appear to have lower expression of several pro-inflammatory genes in the lungs, it was hypothesized that this lower expression at the primary site of infection could be altering the ongoing acute phase response during infection, potentially creating a less bactericidal environment in the host.

Gene expression in the infected livers at 48 hours post-infection following 10^4 CFU *K. pneumoniae* inoculum was assessed for several of the principal cute phase reactants. While C reactive protein (CRP) is one of the most commonly used acute phase biomarkers clinically (173,174), its murine homolog is not induced during infection. That role is fulfilled by another opsonin, serum amyloid P component (*Apcs*)(175), which demonstrated no change in expression. A second gene is *Lbp*, lipopolysaccharide binding protein, which as the name implies, binds LPS shed by Gram negative bacteria during infection and presents it to TLR4 to initiate downstream signaling (172). This protein has been utilized clinically to distinguish infectious and non-infectious cases of sepsis (176), however, no change in hepatic expression was observed (Fig. 3.6).

Serum amyloid A is a protein that is dramatically upregulated during infection, upwards of 1,000-fold at the protein level, and serves several roles including inducing cytokine and chemokine expression while itself being a chemoattractant protein for a variety of immune cells (177). There are four genes present in the mouse genome (*Saa1-4*), with *Saa3* and *Saa4* being constitutively expressed, while *Saa1* and *Saa2* are inducible. Gene expression of *Saa1* and *Saa2* was found to be dramatically upregulated in both groups, but significantly higher in propofol-sedated mice at 48 hours post-infection (Fig. 3.6).

Lastly, the small protein hepcidin was originally identified as an antimicrobial peptide, but eventually was found to be a master regulator of host iron homeostasis (160,178). Ferroportin is the only known mammalian iron exporter and hepcidin targets this transporter for degradation. During homeostasis, senescent erythrocytes are phagocytosed by macrophages in the spleen, resulting in an excess of iron. This can be recycled to hepatocytes through the action of ferroportin moving the excess iron out into circulation. As iron acquisition has been identified as a key virulence determinant in *K. pneumoniae* and other Gram negative bacteria (Chapter 1.4), it is critical for the host to limit the availability of iron to the pathogen, thus hepcidin is upregulated. The net result is increased ferroportin

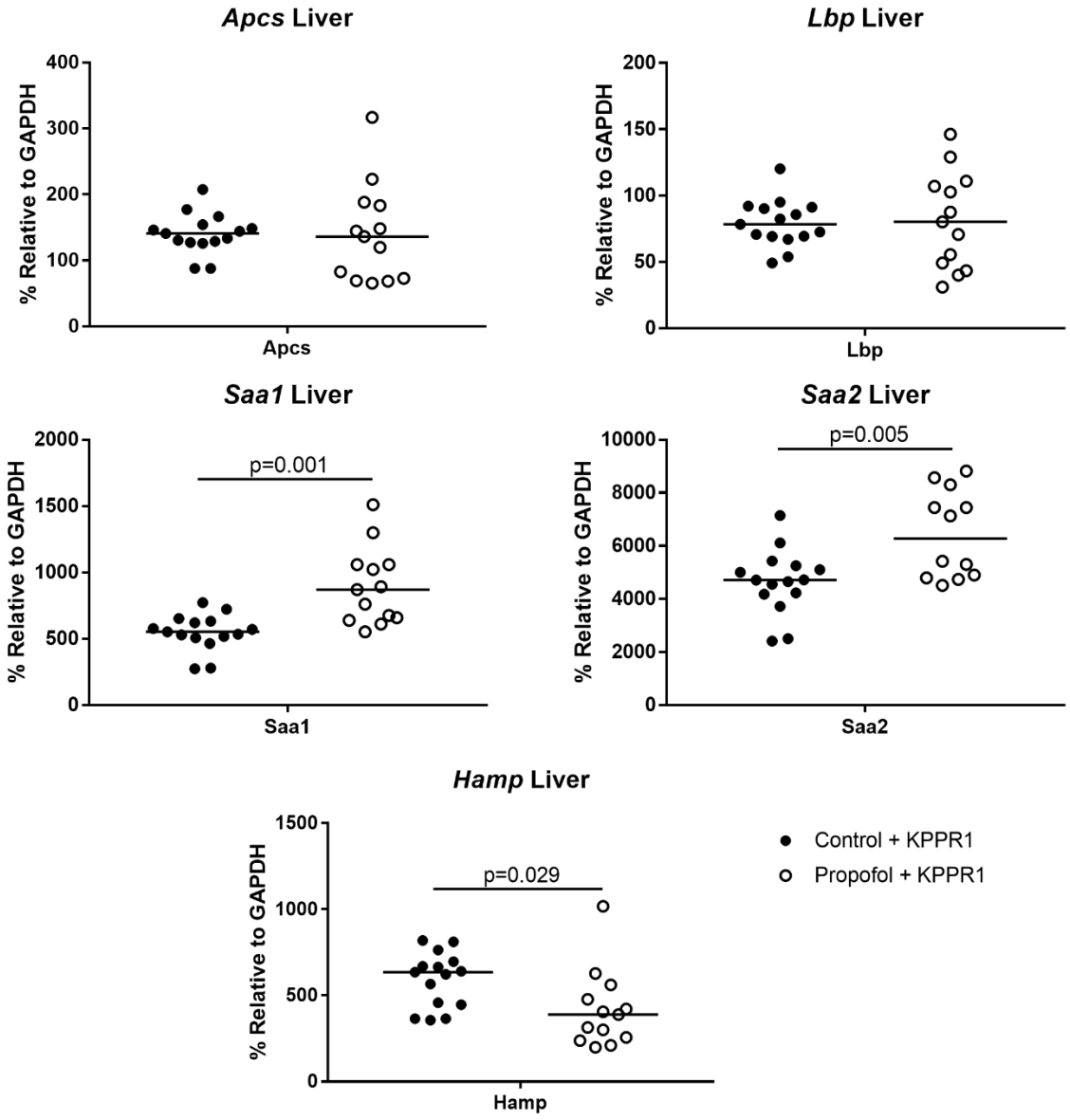

1100

1101 **Figure 3.6. Propofol may alter the acute phase response to *K. pneumoniae*.** Gene expression of acute

1102 phase reactants was assessed in the livers of Swiss Webster mice infected with 10^4 CFU *K. pneumonia* at

1103 48 hours post-infection. Data were linearized and normalized to GAPDH. Statistical significance was

1104 determined with a two-tailed Student's T test with Welch's correction. Insignificant p values are not

1105 shown.

1106

degradation and ~90% decrease in serum iron levels, resulting in a transient anemic state. Hepatic expression of the gene encoding hepcidin, *Hamp*, was assayed and at 48 hours post-infection, propofol-sedated mice demonstrated little to no increase in *Hamp* expression, potentially indicating a reduced ability of the host to limit access to iron (Fig. 3.6). It has been suggested experimentally that hepatic expression of several pro-inflammatory cytokines may affect the expression of acute phase reactants (172,179), thus the gene expression of *Il1a*, *Il1b*, and *Tnfa* were assessed in the liver at 48 hours. No differences were noted (Fig. 3.7), suggesting that the lung is the primary source of these pro-inflammatory signals. With propofol-sedated mice demonstrating altered expression of both serum amyloid A and hepcidin in the liver, further investigation may be warranted to characterize other acute phase reactants following propofol sedation.

3.8. Discussion

To date, peer-review research investigating propofol has primarily utilized simplified *in vitro* approaches to careful identify and define potential molecular targets and their associated pathways and as a result, multiple putative mechanisms have been suggested to explain, at least in part, how propofol may be altering immune responses *in vivo*. However, as Inada et al (145) identified in a macrophage:NK cell co-culture model, macrophages synthesized leukotriene B_4 in response to LPS stimulation, which in turn suppressed IFNγ production by natural killer cells, highlighting an excellent example of cross talk between immune cell populations. The experiments described in this chapter were attempts to establish a line of investigation into the complex *in vivo* regulatory networks of the immune response during a clinically relevant pneumonia model. It is clear from these experiments and those described in Chapter Three that in this model of infection, the initial infectious dose has a significant impact on the readouts of dozens of relevant genes and proteins. As mentioned, all experiments in this chapter were performed with an initial dose of 10^4 CFU *K. pneumoniae* and results were largely similar between propofol and control animals, while gene and protein expression were dramatically altered with an

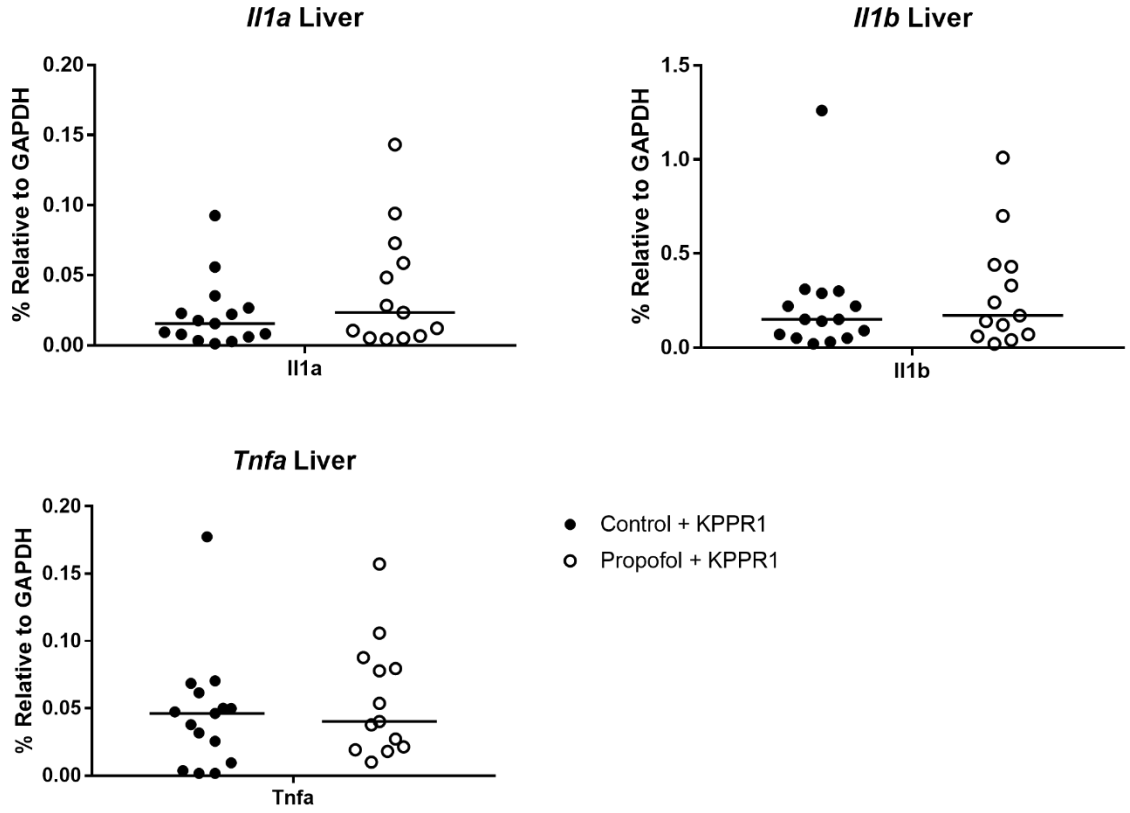

1131

1132 **Figure 3.7. Propofol does not alter hepatic pro-inflammatory gene expression.** Swiss Webster mice

1133 were infected with 10^4 CFU K. pneumoniae and sacrificed at 48 hours post-infection. Gene expression

1134 was assessed for several pro-inflammatory cytokines. Data were linearized and normalized to GAPDH.

1135 Statistical significance was determined with a two-tailed Student's T test with Welch's correction.

1136 Insignificant p values are not shown.

1137

initial dose of 10^3 CFU. These low dose experiments investigated outcomes in mice out to 48 hours, whereby the heightened gene expression in propofol-sedated mice appeared to decrease to levels comparable to control-sedated, infected mice. Thus, it stands to reason that significant phenotypes were not detected in the majority of these experiments due to either the initial dose, the time(s) investigated, or a combination thereof. Therefore, in light of recent findings at the lower dose, revisiting hypotheses such as vascular permeability and alterations in the acute phase response are warranted.

For much of these early investigations into the progression of *K. pneumoniae* lung infection and septicemia, organ burdens were the primary readout. This extensive collection of data demonstrated that propofol did not have an impact on dissemination in Swiss Webster mice at a wide range of relatively high infectious doses, but recent results strongly suggested that with low infectious doses ($\leq 10^3$ CFU), there is a subpopulation of animals that fail to control local infection and experience more severe systemic dissemination following propofol sedation (Fig. 3.8). By 48 hours post-infection, there is a distinct bimodal distribution in propofol-sedated spleen burdens which suggests that 10^3 CFU represents a tipping point following propofol sedation (Fig. 3.8). Nonetheless, at higher infectious doses, liver and spleen burdens had clear correlations to lung burdens regardless of anesthetic choice, suggesting that the Swiss Webster mouse is already incapable of handling these initial doses and as a result, the immune system is responding maximally. This is important in light of propofol's enhancement of pro-inflammatory gene expression at low infectious doses, strongly suggesting that propofol's effects are not principally anti-inflammatory in the context of infection.

While propofol's effects on *L. monocytogenes* bloodstream infection were readily detectable by determining organ burdens (135), they were less so in regards to *S. aureus* infection (136). Organ pathology, however, was significantly more severe in either case. As the spleen is the largest secondary lymphoid organ in the body, it was worthwhile to investigate what immune cells were responding as *K. pneumoniae* disseminated from the lungs to the spleen. It was observed that mobile pools of immune

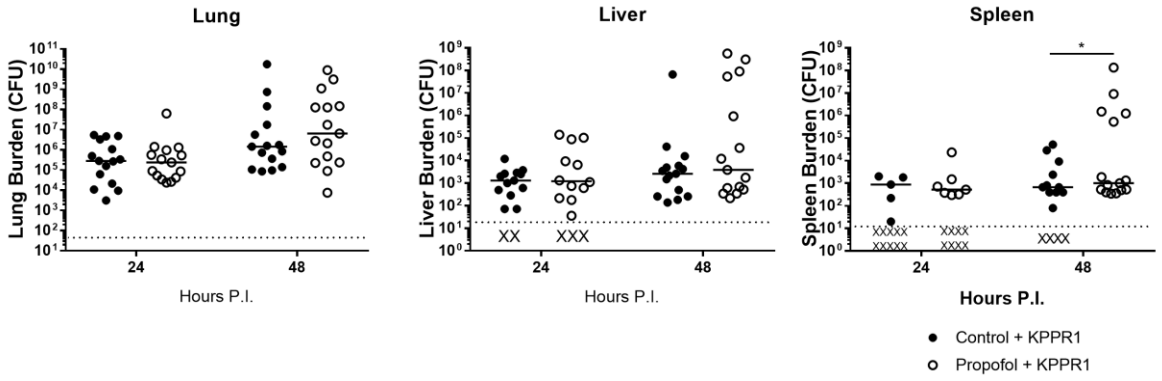

Figure 3.8. A subpopulation of mice experience severe bacteremia following propofol sedation. Swiss Webster mice were infected intra-nasally with 10^3 CFU. Organ burdens were assessed at 24 and 48 hours post-infection. X represents no detectable burdens and the dotted line represents the limit of detection. Significance was determined by a two-tailed Mann Whitney U test. *, $p < 0.05$

responders such as Ly-6G$^+$ neutrophils and Ly-6C$^+$ inflammatory monocytes did not increase in this secondary organ despite increased burdens. In retrospect, this is perhaps unexpected as this data was obtained from mice infected with 10^4 CFU *K. pneumoniae*, a dose which did not have significant effects at the transcriptional level in the lung. Nonetheless, it supports a hypothesis wherein immune mobilization is increased to the primary site(s) of infection in the lung, effectively depleting mature responders available for to respond to later dissemination to secondary sites of infection.

Splenic marginal zone macrophages are a tissue-resident cell type which have a prenatal origin and are not replenished by peripheral monocyte pools under homeostatic conditions (180). Expansion of this cell type requires external cues such as M-CSF to promote self-proliferation and survival before and after inflammation (181). At the lower infectious dose, a transient increase in lung M-CSF expression was observed at 24 and 32 hours post-infection in propofol-sedated mice (Fig. 2.4), which could explain in part the initial expansion of MZMs observed at 24 hours, however, this was not observed in control mice. It must be considered that in control mice, the proliferative signal is either not M-CSF or is M-CSF expressed from a cell population outside the lung that would be readily assessed through assessing serum levels of these colony stimulating factors.

In retrospect, it is not surprising that no changes in vascular permeability were detected in propofol-sedated mice due to the dissemination relationship observed in Figure 3.1. Just as higher bacterial inocula masked changes in gene expression, so too could it be masking any alterations propofol may have on vascular permeability. It is still plausible that propofol could indirectly alter vascular permeability through the increased recruitment of immune responders. Similarly, that no significant differences were found with the serum levels of IL-6Rα after a 10^4 CFU dose does not preclude there being important alterations that would be detectable at a 10^3 CFU dose. Indeed, in light of the hyper-expression of *Il6* found in the lungs and IL-6 protein in the serum, determining expression of *Il6ra* could potentially indicate a significant pro- or anti-inflammatory mechanism in the context of propofol.

The acute phase is a complex entity with manifold actors, some of which have not been well characterized. Nevertheless, the proteins that have been characterized play important roles in fighting inflammatory conditions, including bacterial infections. Mobilization of opsonins, complement factors, chemotactic proteins, and more represent critical defenses against extracellular pathogens such as *K. pneumoniae*. It is interesting that significant differences were detected in propofol-sedated mice at a 10^4 CFU dose, considering some of the major inducers of these proteins are the pro-inflammatory cytokines IL-1β, IL-6, and TNFα, none of which were significantly different following propofol sedation. Nevertheless, inducible serum amyloid A genes were more upregulated while simultaneously hepcidin mRNA was down, clearly demonstrating that the aforementioned cytokines are only partly responsible for regulating expression of these genes during infection. A deeper investigation into the regulation of these three genes during infection could yield important clues into their differential expression in this model.

Propofol-dependent alterations in the immune responses appear to be widespread and now it would appear that the appropriate tools with appropriate parameters are in place to further investigate the far-reaching consequences of propofol sedation preceding a lung infection by *K. pneumoniae*. While these observations may be translatable to the clinic, they still only amount to broad suggestions when we consider the underlying mechanism or mechanisms of propofol during infection.

Chapter 4: Propofol sedation alters *Klebsiella pneumoniae* virulence determinant repertoire during lung infection

(This chapter presents data from a collaboration with Dr. Mark Mandel, Dr. Ella Rotman, and Acadia Kocher of Northwestern University, who are responsible for all strains created, in vitro characterization, and bioinformatics. All in vivo work and manuscript preparation was performed by David Mains.)

4.1. Summary

Klebsiella pneumoniae make up 85% of Carbapenem-resistant Enterobacteriaceae (CRE), bacteria that are developing as an urgent threat to public health. As an emerging infectious disease, little is known about the molecular mechanisms by which *K. pneumoniae* colonize and cause damage to their hosts. *K. pneumoniae* is largely transmitted in a healthcare setting, where inpatients and outpatients are often anesthetized with the ubiquitously used anesthetic induction agent propofol. Recent evidence indicates that propofol exposure can dramatically increase host susceptibility to microbial infections. Given that intubated patients are often given propofol and are at risk for *K. pneumoniae* lung infections, we investigated the outcome of *K. pneumoniae* infections in mice sedated with either propofol or ketamine/xylazine as control. Propofol-sedated mice appeared to experience quicker dissemination from the lungs to secondary sites of infection and to develop more severe lung pathology. Based on these observations, we sought to determine whether the arsenal of bacterial factors involved in infection and dissemination in mice differs with and without propofol sedation using a high throughput insertion sequencing (INSeq) approach. We identified numerous potentially novel as well as previously identified factors, the latter of which served to confirm the validity of our screen. Deletions of select genes were characterized *in vitro* and for virulence *in vivo* with and without propofol sedation. Of the eight genes investigated, *VK055_1993* and *glnB* mutants were found to have competitive defects only after control sedation, while *VK055_1398* and *virK* only demonstrated defects following propofol sedation. Furthermore, six of the eight mutants demonstrated clear virulence

defects depending on the sedative used. This study, in addition to identifying novel virulence factors for *K. pneumoniae*, also indicates that anesthetic choice impacts the global virulence repertoire required for infection *in vivo*.

4.2. Introduction

In the nearly thirty years since its introduction, the general anesthetic propofol has grown to become the predominant anesthetic in clinical use throughout the world, lauded for its rapid on- and off-set, relatively mild side effects, and flexibility in both the induction and maintenance of anesthesia (70,182). While there have been multiple reports on propofol's immunomodulatory effects *in vitro* (118,123–125,183,144,145,184,146,121,128,155,147,148), *in vivo* evidence has only recently begun to be reported. Visvabharathy et al. (135,136) reported that acute propofol sedation dramatically increased susceptibility to both *Listeria monocytogenes* and *Staphylococcus aureus* bloodstream infections in a mouse model and additionally led to more severe pathology at primary sites of infection. This susceptibility correlated with a reduced capacity to effectively recruit mature immune effector cells to sites of infection following propofol sedation.

Healthcare-associated infections (HAIs) are a significant risk for all patients undergoing invasive procedures and thus we sought to investigate whether this increased susceptibility to bloodstream infections is representative of a systemic defect. Patients requiring mechanical ventilation are frequently administered sedatives (185) and are at increased risk for a variety of complications including pneumonia, collectively referred to as ventilator-associated events (VAEs)(186). Recently, Klompas et al. (71) correlated propofol sedation in mechanically-ventilated patients with a significantly increased risk of VAEs, including pneumonia, compared to patients not receiving propofol. To address this growing concern, we developed a mouse model of lung infection using the Gram-negative opportunistic

pathogen *Klebsiella pneumoniae*. *K. pneumoniae* is a growing threat worldwide as a nosocomial pathogen that is rapidly acquiring antimicrobial resistance (9).

Genome-wide approaches for the discovery of virulence factors required for *in vivo* growth have been applied in *K. pneumoniae* previously with considerable success (187,188,42,189–191). In addition to examining the impact of propofol on *K. pneumoniae* lung infection, we also sought to investigate what impact propofol might have on the *K. pneumoniae* global virulence repertoire required for successful growth in the lung. Transposon insertion sequencing (INSeq) is a powerful, high resolution approach to analyze whole genomes through coupling Mariner transposon mutagenesis with high-throughput sequencing to rapidly and comprehensively quantify the relative fitness of large pools of transposon mutants (192,193). We applied this approach by mutagenizing *K. pneumoniae* strain KPPR1 (ATCC 43816), sedating mice with either ketamine/xylazine or propofol, and infecting mice via an intranasal route. Ketamine and xylazine sedation was previously found to have no discernable effects on immunity *in vivo* (135). Analysis of recovered bacterial populations revealed numerous putatively required virulence factors in addition to factors previously identified (22) and furthermore identified differentially required genes based on the host's previous anesthetic exposure.

4.3. Materials and Methods

Bacterial media and strains.

K. pneumoniae and *E. coli* strains used in this study are listed in Table 4.1. Strains were grown at 37 °C in lysogeny broth (LB; per liter, 10 g Bacto-tryptone [BD], 5 g yeast extract [BD], 10 g NaCl [Sigma-Aldrich]). When cells were grown in the presence of hygromycin, low-salt LB was used (i.e., 5 g NaCl per liter). When necessary, antibiotics (Gold Biotechnology) were added to the media at the following concentrations: hygromycin 100 μg ml^{-1}, kanamycin 50 μg ml^{-1}, and carbenicillin 100 μg ml^{-1}. When necessary, the following compounds were added to the media to the indicated final concentrations:

sodium salicylate (Sigma-Aldrich): 2 mM; diaminopimelate (DAP; Sigma-Aldrich): 0.3 mM; arabinose (Gold Biotechnology): 100 mM. Growth media were solidified with 1.5% agar as needed. Standard molecular biology techniques were used to introduce plasmids into *E. coli* (i.e. electroporation) and into *K. pneumoniae* (i.e., electroporation or conjugation).

Animal infections

All animal procedures were approved by the University of Illinois at Chicago Animal Care Committee and were conducted in the Biological Resources Laboratory. *Klebsiella* strains were cultured overnight, shaking (37°C, 180 rpm) in LB broth. The following morning, strains were sub-cultured 1:50 in fresh LB and incubated with shaking for one hour to an OD_{600nm} of 0.2-0.4. Optical density was adjusted to 0.2 with LB broth and diluted to the desired density in sterile 1X phosphate-buffered saline (PBS) for infection. Strains were kept on ice until immediately before infection. Animals were sedated via tail vein injection with ketamine (25 mg/kg) and xylazine (4 mg/kg) as control or propofol (20 mg/kg; Zoetis, Kalamazoo, MI). For non-competitive infections, approximately $1x10^4$ colony forming units of each strain was administered via intranasal route into 6- to 8-week old Swiss Webster mice (Envigo, Madison, WI, USA) and for competitive infections, approximately $5x10^3$ CFU of WT and a mutant were premixed and administered via intra-nasal route for a total $1x10^4$ CFU dose. For non-competitive infections, mice were sacrificed after 24 or 48 hours and lungs, livers, and spleens were isolated, homogenized, and plated in triplicate on LB agar containing 30 μg ml^{-1} rifampicin for enumeration of bacterial burdens in each organ. For competitive infections, mice were sacrificed after 24 hours and lungs were homogenized and plated in triplicate on LB agar containing 30 μg ml^{-1} rifampicin and on LB agar containing 30 μg ml^{-1} rifampicin and 50 μg ml^{-1} kanamycin.

Histology

For histological analysis, mice were sacrificed via isoflurane (Henry Schein, Dublin, OH). The lung vasculature was perfused with 10 ml ice cold PBS containing 50U/ml heparin to remove blood and lungs were infused with one milliliter of neutral buffered formalin solution (Millipore Sigma). Lungs were placed in 20 ml of neutral buffered formalin for 48 hours, then transferred into 70% ethanol. Paraffin-embedded sections were prepared by the UIC Research Histology and Tissue Imaging core facility. Five micron-thick sections were stained with hematoxylin and eosin (H&E) and mounted. Digital scans of H&E stained lung sections were captured on a ScanScope CS and analyzed using ImageScope software (Aperio/Leica).

Immunofluorescence

For immunofluorescent analysis, mice were sacrificed via isoflurane (Henry Schein, Dublin, OH). The lung vasculature was perfused with 10 ml ice cold PBS containing 50U/ml heparin to remove blood and lungs were infused with one milliliter of neutral buffered formalin solution (Sigma). Lungs were placed in 20 ml of neutral buffered formalin for 48 hours, then transferred into 70% ethanol. Unstained, paraffin-embedded sections of 5µm thickness were prepared by the UIC Research Histology and Tissue Imaging core facility. Paraffin was dissolved in xylenes and sections were rehydrated in graded ethanol washes, followed by washing in tris-buffered saline (TBS, pH 7.6). Antigen retrieval was carried out in 10mM sodium citrate buffer with 0.05% Tween-20 (pH 6.0) in a pressure cooker on high temperature for fifteen minutes. Slides were blocked with Background Buster (Innovex, Richmond, CA). Primary antibody was *K. pneumoniae* rabbit polyclonal (ThermoFisher, Waltham, MA) and secondary antibody was goat anti-rabbit-FITC (Invitrogen, Carlsbad, CA). Slides were mounted with ProLong Gold antifade with DAPI (ThermoFisher), imaged using a Zeiss Axio Imager A2 upright microscope (Carl Zeiss, Thornwood, NY), and analyzed on Zen 2012 (Carl Zeiss) imaging software.

Generation of KPPR1 transposon mutant library

KPPR1 and MJM2382 saturated cultures were diluted 1:80 in 3 ml LB and LB carb DAP, respectively, and grown for 2 hours and 40 minutes at 37˚C. 2.5 ml of *E. coli* and 5 ml of *K. pneumoniae* were pelleted and combined together in 500 µl LB, which was spotted in fifty 10-µl spots on LB. After 3.5 hours at 37˚C, each spot was swabbed into 500 µl LB, vortexed, and 50 µl was spread onto LB kan sal for overnight incubation at 37˚C. An estimated 50,000 colonies were swabbed into 25 ml LB mixed with 12.5 ml 50% glycerol on ice and frozen at -80˚C with a final density of 3 x 10^{11} cfu/ml.

Preparation of samples for INSeq

Genomic DNA was extracted using a Maxwell 16 robot (Promega, Madison, WI). Transposon insertion junctions were amplified from three input samples and six output samples according to the previously published protocol (194). Samples were single-end sequenced with an Illumina HiSeq 2500 (Illumina, San Diego, CA) platform at the Tufts University Genomics Core Facility in Boston with 45 million reads generated.

Analysis of INSeq samples

The Illumina files were run through pyinseq pipeline (https://github.com/mandel01/pyinseq; v.0.1) using the KPPR1 complete genome sequence (195). The program demultiplexed the samples and organized the reads into the following categories: contig, nucleotide, Lcounts, Rcounts, totalCounts, cpm, threePrimeness, and locus_tag. The KPPR1 contig was CP009208 for all genes (there are no plasmids in this strain); the nucleotide position was the location of the transposon insertion; Lcount, Rcount and totalCount enumerated the sequences on either side of the transposon (with a roughly 50/50 percentage expected – hits with a skewer greater than 1:10 were omitted); cpm (counts per million) was the total reads generated per individual transposon hit divided by 10^6; threePrimeness was only if the hit was present in an annotated gene and indicated where insertion fell between the start and stop codon; locus tag identified the name or position of the gene (represented by VK055_xxxx in

KPPR1). The cpm counts of the three different biological replicates was first analyzed by the average value and then by the median. The list of genes was sorted by the log10(output/input).

Construction of deletion-replacements in KPPR1

Gene deletions in KPPR1 were constructed by a modified Lambda-Red method of deletion-replacement using the protocol of Huang et al (196). In brief, 90-mer primers (table 4.2) were designed to amplify the kanamycin resistance cassette from pKD4 (197) with 65-70 bp of homology flanking the gene to be deleted. The deletion was designed to include the start codon and last six amino acids of the protein product as suggested by Baba et al (198). The resulting PCR product was electroporated into arabinose-induced KPPR1 carrying the Lambda-Red functions on pACBSR-Hyg. Colonies that grew on LB kan were screened by PCR for the insertion-deletion and serially streaked on LB until they lost Hygromycin resistance.

Doubling time analysis.

Cultures were grown overnight in LB kan media at 37˚C with aeration. Saturated cultures were diluted 25 µl into 2 ml LB and grown for 1 hour at 37˚C. 11 µl were subcultured into 2 ml LB and grown for 3 hours at 37˚C, with 20 µl aliquots removed every 30 minutes into 180 µl 1% NaCl. Each time point was serially diluted in 1% NaCl and 10 µl spots of each dilution was placed in duplicate on LB agar at 25˚C. The CFU/ml of the cultures was determined from counting microcolonies. The log2 of the cell number was plotted, with the inverse of the slope equal to the doubling time of the culture. The normalization for the graphs were obtained by subtracting the value of the first time point from all the time points.

***In vitro* competition assay**

Cultures were grown overnight in LB kan media at 37˚C with aeration. Saturated cultures were diluted 25 µl into 2 ml LB and grown for 1 hour at 37˚C. 5.5 µl of KPPR1 and 5.5 µl of the mutant culture was

diluted into 2 ml LB and grown for 3 hours at 37˚C. At t = 0 hours and t = 3 hours, 20 µl aliquots were diluted in 1% NaCl. The t = 0 time point was diluted to 10^{-2} and the t = 3 time point was diluted to 10^{-5}, with 40 µl spread on LB and LB kan plates in duplicate. The ratio of kan^S:kan^R colonies, reflecting WT vs mutant, was determined from the colonies that grew.

Table 4.1. Bacterial strain and plasmid list.

Strain	**Relevant Genotype**	**Reference**
K. pneumoniae		
MJM2383	KPPR1	(195)
MJM2402	Transposon mutant library in KPPR1	This Study
MJM2462	KPPR1 VK055_5015::kan	This Study
MJM2793	KPPR1 ΔVK055_3462::kan	This Study
MJM2794	KPPR1 ΔVK055_1993::kan	This Study
MJM2795	KPPR1 ΔVK055_0094::kan	This Study
MJM2796	KPPR1 ΔVK055_1930::kan	This Study
MJM2797	KPPR1 ΔVK055_3875::kan	This Study
MJM2784	KPPR1 ΔVK055_4623::kan	This Study
MJM2816	KPPR1 ΔVK055_3638::kan	This Study
MJM3001	KPPR1 ΔVK055_1398::kan	This Study
***E. coli* strains**		
Strain	Genotype	Reference
MJM537	DH5α λpir	This Study
MJM1424 (β3914)	F- RP4-2-Tc::Mu Δ*dapA*::(erm-pir) *gyrA*462 zei-298::Tn10 (ErmR KanR TetR)	(199)
MJM2382	B3914 pJNW684	(200)
MJM534	CC118 λpir / pEVS104	This Study
MJM2532	MJM1424 pACBSR-Hyg	This Study
MJM2698	MJM2383 pACBSR-Hyg	This Study
Plasmids	Genotype/Description	
pJNW684	Transposon vector	(200)
pACBSR-Hyg		(196)

Strains developed and bacterial genetics performed by Ella Rotman.

1374 **Table 4.2. Primers used in this study.**

Name	Sequence (5'-3')	Construct/Purpose[1]
wza_for	TCAATTAACAAGGCATTCCC	ΔVK055_5015::kan (V)
wza_rev	CATTGTCTTACCTCGTGCTT	ΔVK055_5015::kan (V)
Tn5pr_for	ggatttgaacgttgcgaAGCAACGGCCCGGAGGGT	Transposon-specific primer (V)
P7	AAGCAGAAGACGGCATACGA	ΔVK055_4268::kan (V)
4628_up	TCATCGACCACATAAACTGG	ΔVK055_4268::kan (V)
1993_KO_for	CGCTGCCCGGCAGAAAGGCGAGCATATTAGCGAAAACAGGTTTGTCATCAGTCTCAAGGAATGCCTATGtgtgtaggctggagctgcttc	ΔVK055_1993::kan (P)
1993_KO_rev	CGCGACTGAGCGCGGCCTGAGTGGTTAGCGTTCTCAACGCGAGCTTATTTTTTTCTCCACCTGCCCGTTGGAcatatgaatatcctcctta	ΔVK055_1993::kan (P)
1993_ver_down	CCTTTTTAACGTCCACATGC	ΔVK055_1993::kan (V)
1993_ver_up	AAAGGCGAGCATATTAGCG	ΔVK055_1993::kan (V)
3462_KO_for	AGTTCTGGCGTTTACCTGTCTTACCTGTCGTCGTATTCTTGCTGAAAAAAACGACAGGAGACAGGCATGtgtgtaggctggagctgcttc	ΔVK055_3462::kan (P)
3462_KO_rev	GGGAGCCCGGCCTAGCACAGCGCAAGCCGGGCTTTCTTTTGCCGTTACAGTTTCCCCAACAGCTGGTTGGAcatatgaatatcctcctta	ΔVK055_3462::kan (P)
3462_ver_for	GAACATATGGGACGCTTCG	ΔVK055_3462::kan (V)
3462_ver_rev	AGCGTAATTCGCTTTTCCC	ΔVK055_3462::kan (V)
1930_KO_for	CGGTATTTACCTTATTGCATTGTTGATTCAGGAGTCCCGCAAAAAATGAGTGCTGTCCCCTCCCGTTTGtgtgtaggctggagctgcttc	ΔVK055_1930::kan (P)
1930_KO_rev	CAGGTAGCCCGGCTCAGCGTAGCGCAAGCCGGGGAAAGAGGAGATTACCGGCGGCCCAGCGGGACGTTGGAcatatgaatatcctcctta	ΔVK055_1930::kan (P)
1930_ver_up	ATCTCATTTATCGCGCTGG	ΔVK055_1930::kan (V)
1930_ver_down	ATTCTGGGGTAACGGTTGA	ΔVK055_1930::kan (V)
3638_KO_up	AAAGTGGCCGGACAGGTCGCCTACCGTCTTTACCAACGTGAGGCCCAAGGAGAGCACCATGCTGATTAA tgtgtaggctggagctgcttc	ΔVK055_3638::kan (P)
3638_KO_down	GGGCACAGCGTTCGTGGCGTTTACGCCCGATCCCTGAGCCCTTTTCAGGACTATTTTTTCAGCGTCGCCTTcatatgaatatcctcctta	ΔVK055_3638::kan (P)
3638_ver_down	GCAGTGAGATGCGCTATG	ΔVK055_3638::kan (V)
3638_ver_up	AAGTCGAAAACGGCTTACC	ΔVK055_3638::kan (V)
3875_KO_for	GCAGAAGGTCATACTGACGCGACGCCGGCAGCCGGCACGACGCATTAATTTCAGGAGAAATACGATATGtgtgtaggctggagctgcttc	ΔVK055_3875::kan (P)
3875_KO_rev	CGCCAGCGTCTCGCCCTCGCGAGTCCAGCTCAGCTGCCCGCTCATTATTTTTTCTGTTCCAGGGTGTTGGAcatatgaatatcctcctta	ΔVK055_3875::kan (P)

3875_ver_up	CACGACGCATTAATTTCAGG	ΔVK055_3875::kan (V)
3875_ver_down	CACAAAATGCACTAACAGCG	ΔVK055_3875::kan (V)
0094_KO_for	GCCAGAGGATTAAGCTTGTCAGTGGCTCGCTTTAAAATAGGGGGAAATCACAACGAGGTGTTTATCGTGtgtgtaggctggagctgcttc	ΔVK055_0094::kan (P)
0094_KO_rev	TAAGCAAACGCCATGTTGTAATTCGGCTTCACCGACAGCGCAATTTAGTCACCGGCATGCCGCTGGTTGGAcatatgaatatcctcctta	ΔVK055_0094::kan (P)
0094_ver_down	AAACGCCATGTTGTAATTCG	ΔVK055_0094::kan (V)
0094_ver_up	CAAATATAGTCCGCCAGAGG	ΔVK055_0094::kan (V)
4323_KO_for	GCTCCGCACTATAGCGCAAGTTATGATACGGTAAGCAACCGGTTACGCGATTAAGACAGGAACCCCATGtgtgtaggctggagctgcttc	ΔVK055_4623::kan (P)
4323_KO_rev	GTAAGCGCAGCGCCACCCGGCAATACTGCAGCGAGCGGCGAGCGTTAAATCGCCGCGTCGTCTTCGTTGGAcatatgaatatcctcctta	ΔVK055_4623::kan (P)
4623_ver_up	TCAGTTTGAGCTGAACTACC	ΔVK055_4623::kan (V)
4623_ver_down	ATGCAGTATTATCTCTGCGG	ΔVK055_4623::kan (V)
1398_KO_for	TAAACGGCGGGCATGATATAGCAAAGCTAATTAATTTACATCCCTACATTTTACGCTACATTTCTCTCAtgtgtaggctggagctgcttc	ΔVK055_1398::kan (P)
1398_KO_rev	AGGCCGATACCCAGCCACAGCAGCCAATAGCGCGGATGCAACAGCGCCGGAGAAAATTTAGGCAAATGAGTcatatgaatatcctcctta	ΔVK055_1398::kan (P)
1398_ver_up	CAGATAGATGCGGCCAAAG	ΔVK055_1398::kan (V)
1398_ver_down	AAGTTCATCACCACCATTCG	ΔVK055_1398::kan (V)

[1] Primer used for (P) PCR during construction, PCR to verify insertion/orientation (V), and/or (S) sequencing to confirm the construct.

Primers designed by Ella Rotman.

4.4. Results

The anesthetic agent propofol leads to increased intranasal infection with *K. pneumoniae*. Previous investigations into propofol's impact on blood stream infections using the Gram-positive pathogens *Listeria monocytogenes* and *Staphylococcus aureus* identified significant alterations in bacterial colonization, growth, and pathology in target organs. Using *Klebsiella pneumoniae* as a model extracellular pathogen, we assessed whether propofol affected lung infection via an intra-nasal route. Brief propofol sedation had no measurable impact on lung burdens 24 hours post-infection, but burdens were increased nearly 100-fold by 48 hours compared to ketamine/xylazine-sedated controls (fig. 4.1A). We also assessed the impact on dissemination from the lungs and again found that while secondary organs had comparable burdens at 24 hours, average burdens in both livers and spleens were more than 1000-fold higher than controls (fig. 4.1BC). We conclude that the immunosuppressive phenotype observed with propofol sedation is broad enough to impact multiple routes of infection with both Gram-positive and –negative bacteria.

Propofol exacerbates lung pathology by *K. pneumoniae*. Previous research on propofol sedation prior to infection also identified gross changes in pathology at primary sites of infection (135,136). Using a histological approach, we observed that by 72 hours post-infection, severe damage was widespread in lungs regardless of sedation agent (fig 4.2AB), however, propofol-sedated mouse lungs featured large areas of de-cellularized or denuded tissue containing little identifiable structure and only sporadic immune infiltration. Quantification of these regions showed that propofol-sedated mice contain significantly larger denuded regions within the lungs (fig 4.2C). Immunofluorescent examination of these regions revealed that *K. pneumoniae* had completely overrun local containment and appeared to have developed a replicative niche (fig 4.2D). It is reasonable to conclude that these regions could likely be a reason behind the disparate burdens observed between sedation groups.

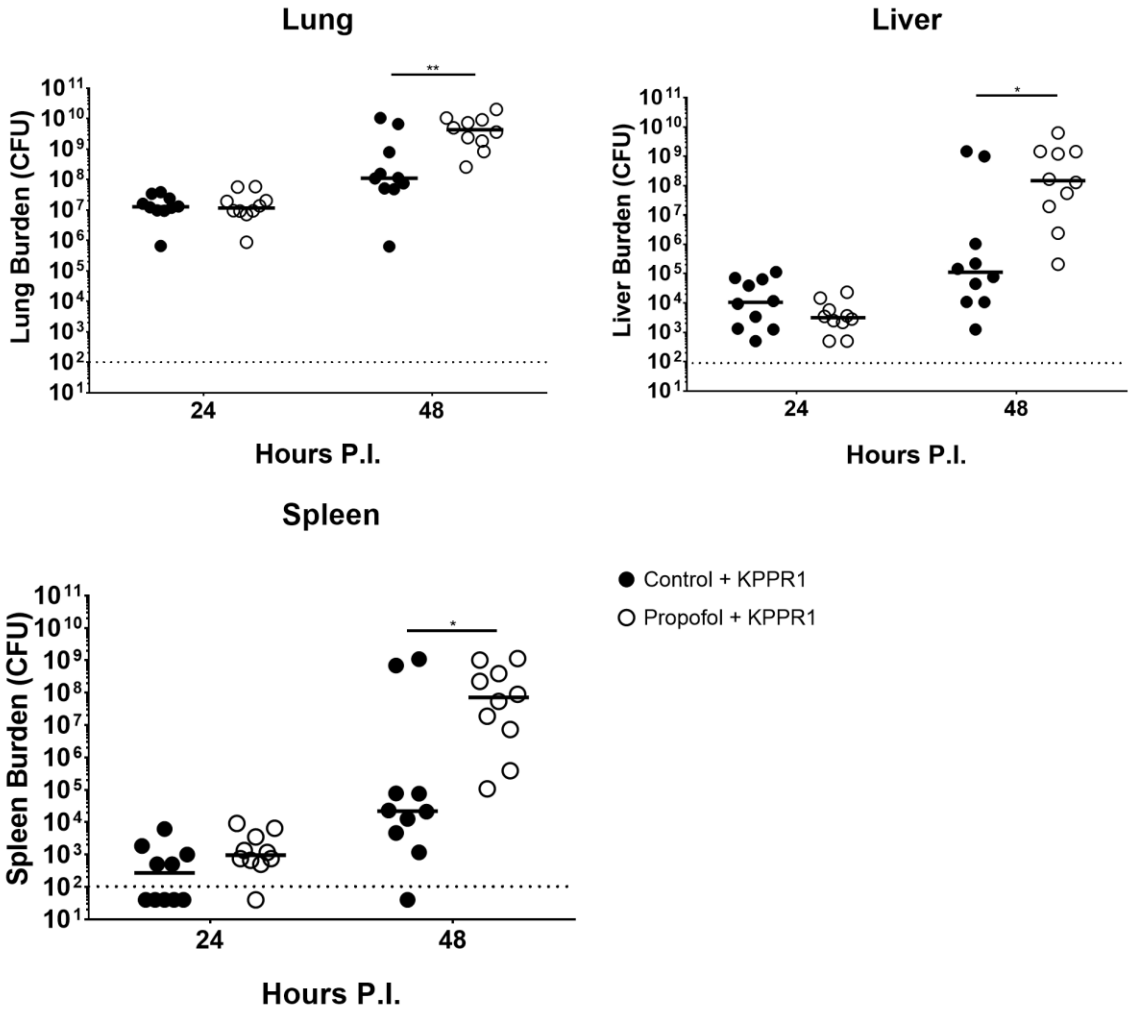

1402

1403 **Figure 4.1. Acute propofol sedation increases *Klebsiella* lung burdens and dissemination to secondary**

1404 **tissues**. Swiss Webster mice were sedated with either ketamine/xylazine (closed circles) or propofol

1405 (open circles) and infected with $3x10^4$ CFU intra-nasally and organ burdens were assessed at 24 and 48

1406 hours post infection. Statistics were calculated using a two-tailed Mann Whitney U test (*, $p \leq 0.05$; **,

1407 $p \leq 0.01$).

1408

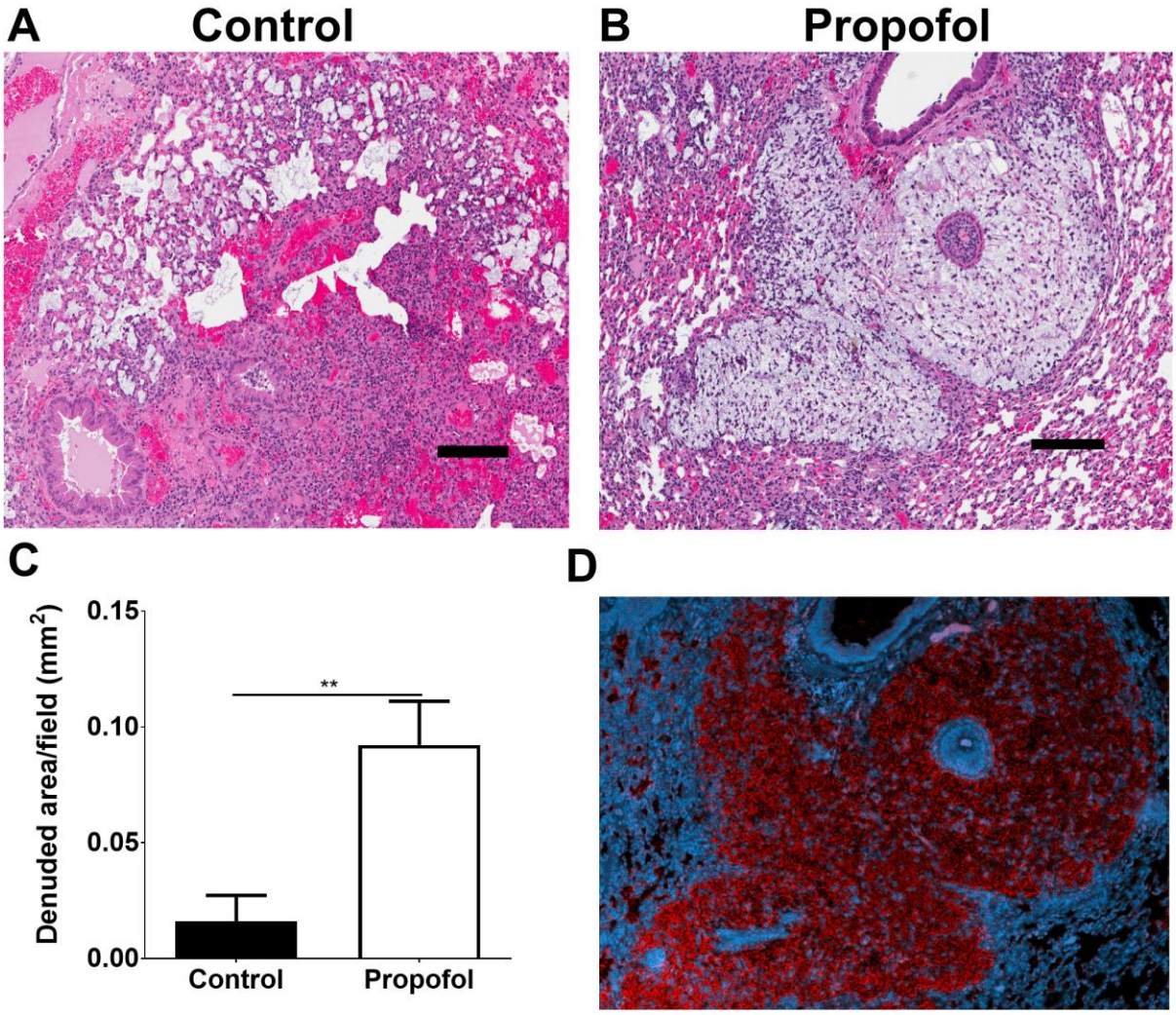

Figure 4.2. Histological analysis of *K. pneumoniae* lung pathology 72 hours post-infection. Swiss Webster mice (n = 3 per group) were infected with $1x10^4$ CFU KPPR1. (A and B) After 72 hours, mice were euthanized and lungs harvested and processed for histological analysis. Representative H&E staining of ketamine/xylazine-sedated (A) and propofol-sedated (B) animals. Black bar = 100 µm (C) Quantification of average denuded area in lung sections from 10 fields per mouse (n=3 per treatment). Statistics were calculated using an unpaired, two-tailed Student's t-test (**, $p \leq 0.01$). (D) Immunofluorescent staining of *K. pneumoniae* (red) in lung tissue (blue, DAPI).

Transposon insertion sequencing identifies *K. pneumoniae* genes that are required for outgrowth in the lung. We generated a 50,000 mutant transposon library in KPPR1 using the plasmid pJNW684 (200). The distribution of the hits was spread evenly throughout the chromosome, averaging approximately 9.1 insertions per kb. The experimental approach is outlined in figure 4.3. Propofol- and control-sedated mice were intra-nasally infected with the library at a dose of $6x10^5$ CFU for 24 hours, after which the lungs were harvested and genomic DNA was extracted. Genomic DNA was also extracted from aliquots of the input library grown under conditions identical to the lung input. Relative fitness was calculated by taking the average number of output reads for each treatment, dividing by the average number of input reads, and taking the log of the quotient. The top 25 candidates following control sedation are listed in table 4.3. For comparison, the top 25 candidates reported by Bachman et al (191) were largely present in our screen and are presented in table 4.4, confirming the validity of our screen. In total, 5,005 genes contained insertions in our input pools with the top 737 genes representing 50% of all insertions.

Transposon insertion sequencing identifies *K. pneumoniae* genes that are required for outgrowth in the lung in a sedative-dependent manner. The screen identified 81 candidate genes that appeared to have at least a 10-fold greater requirement following control sedation and an additional 80 genes with at least a 10-fold differential requirement under propofol-sedation, excluding 76 genes that had no reads in one or the other output (fig 4.4). To maximize the likelihood that a given mutant would accurately reflect its defect(s) following validation, we imposed several conservative statistical cutoffs. For preliminary analyses, we excluded genes with less than 20 cpm in the input pools and then further excluded genes that demonstrated high intra-replicate variability (CV≥75%) in either the input or output

Table 4.3. The top 25 genes required for lung growth under ketamine sedation.

VK055_x	Gene	Control in/out	Propofol in/out
3696	*ompR*	-4.02	-2.13
1783	*tolA*	-3.87	-3.62
4686	*purM*	-3.82	-3.35
3303	-	-3.61	output = 0
0137	*dsbB*	-3.61	-2.11
5015	*wza*	-3.55	-2.40
1782	*tolB*	-3.50	output = 0
4811	*purF*	-3.45	-2.41
4794	*aroC*	-3.36	output = 0
3505	-	-3.25	-3.31
1785	*tolQ*	-3.22	-2.91
5040	*hisA*	-3.21	-2.97
1196	*trpB*	-3.18	-3.50
3852	*gltD*	-3.16	-2.98
1772	*nadA*	-3.14	-0.45
3504	-	-3.14	-3.20
2794	*pepA*	-3.10	-2.94
3941	-	-3.04	-0.66
3499	-	-3.03	-3.49
3502	-	-3.02	-3.37
1193	*trpE*	-3.02	-1.10
1518	*ssuB*	-2.89	-1.88
3088	*purD*	-2.86	-2.20
2493	*leuA*	-2.86	-2.14
1549	*serC*	-2.86	-3.27

Table 4.4. Comparison to Bachman Top 25 (log10 output/input results)

VK055_x	Gene	Bachman score	Control in/out	Propofol in/out	Comment
5014[a]	*wzi*	-3.45	-2.45	-2.45	
3141[a]	*rfaH*	-3.43	-1.13	-0.54	
5096	*hyp*	-3.40	NA	NA	Absent in input
3202	*ilvC*	-3.35	-1.01	-1.24	
3832	*argR*	-3.06	output = 0	-1.01	
5025[a]	*wcaJ*	-2.92	-1.97	-1.46	
5012[a]	*galF*	-2.85	-1.21	-3.08	
3206	*ilvE*	-2.76	-1.51	-2.30	
3515	-	-2.71	-0.39	-0.14	
4417	-	-2.65	-1.66	-0.31	
4811	*purF*	-2.58	-3.46	-2.41	
4619	*purL*	-2.49	-2.56	-2.51	
1194	*trpD*	-2.48	output = 0	-2.82	
4135	*serA*	-2.40	-1.55	-0.83	
2495	*leuC*	-2.39	-0.31	-2.10	
3142	*tatC*	-2.34	-0.66	-0.74	
3205	*ilvD*	-2.31	-0.64	-1.21	
5023[a]	-	-2.24	-1.06	-2.55	
4883	*rcsB*	-2.10	-0.62	-2.08	
2215	*phoR*	-2.05	-2.30	-2.43	
4579	*pheA*	-1.98	-0.23	-0.46	
3368	*dgoA*	-1.95	0.04	-0.26	
2084	*copA*	-1.84	-1.42	-1.13	
3086	*purH*	-1.83	-2.18	-3.66	
3791	*aroE*	-1.79	output = 0	-2.15	

*a, capsule gene

List compiled by Ella Rotman.

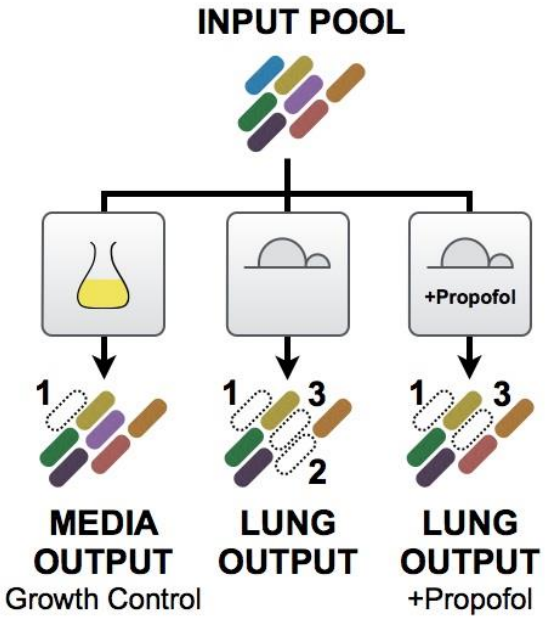

Figure 4.3. Diagram of INSeq overview. The colored rods symbolize separate mutants from a 50,000 transposon-mutant INSeq library in *K. pneumoniae* strain KPPR1. The outlined rods represent mutants that are expected to be absent after each selection. Examples are shown for mutants that exhibit (1) a growth defect; (2) inability to colonize immunocompetent mice; and (3) inability to colonize propofol-immunocompetent mice. Figure created by Ella Rotman.

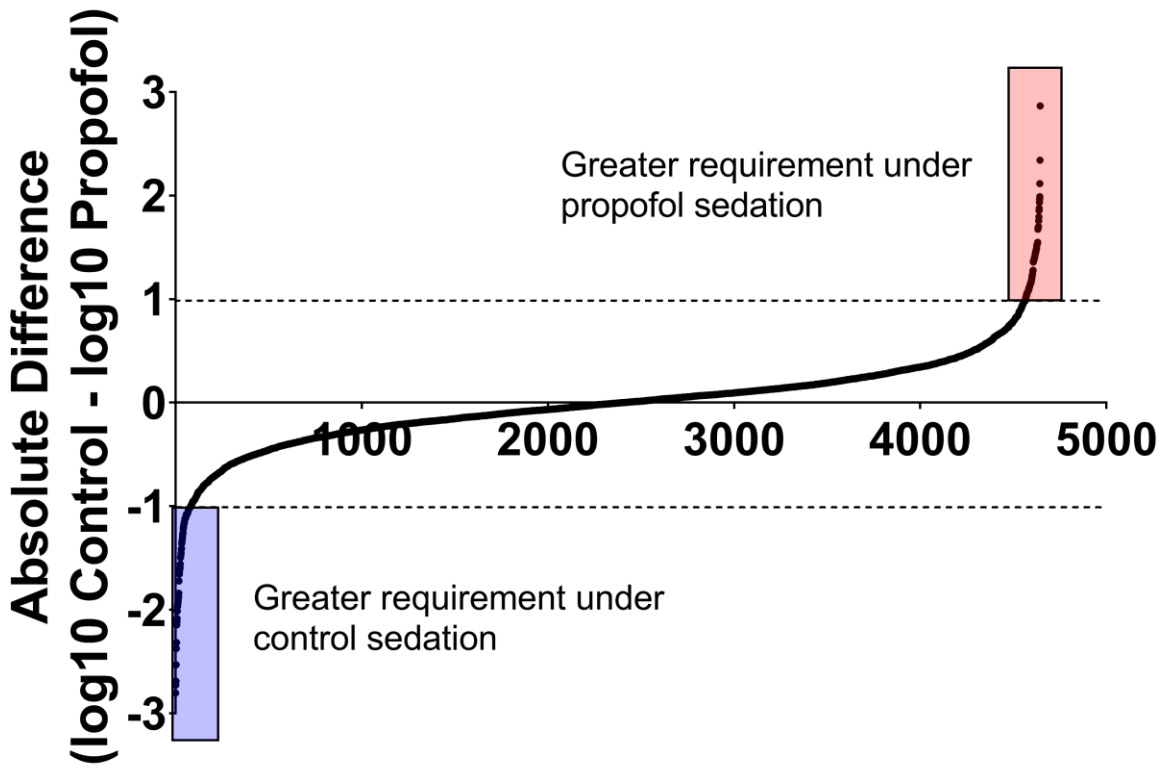

Figure 4.4. Absolute difference of log10 competitive indices. The dataset contained 4,565 genes with nonzero reads in the input and both outputs. The log10 index for each gene was calculated $CI=\log(AVG_{output}/AVG_{input})$. The absolute difference is plotted from smallest (more critical following control sedation) to largest (more critical following propofol sedation).

pools. Finally, genes that had no reads in either output were also excluded. This narrowed the list of genes to approximately 2,625, which we used to identify primary candidates that may be differentially required following different sedatives.

Eight genes were selected for validation and deletions were made in the KPPR1 background using lambda Red recombination (fig 4.5). The genes *copA* and *ilvC* were previously validated as genuinely defective in virulence (191) and serve to confirm the success of the screen (fig. 4.5). Additionally, we chose *mlaC* as it was identified as having a defect regardless of sedative choice and was furthermore representative of the entire *mla* operon. The genes *virK, VK055_1993*, and *glnB* were identified as potentially only required following control sedation, while the genes *VK055_1398, VK055_3638, VK055_3462*, and *fepC* were likely to be more important following propofol sedation. *In vitro* characterization of these mutants revealed that all demonstrated WT-like growth in broth, except Δ*fepC* which had a 16% increase in doubling time (20.92±0.55 min) (fig 4.6).

Validation of candidate genes in a mouse model of infection. Gene candidates were assessed for virulence defects *in vivo* using the same intra-nasal infection route as before with burdens being assessed 24 hours post-infection. Of the eight genes tested, statistically significant virulence defects were detected in six mutants following propofol sedation, and four mutants following control sedation (fig. 4.7A). Interestingly, one gene, Δ*VK055_1398*, which encodes an unknown protein, displayed a significant virulence defect only after propofol and not control sedation. In light of the screen essentially being a large scale competitive infection, we additionally assessed whether these genes had competitive defects compared to WT *in vivo* (fig. 4.7B). Δ*VK055_3462* again demonstrated no virulence defect, while Δ*fepC, ΔVK055_3638*, and Δ*mlaC* showed modest competitive defects that were not significantly altered by sedative choice. Both Δ*VK055_1993* and Δ*glnB* demonstrated competitive virulence defects only after control sedation, while Δ*virK* and Δ*VK055_1398* were only defective

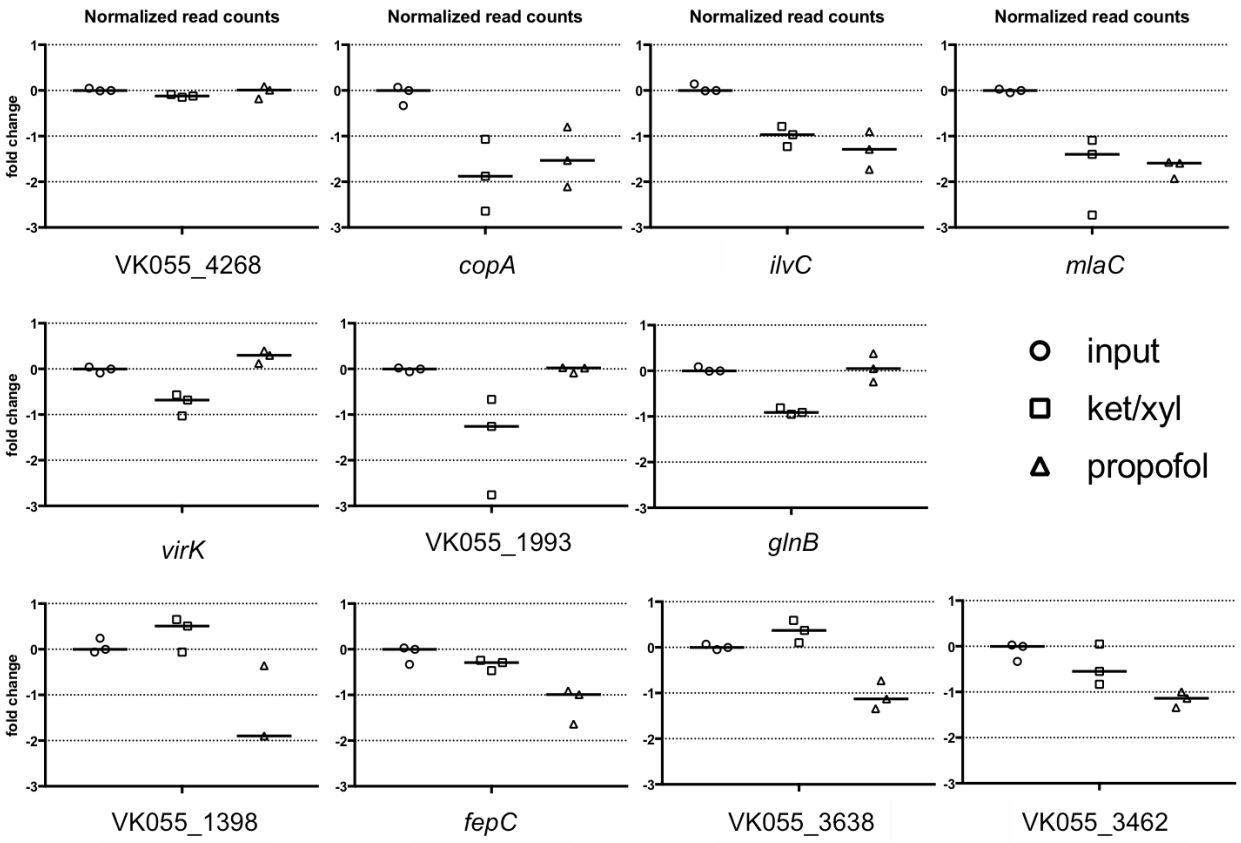

1481

1482 **Figure 4.5. Genes with competitive defects identified by INSeq.** Log10 competitive results. First row

1483 contains an example of a gene not important for virulence (VK055_4268). Genes copA and ilvC were

1484 previously validated. MlaC is a novel general virulence factor. Second row (virK, VK055_1993, glnB) are

1485 genes expected to have defects in control-sedated mice only. Third row (VK055_1398, fepC,

1486 VK055_3638, VK055_3462) are genes expected to have defects preferentially under propofol sedation.

1487 Data analyzed and prepared by Mark Mandel and Ella Rotman.

1488

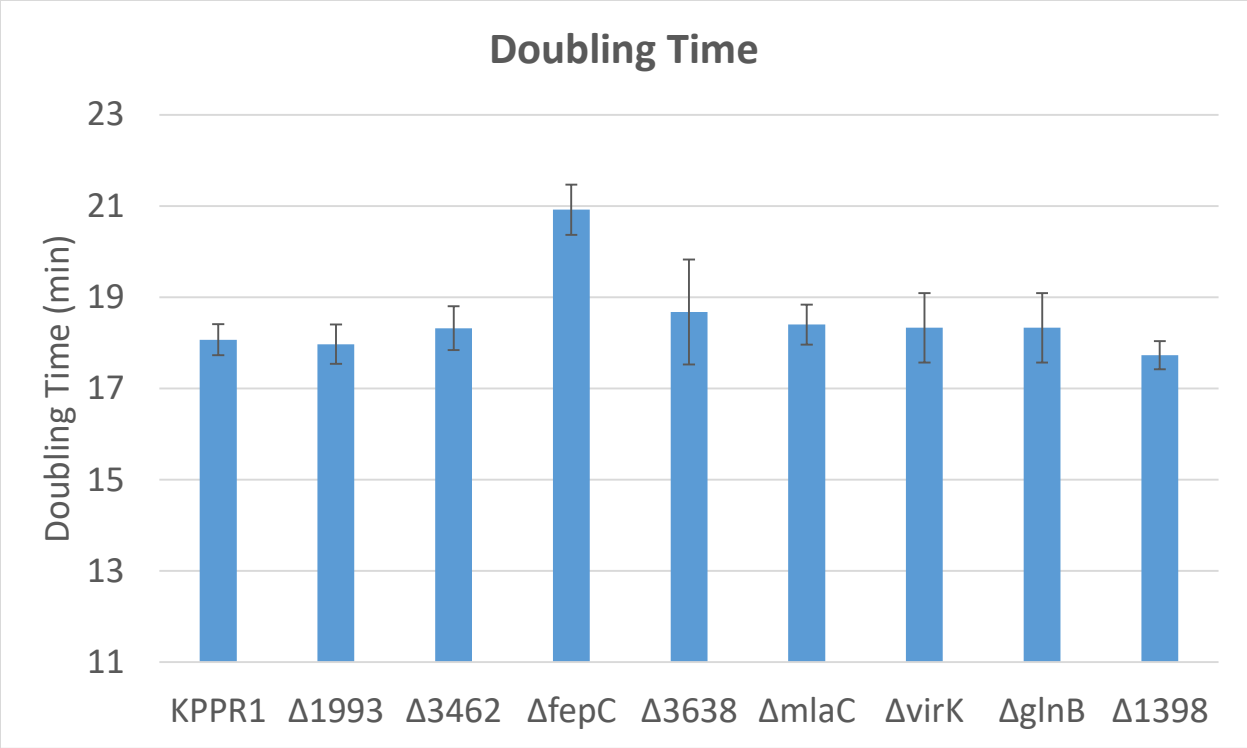

Figure 4.6. Most mutants have no *in vitro* growth defects. Doubling time in LB was assessed as described in the materials and methods section. Bars are the average of three independent experiments and error bars represent standard error (SEM). Experiments performed by Ella Rotman and Acadia Kocher.

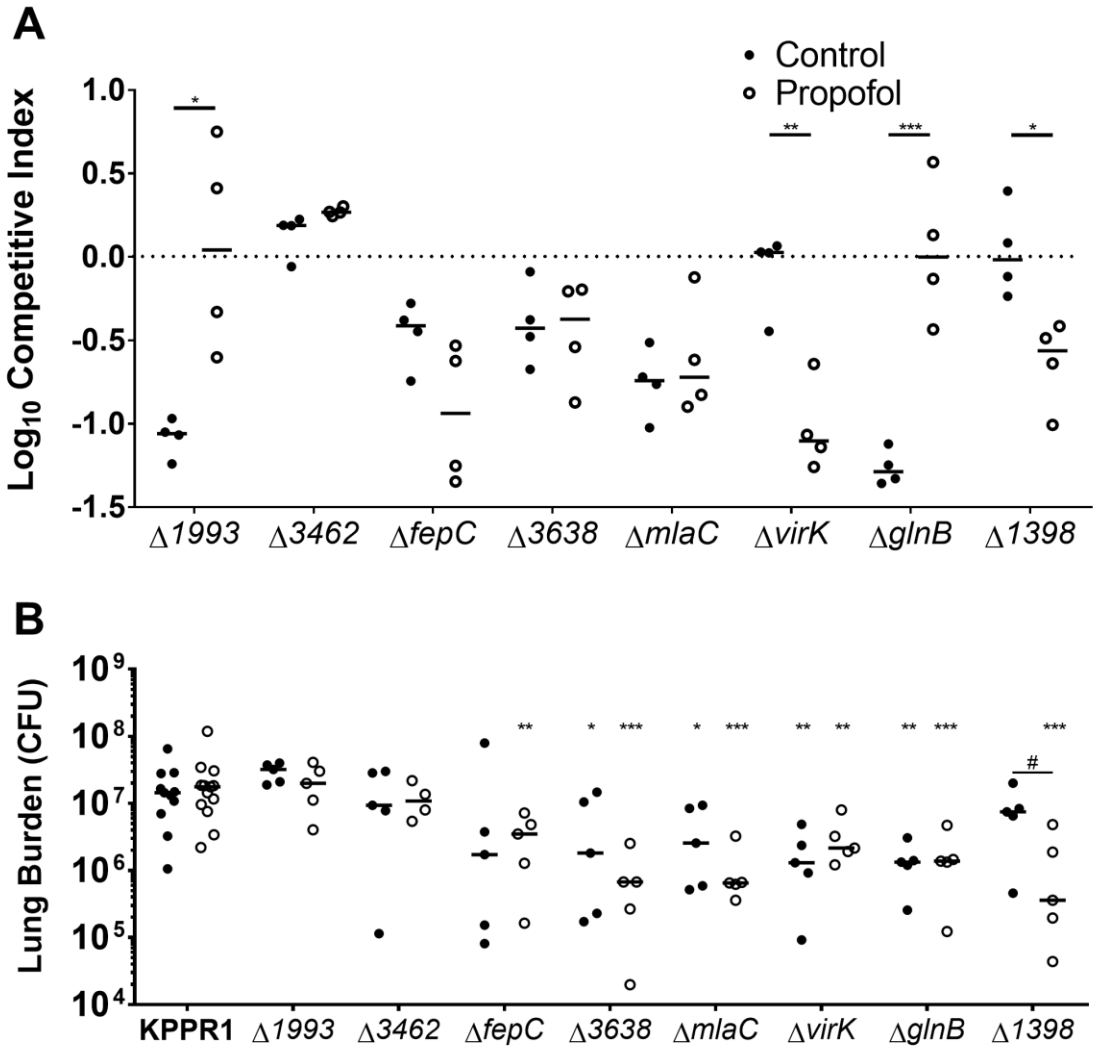

Figure 4.7. Quantification of lung burdens 24 hours post-infection for wild type and mutant KPPR1 strains. (A) Competitive indices of each mutant against WT 24 hours post-infection (n=4 per group). Statistics were calculated using an unpaired, two-tailed Student's T-test. (B) Swiss Webster mice (n=5 per group) were control- (closed circles) or propofol-sedated (open circles) and infected with $1x10^4$ CFU intranasally. Statistics were calculated using a two-tailed Mann-Whitney U test (*, $p \leq 0.05$; **, $p \leq 0.01$; ***, $p \leq 0.001$) and significance is compared to KPPR1 under the same sedative.

following propofol sedation. Thus, sedative choice has a significant impact on the requirement of a subset of *K. pneumoniae* virulence factors.

4.5. Discussion

Previous work in the Freitag lab had identified the significant impact acute propofol sedation has on the mammalian host's ability to combat bacterial bloodstream infections with Gram-positive pathogens (135,136). Here, we have extended the model to demonstrate that propofol's immunomodulatory phenotype is applicable to both a new route of infection and to a Gram-negative pathogen, *Klebsiella pneumoniae*. Propofol sedation increased lung burdens approximately 100-fold compared to control-sedated mice and furthermore increased dissemination to secondary organs approximately 1,000-fold at 48 hours post-infection (fig. 2.1). We further identified that propofol sedation resulted in significantly larger areas of denuded or destroyed lung tissue, likely forming a replicative niche for rapidly dividing *K. pneumoniae in vivo* and possibly accounting for the increased lung burdens measured at 48 hours post-infection. These data clearly demonstrate that propofol is negatively impacting the host's ability to address *K. pneumoniae* lung infection and subsequent bacteremia.

Genome-wide mutagenic approaches such as signature-tagged mutagenesis (STM) and transposon mutagenesis have previously been applied to *K. pneumoniae in vivo* virulence screens and have identified dozens of putative virulence factors, which have been comprehensively reviewed by Paczosa and Mecsas (22). The screen described herein yielded novel gene products not only through the utilization of a library of unprecedented complexity, but by considering sedative exposure as a key variable in subsequent lung outgrowth. By comparing outputs from infected lungs to their inputs, we were able to quantify the relative requirement of numerous genes following either control or propofol

sedation. This approach enabled us to identify novel virulence determinants and begin to define the broad impact that sedation has on lung fitness.

Membrane lipid asymmetry has not been previously investigated in *K. pneumoniae*, however, the *mla* (maintenance of outer membrane lipid asymmetry) pathway has been well characterized in *Escherichia (E.) coli*. Mla comprises a transport system thought to shuttle phospholipids from the outer membrane to the inner membrane (201). MlaFEDB forms an ABC transporter, while MlaA is a lipoprotein attached to the outer membrane and MlaC is the periplasmic shuttle between the two. Interestingly, *mlaA* was identified in our screen as being differentially required, with a log10 defect of -0.69 following control sedation, but -1.78 following propofol. The implications of this dichotomy remain unclear and unvalidated. *MlaC* was found to have a significant competitive defect under both sedative conditions, both in our screen and subsequent validation, and similar defects are predicted for *mlaD*, *mlaE*, and *mlaF*. Finally, loss of *mlaB* does not appear to carry a significant defect, a reasonable finding considering that MlaB is a minor subunit in the transporter. Clearly, perturbation of this membrane lipid homeostatic mechanism is a critical factor in the resistance of *K. pneumoniae* to host antimicrobial strategies.

Of the four genes demonstrating differential competitive defects, only *glnB* had been previously characterized, while the other three remain annotated as unknown or hypothetical. *GlnB* encodes P_{II}, a regulator of glutamine synthetase (GS). This protein effectively senses the nitrogen status of the bacterium through allosteric regulation by α-ketoglutarate and glutamine (202,203). High intracellular glutamine levels cause P_{II} to adenylylate GS, effectively turning it off, while α-ketoglutarate binding to P_{II} leads to de-adenylylation of GS and its activation. This differential requirement under control sedation was also noted, although not confirmed, in the gene *glnS* (VK055_1830), encoding glutamine--tRNA ligase, but not in any of the other six *gln* family genes. It is plausible that propofol administration is increasing the bio-availability of nitrogen in the host during infection, either through the co-

administration of the intralipid carrier propofol is emulsified in, or through direct action on host nitrogen regulation. Based on the similarity of lung, liver, and spleen burdens in either treatment group after 24 hours, it is more likely that host nitrogen is the primary source. Metabolic modeling has found that KPPR1 is capable of utilizing a diverse array of nitrogen sources (204) and the possibility of a shift in host nitrogen metabolism could explain the indifference of the *glnB* mutant following propofol sedation.

Our dataset suggests numerous other genes that are potentially differentially required depending on host anesthetic exposure. Functional grouping of these genes may identify common pathways that could hint at the underlying shifts in the propofol-sedated patient, although 48 of the 161 (29.8%) candidate genes identified are annotated as hypothetical. Further validation and characterization of these gene products would provide significant clarity to these findings. This screen identified numerous genes with relatively mild putative virulence defects and it is a testament to the sensitivity and resolution of the screen that we could confirm several subtle virulence defects in our subsequent validation.

A majority of validated genes revealed general virulence defects *in vivo* despite utilizing a non-competitive infection assay, and furthermore identified *VK055_1398*, which as predicted, was defective for growth only following propofol sedation. This hypothetical gene product is thus an excellent candidate for further characterization. Together, these results reveal that propofol sedation leads to a broad effect on colonization by bacterial pathogens and that identifying colonization factors under multiple sedation conditions yields useful information for probing pathogenesis *in vivo*.

Chapter 5: Discussion, Future Directions, and Conclusions

5.1. Swiss Webster mice are relevant models for *K. pneumoniae* lung infection

These studies have demonstrated conclusively that propofol sedation affects pulmonary infection by the Gram negative pathogen *Klebsiella pneumoniae* in both the outbred Swiss Webster mouse and the inbred C57BL/6 mouse and furthermore, these alterations are reflected in the virulence repertoire required for successful intrapulmonary growth *in vivo*. Initial time course investigated whether propofol had a significant impact on infection as detected through the recovered organ burdens across numerous initial dose points. While increased lung, liver, and spleen burdens were observed at 48 hours post-infection following an initial dose of $3x10^4$ CFU *K. pneumoniae* (Fig. 4.1), repeated experiments at both lower and higher inocula did not demonstrate clear alterations, suggesting propofol does not affect *K. pneumoniae* fitness during lung infections.

Lowering the initial infectious dose to 10^3 CFU still failed to yield significantly different burdens beyond ten hours post-infection, however, gene expression analysis revealed a radically different story at this lower dose. This led us further probe the 10^3 CFU dose outcome and by aggregating multiple experiments, it was revealed that propofol may have a more significant impact on dissemination than initially appreciated, although further examination is required. Six out of fifteen propofol-sedated mice inoculated with 10^3 CFU had lung burdens $\geq 10^8$ CFU by 48 hours post-infection, compared to three of fifteen control mice, however, these propofol-sedated mice had liver and spleen burdens often several orders of magnitude higher than their control counterparts (Fig 2.8). As discussed in Chapter Two, this suggests that the 10^3 CFU dose is at a tipping point for propofol-sedated mice, but it remains possible that this bifurcation could be an artifact of the inoculation method. The intranasal route of infection was selected for this model due to its non-invasive nature, the quickness with which the bacterial suspension can be delivered, and that it is well tolerated by the mice. The tradeoff is that it is not

possible to accurately gauge the precise initial dose because liquid may go into the esophagus instead of the trachea, or may remain in the nasopharynx, or may be expelled by the animal. The common alternative approach is intratracheal (IT) instillation, in which a cannula is inserted into the trachea to directly deliver the infectious dose into the lungs, however this is an invasive procedure that requires a longer duration of sedation as well as tissue injury and thus was incompatible with the acute sedation experimental approach. Nevertheless, refinement of intranasal inoculation experimental technique has resulted highly consistent lung burdens at both ten and 24 hours post infection, as well as the identification of a remarkably consistent transcript-based signature of propofol-immunomodulation at a lower infectious dose, demonstrating that inter-murine variation in the actual initial inoculum has a negligible impact on outcomes.

5.2. What host pathways are affected by propofol sedation?

On the host side, it was interesting to find such a broadly shared hyper-expression phenotype amongst pro-inflammatory genes and that this translated to increased serum levels for these proteins, corroborating the serum protein findings of Schläpfer et al with their rat sepsis model (134). These results suggest that propofol is antagonizing a broadly conserved negative regulator of immune modulation. The NF-κB pathway has been experimentally linked to numerous aspects of development, apoptosis, and immunity (205), and furthermore has been implicated in previous studies of propofol immune suppression (127–129,144,148,149), thus this would be a reasonable pathway to investigate.

The NF-kB family of transcription factors consists of five members: RelA, RelB, c-Rel, p50, and p52, with these last two not demonstrating transcriptional activity (206). These factors are retained in the cytosol, bound by IκB proteins inhibiting their function. Signal-induced phosphorylation of IκB by IκB kinases (IKKs) result in degradation of IκB and the release of the NF-κB protein. These factors may then form either homo- or heterodimers and translocate to the nucleus to regulate distinct sets of genes.

There are several well characterized negative regulators of the NF-κB pathway. Both IkB alpha and IkB epsilon can enter the nucleus, bind to DNA-bound NF-κB dimers, and by virtue of a nuclear export sequence, remove the transcription factor back into the cytosol. Conversely, IκB beta does not contain the nuclear export signal and its binding to active dimers renders them resistant to IκBα and IκBε inhibition (205,206).

There are several deubiquitinase enzymes that negatively regulate NF-κB signaling with the best studied being A20 (207–210). A20 targets multiple IKK activators for degradation, thus preventing further signal transduction. Similarly, cylindromatosis (CYLD) targets IKKs and other activators and attenuates signaling following TLR2 and TLR4 stimulation (211,212). Additional mechanisms inhibiting NF-kB signaling include factors that can actively displace dimers from DNA and factors can target dimers for degradation while in the nucleus (213–215). In total, there are numerous potential regulatory factors in the NF-κB pathway that propofol could be interacting with and inhibiting the function thereof. While these diverse mechanisms present a significant volume of work for a future researcher, the experimental approaches to test these pathways are straightforward and reagents are readily available.

While the hyper-inflammatory phenotype broadly affected dozens of genes, both gene expression and serum protein analysis identified several notable peculiarities in propofol-sedated mice. The first identified was a delay in the induction of *Il23a* expression. The heterodimeric cytokine IL-23 is composed of the IL-23p19 subunit and the IL-12p40 subunit. This bioactive cytokine regulates mucosal barrier function under homeostatic conditions and is critical for defense against extracellular pathogens by contributing to robust activation of the innate immune response (216). IL-23 is primarily produced by activated macrophages and DCs in the lungs and in the context of infection, expression is driven by sensing of microbial products. Signaling through TLR4 utilizes both NF-κB and p38 MAP kinase pathways to upregulate transcription, while interferon gamma signaling through its cognate receptor can inhibit transcription via interferon regulatory factor (IRF)-1 (217). While an increase in *Ifng* transcripts and

serum protein was detected, it was not until well after this early inhibition, suggesting that propofol is blocking activation, possibly through NF-κB antagonism.

Serum protein analysis noted that despite the rapid and significant increases in *Csf3* expression, serum G-CSF was not increased at ten hours post-infection in propofol-sedated mice. A recent study demonstrated that LPS-induced production of G-CSF primarily originated from endothelial cells in a TLR4/MyD88-dependent manner (218). The absence of a response suggests that propofol-sedated mice may additionally have non-immune cell suppression for at least ten hours after brief sedation, then by 24 hours, this initial suppression is reversed to seemingly unrestrained expression. This raises the possibility of two distinct molecular mechanisms antagonizing the appropriate signaling for cytokine expression. First, early suppression of cells such as alveolar macrophages takes place when propofol plasma levels are still relatively high as propofol continuously diffuses back out of fatty tissues into the circulation. Propofol's interactions with this target would imply a relatively low affinity, consistent with *in vitro* studies finding little to no effect with propofol concentrations below 10 μM. The second mechanism is the inhibition of the negative feedback loop(s) for NF-κB or a related pathway. At this point in time, the evidence for this is circumstantial, but future mechanistic studies should take this phenotype into account.

It is possible that propofol may directly bind to one (or more) of the diverse members of the nuclear receptor (NR) superfamily. Humans express at least 48 unique NRs sorted into four subclasses by mechanism of action and act as transcription factors upon activation. At least fifteen of these receptors act as xenobiotic sensors and induce the expression of specific cytochrome P450 (CYP) enzymes in the liver to metabolize exogenous substrates. In Chapter 1.6, it was discussed that propofol is primarily metabolized by CYP2B6 in humans (98,219). Human CYP2B6 and murine homolog CYP2B10 have been shown to be transcriptionally co-regulated by the constitutive androstane receptor (CAR), which is indirectly activated by propofol, and the pregnane X receptor (PXR), likely binding directly to

propofol (220–222). Whether propofol could activate other NR pathways has not been described, let alone in the context of an active infection, therefore this represents a plausible mechanism of immune alteration.

5.3. Does propofol potentiate clinical signs of sepsis?

This model of lung infection and septic progression potentiated by acute propofol sedation presents an excellent opportunity to address several important questions. While the data presented in Chapter Two strongly suggests that propofol-sedated mice are experiencing a hyper-inflammatory response in the lung, and that this appears to promote a systemic inflammatory response to severe bacteremia, further analysis of the characteristics of this altered response are needed. These alterations appear to mimic several classic signs of clinical sepsis and thus it is critical that other manifestations of sepsis be investigated.

In addition to the over-expression of both pro- and anti-inflammatory genes found during sepsis, activation of the complement pathway and the coagulation system occur. As discussed in Chapter 1.3, the complement cascade is an important defense against *K. pneumoniae* through opsonization and formation of the membrane attack complex, but excessive activation can lead to tissue damage and organ dysfunction. This pathway could be analyzed in significant detail through both gene expression analysis of liver tissue and protein quantitation in both bronchoalveolar lavage (BAL) fluid from infected lungs and serum. This could enable temporal profiling of both the initial response and subsequent systemic cascade as sepsis progresses. Likewise, the coagulation system is tightly linked to the inflammatory response and excessive activation can lead to both hemorrhage and microvascular thrombosis, again precipitating tissue damage and organ dysfunction (223,224). This pathway, as well as its counter-regulation by anticoagulation mechanisms, can also be analyzed through liver and lung gene expression and protein analysis in parallel to the complement pathway.

Diagnostic testing is a routine method of analyzing organ function in the clinic and would be valuable information toward a broad understanding of the immune status of infected mice. Serum chemistry can be analyzed with a variety of metabolic panels that provide a snapshot of a patient's health and are required in the diagnosis of sepsis. Total protein levels increase during infection while albumin levels decrease and both can indicate infection in a patient. Blood urea nitrogen (BUN) and creatinine levels also increase and these serve as biomarkers of kidney dysfunction. For detecting liver injury, the combination of alanine aminotransferase (ALT), aspartate aminotransferase (ALT), and bilirubin are frequently assessed (159,165). While these tests are well established clinical metrics, extensive research has identified dozens of other proteins that may serve as biomarkers of acute organ injury and dysfunction, or of sepsis in general. These serum chemistry panels are conveniently available through the Biological Research Laboratory (BRL) and would serve as a critical litmus test of the hypothesis that propofol is potentiating sepsis with acute organ dysfunction.

Similar to serum chemistry, complete blood counts (CBC) are frequently utilized to obtain a snapshot of the status of both the white and red blood cell compartments, as well as platelets. Abnormally high or low white cell counts are one of the criteria identified for the diagnosis of systemic inflammatory response syndrome (SIRS) and thus sepsis. When ordered with a "differential," the white cell counts are further subdivided in to lymphocytes, monocytes, neutrophils, basophils, and eosinophils, which can not only indicate infection, but potentially distinguish the type of pathogen and thus dictate the treatment plan pursued.

5.4. How does propofol alter host recruitment?

As identified in Chapter Two, G-CSF expression was significantly increased following propofol sedation and subsequent *Klebsiella* infection and this highlighted the likelihood that propofol was increasing emergency granulopoiesis, thus an interesting direction to follow up on would be to analyze

the hematopoietic compartment. Granulopoiesis takes place in the bone marrow (BM) and is the process by which hematopoietic stem and progenitor cells (HSPCs) differentiate into granulocytes such as neutrophils. Emergency granulopoiesis is primarily driven by G-CSF derived from endothelial cells in a TLR4/MyD88-dependent manner (218). Having found that propofol precipitated large increases in G-CSF expression during infection, a relevant follow-up would be to assess how propofol is affecting the cellularity in the BM and the relative maturity of these neutrophils both in the BM and as they enter the periphery using flow cytometry. Another clinical aspect of sepsis is lymphocyte exhaustion and apoptosis (223), highlighted by depletion of T, B, and dendritic cells both in the spleen and periphery. While there is a clear role for both dendritic cells and T cells in the innate response to *K. pneumoniae* as highlighted in Chapter 1.3, it appears that the Swiss Webster mouse is a poor model for adaptive immunity to *K. pneumoniae* due to the exceptional susceptibility found. The propofol gene hyper-expression phenotype was recapitulated in the more resistant C57BL/6 mouse, which could likely serve as a superior model for studying the adaptive immune response to *K. pneumoniae* lung infection/sepsis in the context of propofol.

An in depth analysis of the responding immune cells in infected lungs could provide valuable insight into whether or not propofol is simply increasing the number of cells being recruited or is fundamentally altering recruiting patterns. Furthermore, *ex vivo* stimulation of *K. pneumoniae* infection control-critical immune populations sorted using fluorescence-activated cell sorting (FACS) would enable assessments of functionality and responsiveness, specifically addressing phagocytosis, the oxidative burst, cytokine and chemokine production, and chemotaxis. As was discussed earlier, propofol appears to suppress pro-inflammatory programming in macrophages *in vitro* and so it would be important to investigate this phenotype *in vivo* with physiological cross talk occurring. It is important to remember that both airway epithelium (antimicrobial peptides, cytokine/chemokine expression) and vascular

endothelium (primary source of G-CSF) are contributing to the observed hyper-inflammatory response and thus it would be prudent to delineate the effects propofol has on them in the context of infection.

This level of analysis could potentially highlight one or more specific cell populations that display the most significantly altered phenotypes *in vivo* and would be exceptional candidates for transcript analysis. While qRT-PCR was a viable approach for broad phenotyping in the lung, working toward a molecular mechanism of propofol will require a global approach to profile gene expression changes. This would be accomplished via RNA sequencing (RNAseq), comparing the transcriptomes of the target cell type from naïve mice, control-sedated infected mice, and propofol-sedated infected mice. Relative changes for each gene would be quantified and statistically significant results identified. Once these targets are validated with qRT-PCR, pathway analysis could be utilized to identify distinct circuitry affected by propofol, potentially leading back to one or a handful of potential proteins propofol could be acting on directly. Validated genes could also be cross referenced against published transcriptome datasets to identify potential upstream targets.

While an *ex vivo* transcriptome would likely gather the most physiologically relevant data, it is possible that critical information could be lost during the harvesting and sorting of individual cell populations. Therefore a standard cell culture model could be employed, stimulated with either live or heat-killed bacteria in the presence or absence of propofol, allowing total RNA to be extracted much faster. These datasets would then require validation and pathway analysis as previously discussed.

Continuing with the use of a cell culture model, initial ground work has been started to establish a line of inquiry into what cell types would be ideal for pursuing mechanistic studies. As discussed earlier, it appears that certain immune cells, despite a restricted $GABA_AR$ subunit repertoire, still form functional $GABA_A$ receptors. Using RAW 264.7 murine macrophages as a starting cell line, qRT-PCR primers were validated for all known proteins associated with the GABA machinery in the nervous

system (excluding specific subunits). Several transcripts were detected, although no coherent picture of how this fragmented pathway may function has been formed. Moving forward, investigating this pathway *in vitro* and how it may or may not contribute to the propofol effect could be assessed by readily available pharmacological inhibitors and agonists of the $GABA_AR$. Understanding this pathway will aid in teasing apart the involvement of other receptors and pathways that could additionally be contributing to the phenotype. Finally, the use of a cell line would also allow for knock-down or knockout lines to be developed, should a target be identified, using small interfering (si)RNA or CRISPR/Cas9 technology, respectively.

5.5. Propofol alters required *K. pneumoniae* virulence repertoire

That propofol is perturbing the immune response to bacterial infection is clear from these and previous studies in the Freitag lab. These alterations appear to be widespread and clearly affect multiple routes of infection by phylogenetically diverse bacteria with disparate virulence strategies. Based on these observations, it was hypothesized that propofol's effects should be reflected in the required virulence factor repertoire of a given pathogen. While no less than six studies have utilized signature-tagged mutagenesis or transposon mutagenesis to identify *in vivo K. pneumoniae* virulence determinants (42,187–191), our insertion sequencing (InSeq) approach detailed in Chapter Four utilized a library of unprecedented size to identify not only novel lung virulence determinants, but also genes that are differentially required depending on the anesthetic the animal was exposed to prior to infection. Many of the identified mutants were found to have not only competitive defects compared to the wild type (WT) parent stain, but defects in a non-competitive infection as well.

The resolution and consistency of the resulting dataset is remarkable considering these mice were infected with 10^6 CFU, a dose that could have easily overwhelmed lung defenses by 24 hours and dramatically altered the reliability of the output. Indeed, data at 48 hours post-infection was also

attempted, but the majority of animals were unable to survive that long. The mutants identified from the 24 hour data were assayed for virulence at 24 hours as well in follow-up experiments, however, it remains unknown whether the defects identified are transient. This could be assessed by measuring burdens along a time course and comparing viability to WT. It would also be useful to identify whether any of these mutants have defects in dissemination, which could also be assayed during the time course. While this approach presented a novel aspect of propofol's impact on the immune responses to *K. pneumoniae* lung infection, much work remains to understand what these differentially affected virulence factors are contributing during infection.

An in depth analysis of the *K. pneumoniae* genome based on this new dataset could provide significant clarity by identifying specific pathways alternately affected by sedative exposure and could lead to a new understanding of one or more aspects of propofol's underlying mechanisms. Of the genes investigated that subsequently demonstrated differential phenotypes, only *glnB* had been characterized. It encodes the regulatory protein PII that directly controls glutamine synthetase activity in response to the nitrogen status of the bacterium. While the *gln* operon contains at least six members, InSeq results indicated that this phenotype is found only with *glnB*. *VirK, 1993*, and *1398* are all annotated as unknown or hypothetical, and characterization of these gene products would be valuable. Furthermore, dozens more genes were identified in the screen that could potentially have more dramatic differential fitness defects, but were excluded from early consideration due to excessive variance. Relaxing the parameters would highlight the next best candidates for further analysis.

5.6. Comparing and contrasting infectious *in vivo* models

As discussed in Chapter 1.8, the work by Visvabharathy et al (135,136) represents the most in depth analysis of propofol immunomodulation *in vivo* to date. Both of these studies investigated bloodstream infection models with Gram positive bacteria following brief sedation with the anesthetic

propofol, compared to the studies described in chapters two through four using *K. pneumoniae* and an intra-nasal route of infection. Despite these obvious differences, broad trends were identified across all three models. First, differences in elevated bacterial burdens were noted in the primary organs for mice sedated with propofol. While the differences were most dramatic in the *L. monocytogenes* model at 72 and 96 hours post-infection, significant differences were also seen at multiple time points in *S. aureus*-infected kidneys and in *K. pneumoniae*-infected lungs at several dosages. Combined, these results strongly suggest that propofol is causing systemic immunosuppression that is precipitating a non-optimal immune response to infection. Second, all three models demonstrated radical alterations in the physiological structure of the primary organs following propofol sedation. *L. monocytogenes*-infected spleens were found to lose their red pulp/white pulp structure, while *S. aureus*-infected kidneys developed large abscesses that could not be resolved as far out as 32 days post-infection. Similarly, *K. pneumoniae*-infected lungs were found to recruit abnormally large populations of immune cells by 24 hours post-infection and to develop significant areas of dense *K. pneumoniae* replication by 72 hours. It remains unclear in all three systems whether this observed pathology is the result of poorly-restrained bacterial growth and/or the production of bacterial enzymes and toxins, or self-inflicted damage caused by the responding immune cell populations. This question could potentially be addressed using mutant strains of a bacterium that otherwise demonstrate reduced virulence *in vivo* and assessing organ pathology at the same time point(s).

While the both the *L. monocytogenes* and *S. aureus* studies investigated specific immune cell populations being recruited to sites of infection, this was not addressed in the *K. pneumoniae* model directly, instead analyzing gene and protein expression during the course of lung infection and dissemination. As discussed in chapter 5.4, flow cytometric analyses of immune cell populations and *ex vivo* assessment of functionality would test the hypothesis of the systemic immunosuppression by

propofol. Conversely, analysis of gene expression in infected primary organs in both the *L. monocytogenes* and *S. aureus* models could corroborate the hypothesis as well.

Serum protein levels were investigated during infection with *L. monocytogenes* and significant alterations were noted in propofol-sedated mice, however, expression levels and kinetics were not comparable between that model and *K. pneumoniae*-infected mice shown in chapter two. This could be explained most readily by the disparate immune responses elicited *in vivo* and the fact that the bloodstream infection model bypassed mucosal immunity, which could alter the alarm cascade initiated by the bacterium. Furthermore, it is well demonstrated that resolution of *K. pneumoniae* infection requires inflammatory monocytes and neutrophils, whereas resolution of *L. monocytogenes* requires a robust cytotoxic $CD8^+$ T cell response. To determine if these serum protein alterations are the result of the bacterium or the route of infection, intra-nasal infections could be performed with the Gram negative *Klebsiella* relative, *Escherichia (E.)* coli, or with *S. aureus*, as both are significant causes of nosocomial pneumonias (140). While there are notable similarities in all models, more work is needed to comprehensively assess what aspects of propofol immunosuppression could be construed as universal and what aspects are specific to the pathogen in question.

5.7. Conclusions and Proposed Model

The secondary pharmacology of propofol is unquestionably pleotropic and much remains to be elucidated, especially with regards to the use of propofol in infected individuals. The majority of infection-related work has used simplified *in vitro* models with pure LPS as a stimulus on a single, homogenous cell population. These results, combined with clinical data from non-infected patients, have led to propofol being characterized as anti-inflammatory. The *in vivo* studies presented herein and previously published by this lab have highlighted that propofol may present a significant, yet underappreciated, risk factor in the context of infections. Acute sedation with propofol has been linked

to prolonged dysfunction of the immune response to bacterial challenge in a variety of models that, while not always demonstrable in viable CFU counts, results in significant pathology in primary organs and an impaired ability of the host to resolve infection in a timely manner.

With regard to this *Klebsiella pneumoniae* lung infection model, we hypothesize the model illustrated in figure 5.1 to broadly describe how propofol is altering the course of infection. Following sedation, *K. pneumoniae* is aspirated into the lungs, where it begins to replicate. Propofol suppresses the antimicrobial capabilities of the phagocytic immune populations early during infection, but quickly leads to a hyper-inflammatory state in the lungs. This excessive inflammation recruits large numbers of immune cells to the lungs from marginal pools that are also potentially functionally deficient. These responders may resolve the infection, or they may fail and containment is lost, leading to significant dissemination. The uncontrolled infection triggers emergency granulopoiesis, depleting mature reserves of granulocytes necessary for *K. pneumoniae* clearance. Further failure of the immune system to resolve infection results in an exhaustion of effective responders, acute organ dysfunction, and ultimately death.

The immune response is fantastically complex with layers of cross talk and regulation *in vivo*, much of which is still not well understood. *In vitro* models have identified several potential mechanisms by which propofol could affect the ability of various immune cell populations to appropriately respond to a pathogen, including potential suppression of both leukotriene and prostaglandin synthesis, suppression of cytokine and chemokine transcription, and competitive inhibition of fMLP binding to its receptor (Fig. 1.3). These hypotheses need to be investigated in an *in vivo* model of infection to determine their validity and applicability to understanding the hyper-inflammatory phenotype highlighted in chapter three. Concurrently, the digitalization of highly-detailed hospital records needs to be exploited to mine for associations and potential unidentified risks, such as exposure to propofol and the risk of subsequent infection.

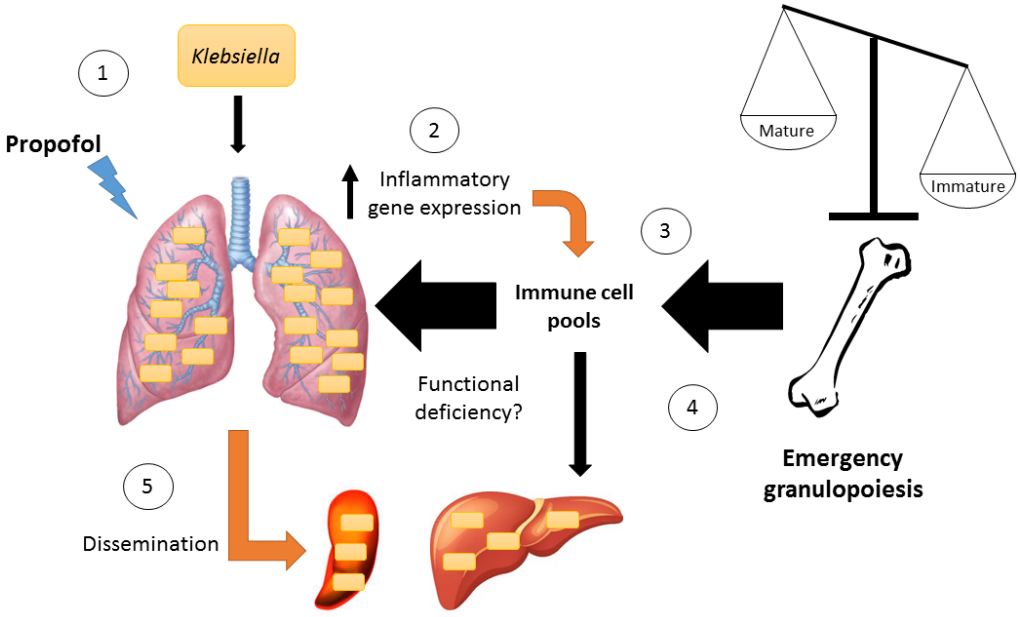

Figure 5.1. Proposed model of propofol's effects on *Klebsiella* lung infection. **(1)** Mice are sedated with propofol and infected with *K. pneumoniae*. **(2)** *Klebsiella* begins multiplying in the lung, triggering a hyper-inflammatory gene expression response in lung tissue. **(3)** The hyper-inflammatory response results in dramatically increased immune cell responder recruitment to the lungs from marginal pools, however these responders may have functional deficiencies preventing optimal clearance of *Klebsiella*. **(4)** Depletion of marginal pools plus increasing colony-stimulating factor production switches the hematopoietic compartment from steady-state to emergency granulopoiesis and mobilizes a large population of mature granulocytes to attack increasing *Klebsiella* threat, depleting mature populations. **(5)** *Klebsiella* disseminates from the lungs to distal organs; uncontrolled burdens result in mature granulocyte depletion and ineffective utilization of immature populations, ultimately resulting in death.

6. LITERATURE CITED

1. Trevisan. Sul micrococco della rabia e sulla possibilità di riconoscere durante il periodo d'incubazione, dall'esame del sangue della persona morsicata, se ha contratta l'infezione rabbica. R C Ist Lomb Ser II. 1885;20:88–105.

2. Brisse S, Grimont F, Grimont PAD. The Genus Klebsiella. In: Dr MDP, Falkow S, Rosenberg E, Schleifer K-H, Stackebrandt E, editors. The Prokaryotes [Internet]. Springer New York; 2006. p. 159–96. Available from: http://link.springer.com/referenceworkentry/10.1007/0-387-30746-X_8

3. Bagley ST. Habitat association of Klebsiella species. Infect Control IC. 1985 Feb;6(2):52–8.

4. Forsythe SJ, Abbott SL, Pitout J. Klebsiella, Enterobacter, Citrobacter, Cronobacter, Serratia, Plesiomonas,and OtherEnterobacteriaceae. 2015 Jun 1;714–37.

5. Diancourt L, Passet V, Verhoef J, Grimont PAD, Brisse S. Multilocus Sequence Typing of Klebsiella pneumoniae Nosocomial Isolates. J Clin Microbiol. 2005 Aug;43(8):4178–82.

6. Brisse S, Fevre C, Passet V, Issenhuth-Jeanjean S, Tournebize R, Diancourt L, et al. Virulent Clones of Klebsiella pneumoniae: Identification and Evolutionary Scenario Based on Genomic and Phenotypic Characterization. PLoS ONE [Internet]. 2009 Mar 25 [cited 2017 Aug 7];4(3). Available from: http://www.ncbi.nlm.nih.gov/pmc/articles/PMC2656620/

7. Bialek-Davenet S, Criscuolo A, Ailloud F, Passet V, Jones L, Delannoy-Vieillard A-S, et al. Genomic Definition of Hypervirulent and Multidrug-Resistant Klebsiella pneumoniae Clonal Groups. Emerg Infect Dis. 2014 Nov;20(11):1812–20.

8. Holt KE, Wertheim H, Zadoks RN, Baker S, Whitehouse CA, Dance D, et al. Genomic analysis of diversity, population structure, virulence, and antimicrobial resistance in Klebsiella pneumoniae, an urgent threat to public health. Proc Natl Acad Sci U S A. 2015 Jul 7;112(27):E3574–81.

9. Wyres KL, Holt KE. Klebsiella pneumoniae Population Genomics and Antimicrobial-Resistant Clones. Trends Microbiol. 2016 Dec;24(12):944–56.

10. Ramirez MS, Traglia GM, Lin DL, Tran T, Tolmasky ME. Plasmid-Mediated Antibiotic Resistance and Virulence in Gram-Negatives: the Klebsiella pneumoniae Paradigm. Microbiol Spectr [Internet]. 2014 Oct 24;2(5). Available from: http://www.asmscience.org/content/journal/microbiolspec/10.1128/microbiolspec.PLAS-0016-2013

11. Podschun R, Ullmann U. Klebsiella spp. as Nosocomial Pathogens: Epidemiology, Taxonomy, Typing Methods, and Pathogenicity Factors. Clin Microbiol Rev. 1998 Oct;11(4):589–603.

12. Ko W-C, Paterson DL, Sagnimeni AJ, Hansen DS, Von Gottberg A, Mohapatra S, et al. Community-Acquired Klebsiella pneumoniae Bacteremia: Global Differences in Clinical Patterns. Emerg Infect Dis. 2002 Feb;8(2):160–6.

13. Cheng D-L, Liu Y-C, Yen M-Y, Liu cheng-Y, Wang R-S. Septic Metastatic Lesions of Pyogenic Liver Abscess: Their Association With Klebsiella pneumoniae Bacteremia in Diabetic Patients. Arch Intern Med. 1991 Aug 1;151(8):1557–9.

14. Chang FY, Chou MY. Comparison of pyogenic liver abscesses caused by Klebsiella pneumoniae and non-K. pneumoniae pathogens. J Formos Med Assoc Taiwan Yi Zhi. 1995 May;94(5):232–7.

15. Braiteh F, Golden MP. Cryptogenic invasive Klebsiella pneumoniae liver abscess syndrome. Int J Infect Dis. 2007 Jan 1;11(1):16–22.

16. Ku Y-H, Chuang Y-C, Chen C-C, Lee M-F, Yang Y-C, Tang H-J, et al. Klebsiella pneumoniae Isolates from Meningitis: Epidemiology, Virulence and Antibiotic Resistance. Sci Rep. 2017 Jul 26;7(1):6634.

17. Bodey GP, Elting LS, Rodriquez S, Hernandez M. Klebsiella bacteremia. A 10-year review in a cancer institution. Cancer. 1989 Dec 1;64(11):2368–76.

18. Feldman C, Smith C, Levy H, Ginsburg P, Miller SD, Koornhof HJ. Klebsiella pneumoniae bacteraemia at an urban general hospital. J Infect. 1990 Jan 1;20(1):21–31.

19. Chen L, Todd R, Kiehlbauch J, Walters M, Kallen A. Notes from the Field: Pan-Resistant New Delhi Metallo-Beta-Lactamase-Producing Klebsiella pneumoniae — Washoe County, Nevada, 2016. MMWR Morb Mortal Wkly Rep [Internet]. 2017;66. Available from: https://www.cdc.gov/mmwr/volumes/66/wr/mm6601a7.htm

20. Moon WK, Im JG, Yeon KM, Han MC. Complications of Klebsiella pneumonia: CT evaluation. J Comput Assist Tomogr. 1995 Apr;19(2):176–81.

21. Ganesan S, Comstock AT, Sajjan US. Barrier function of airway tract epithelium. Tissue Barriers [Internet]. 2013 Oct 1 [cited 2017 Aug 2];1(4). Available from: http://www.ncbi.nlm.nih.gov/pmc/articles/PMC3783221/

22. Paczosa MK, Mecsas J. Klebsiella pneumoniae: Going on the Offense with a Strong Defense. Microbiol Mol Biol Rev MMBR. 2016 Jun 15;80(3):629–61.

23. Coya JM, Akinbi HT, Sáenz A, Yang L, Weaver TE, Casals C. Natural anti-infective pulmonary proteins: In vivo cooperative action of surfactant protein SP-A and the lung antimicrobial peptide SP-BN. J Immunol Baltim Md 1950. 2015 Aug 15;195(4):1628–36.

24. Merle NS, Noe R, Halbwachs-Mecarelli L, Fremeaux-Bacchi V, Roumenina LT. Complement System Part II: Role in Immunity. Front Immunol [Internet]. 2015 May 26 [cited 2017 Aug 2];6. Available from: http://www.ncbi.nlm.nih.gov/pmc/articles/PMC4443744/

25. Broug-Holub E, Toews GB, van Iwaarden JF, Strieter RM, Kunkel SL, Paine R, et al. Alveolar macrophages are required for protective pulmonary defenses in murine Klebsiella pneumonia: elimination of alveolar macrophages increases neutrophil recruitment but decreases bacterial clearance and survival. Infect Immun. 1997 Apr;65(4):1139–46.

26. Xiong H, Carter RA, Leiner IM, Tang Y-W, Chen L, Kreiswirth BN, et al. Distinct Contributions of Neutrophils and CCR2+ Monocytes to Pulmonary Clearance of Different Klebsiella pneumoniae Strains. Infect Immun. 2015 Sep;83(9):3418–27.

27. Ye P, Garvey PB, Zhang P, Nelson S, Bagby G, Summer WR, et al. Interleukin-17 and Lung Host Defense againstKlebsiella pneumoniae Infection. Am J Respir Cell Mol Biol. 2001 Sep 1;25(3):335–40.

28. Hirche TO, Gaut JP, Heinecke JW, Belaaouaj A. Myeloperoxidase Plays Critical Roles in Killing *Klebsiella pneumoniae* and Inactivating Neutrophil Elastase: Effects on Host Defense. J Immunol. 2005 Feb 1;174(3):1557–65.

29. Kumar V, Sharma A. Neutrophils: Cinderella of innate immune system. Int Immunopharmacol. 2010 Nov 1;10(11):1325–34.

30. Batra S, Cai S, Balamayooran G, Jeyaseelan S. Intrapulmonary Administration of Leukotriene B4 Augments Neutrophil Accumulation and Responses in the Lung to Klebsiella Infection in CXCL1 Knockout Mice. J Immunol Baltim Md 1950. 2012 Apr 1;188(7):3458–68.

31. Bhan U, Lukacs NW, Osterholzer JJ, Newstead MW, Zeng X, Moore TA, et al. TLR9 Is Required for Protective Innate Immunity in Gram-Negative Bacterial Pneumonia: Role of Dendritic Cells. J Immunol. 2007 Sep 15;179(6):3937–46.

32. Moore TA, Moore BB, Newstead MW, Standiford TJ. γδ-T Cells Are Critical for Survival and Early Proinflammatory Cytokine Gene Expression During Murine Klebsiella Pneumonia. J Immunol. 2000 Sep 1;165(5):2643–50.

33. Price AE, Reinhardt RL, Liang H-E, Locksley RM. Marking and Quantifying IL-17A-Producing Cells In Vivo. PLoS ONE [Internet]. 2012 Jun 29 [cited 2017 Aug 7];7(6). Available from: http://www.ncbi.nlm.nih.gov/pmc/articles/PMC3387253/

34. Happel KI, Dubin PJ, Zheng M, Ghilardi N, Lockhart C, Quinton LJ, et al. Divergent roles of IL-23 and IL-12 in host defense against Klebsiella pneumoniae. J Exp Med. 2005 Sep 19;202(6):761–9.

35. Gaffen SL, Jain R, Garg AV, Cua DJ. The IL-23-IL-17 immune axis: from mechanisms to therapeutic testing. Nat Rev Immunol. 2014 Sep;14(9):585–600.

36. Tecle T, Tripathi S, Hartshorn KL. Review: Defensins and cathelicidins in lung immunity. Innate Immun. 2010 Jun;16(3):151–9.

37. Cramer EP, Dahl SL, Rozell B, Knudsen KJ, Thomsen K, Moser C, et al. Lipocalin-2 from both myeloid cells and the epithelium combats Klebsiella pneumoniae lung infection in mice. Blood. 2017 May 18;129(20):2813–7.

38. Ye P, Rodriguez FH, Kanaly S, Stocking KL, Schurr J, Schwarzenberger P, et al. Requirement of Interleukin 17 Receptor Signaling for Lung Cxc Chemokine and Granulocyte Colony-Stimulating Factor Expression, Neutrophil Recruitment, and Host Defense. J Exp Med. 2001 Aug 20;194(4):519–28.

39. Balamayooran G, Batra S, Balamayooran T, Cai S, Pacher P, Jeyaseelan S. Intrapulmonary G-CSF Rescues Neutrophil Recruitment to the Lung and Neutrophil Release to Blood in Gram-negative Bacterial Infection in MCP-1−/− Mice. J Immunol Baltim Md 1950. 2012 Dec 15;189(12):5849–59.

40. Marshall JC. The effects of granulocyte colony-stimulating factor in preclinical models of infection and acute inflammation. Shock Augusta Ga. 2005 Dec;24 Suppl 1:120–9.

41. Aujla SJ, Chan YR, Zheng M, Fei M, Askew DJ, Pociask DA, et al. IL-22 mediates mucosal host defense against Gram-negative bacterial pneumonia. Nat Med. 2008 Mar;14(3):275–81.

42. Lawlor MS, Hsu J, Rick PD, Miller VL. Identification of Klebsiella pneumoniae virulence determinants using an intranasal infection model. Mol Microbiol. 2005 Nov 1;58(4):1054–73.

43. Cortés G, Borrell N, de Astorza B, Gómez C, Sauleda J, Albertí S. Molecular Analysis of the Contribution of the Capsular Polysaccharide and the Lipopolysaccharide O Side Chain to the Virulence of Klebsiella pneumoniae in a Murine Model of Pneumonia. Infect Immun. 2002 May;70(5):2583–90.

44. Yeh K-M, Kurup A, Siu LK, Koh YL, Fung C-P, Lin J-C, et al. Capsular Serotype K1 or K2, Rather than magA and rmpA, Is a Major Virulence Determinant for Klebsiella pneumoniae Liver Abscess in Singapore and Taiwan. J Clin Microbiol. 2007 Feb;45(2):466–71.

45. Fang C-T, Chuang Y-P, Shun C-T, Chang S-C, Wang J-T. A Novel Virulence Gene in Klebsiella pneumoniae Strains Causing Primary Liver Abscess and Septic Metastatic Complications. J Exp Med. 2004 Mar 1;199(5):697–705.

46. Clements A, Tull D, Jenney AW, Farn JL, Kim S-H, Bishop RE, et al. Secondary Acylation of Klebsiella pneumoniae Lipopolysaccharide Contributes to Sensitivity to Antibacterial Peptides. J Biol Chem. 2007 May 25;282(21):15569–77.

47. Llobet E, Martínez-Moliner V, Moranta D, Dahlström KM, Regueiro V, Tomás A, et al. Deciphering tissue-induced Klebsiella pneumoniae lipid A structure. Proc Natl Acad Sci U S A. 2015 Nov 17;112(46):E6369–78.

48. Follador R, Heinz E, Wyres KL, Ellington MJ, Kowarik M, Holt KE, et al. The diversity of Klebsiella pneumoniae surface polysaccharides. Microb Genomics [Internet]. 2016 Aug 25 [cited 2017 Aug 7];2(8). Available from: http://www.ncbi.nlm.nih.gov/pmc/articles/PMC5320592/

49. Merino S, Camprubí S, Albertí S, Benedí VJ, Tomás JM. Mechanisms of Klebsiella pneumoniae resistance to complement-mediated killing. Infect Immun. 1992 Jun;60(6):2529–35.

50. Álvarez D, Merino S, Tomás JM, Benedí VJ, Albertí S. Capsular Polysaccharide Is a Major Complement Resistance Factor in Lipopolysaccharide O Side Chain-Deficient Klebsiella pneumoniae Clinical Isolates. Infect Immun. 2000 Feb;68(2):953–5.

51. Albertí S, Alvarez D, Merino S, Casado MT, Vivanco F, Tomás JM, et al. Analysis of complement C3 deposition and degradation on Klebsiella pneumoniae. Infect Immun. 1996 Nov;64(11):4726–32.

52. Cassat JE, Skaar EP. Iron in Infection and Immunity. Cell Host Microbe. 2013 May 15;13(5):509–19.

53. Fischbach MA, Lin H, Liu DR, Walsh CT. In vitro characterization of IroB, a pathogen-associated C-glycosyltransferase. Proc Natl Acad Sci U S A. 2005 Jan 18;102(3):571–6.

54. Fischbach MA, Lin H, Zhou L, Yu Y, Abergel RJ, Liu DR, et al. The pathogen-associated iroA gene cluster mediates bacterial evasion of lipocalin 2. Proc Natl Acad Sci U S A. 2006 Oct 31;103(44):16502–7.

55. Bach S, de Almeida A, Carniel E. The Yersinia high-pathogenicity island is present in different members of the family Enterobacteriaceae. FEMS Microbiol Lett. 2000 Feb 1;183(2):289–94.

56. Vernet V, Philippon A, Madoulet C, Vistelle R, Jaussaud R, Chippaux C. Virulence factors (aerobactin and mucoid phenotype) in Klebsiella pneumoniae and Escherichia coli blood culture isolates. FEMS Microbiol Lett. 1995 Jul 15;130(1):51–7.

57. Lawlor MS, O'Connor C, Miller VL. Yersiniabactin Is a Virulence Factor for Klebsiella pneumoniae during Pulmonary Infection. Infect Immun. 2007 Mar;75(3):1463–72.

58. Yu W-L, Ko W-C, Cheng K-C, Lee C-C, Lai C-C, Chuang Y-C. Comparison of prevalence of virulence factors for Klebsiella pneumoniae liver abscesses between isolates with capsular K1/K2 and non-K1/K2 serotypes. Diagn Microbiol Infect Dis. 2008 Sep 1;62(1):1–6.

59. Bachman MA, Oyler JE, Burns SH, Caza M, Lépine F, Dozois CM, et al. Klebsiella pneumoniae Yersiniabactin Promotes Respiratory Tract Infection through Evasion of Lipocalin 2 ▽. Infect Immun. 2011 Aug;79(8):3309–16.

60. Tan TY, Ong M, Cheng Y, Ng LSY. Hypermucoviscosity, rmpA, and aerobactin are associated with community-acquired Klebsiella pneumoniae bacteremic isolates causing liver abscess in Singapore. J Microbiol Immunol Infect [Internet]. 2017 Jul 14 [cited 2017 Aug 7]; Available from: http://www.sciencedirect.com/science/article/pii/S1684118217301433

61. Firon N, Ofek I, Sharon N. Carbohydrate-binding sites of the mannose-specific fimbrial lectins of enterobacteria. Infect Immun. 1984 Mar;43(3):1088–90.

62. Sebghati TAS, Korhonen TK, Hornick DB, Clegg S. Characterization of the Type 3 Fimbrial Adhesins of Klebsiella Strains. Infect Immun. 1998 Jun;66(6):2887–94.

63. Kline KA, Fälker S, Dahlberg S, Normark S, Henriques-Normark B. Bacterial Adhesins in Host-Microbe Interactions. Cell Host Microbe. 2009 Jun 18;5(6):580–92.

64. Struve C, Bojer M, Krogfelt KA. Identification of a Conserved Chromosomal Region Encoding Klebsiella pneumoniae Type 1 and Type 3 Fimbriae and Assessment of the Role of Fimbriae in Pathogenicity. Infect Immun. 2009 Nov;77(11):5016–24.

65. Rosenthal VD, Maki DG, Mehta Y, Leblebicioglu H, Memish ZA, Al-Mousa HH, et al. International Nosocomial Infection Control Consortium (INICC) report, data summary of 43 countries for 2007-2012. Device-associated module. Am J Infect Control. 2014 Sep 1;42(9):942–56.

66. Rosenthal VD, Al-Abdely HM, El-Kholy AA, AlKhawaja SAA, Leblebicioglu H, Mehta Y, et al. International Nosocomial Infection Control Consortium report, data summary of 50 countries for 2010-2015: Device-associated module. Am J Infect Control. 2016 Dec 1;44(12):1495–504.

67. Patel G, Huprikar S, Factor SH, Jenkins SG, Calfee DP. Outcomes of Carbapenem-Resistant Klebsiella pneumoniae Infection and the Impact of Antimicrobial and Adjunctive Therapies. Infect Control Amp Hosp Epidemiol. 2008 Dec;29(12):1099–106.

68. Son Y. Molecular mechanisms of general anesthesia. Korean J Anesthesiol. 2010 Jul;59(1):3–8.

69. Butterworth JF, Mackey DC, Wasnick JD. Chapter 8. Inhalation Anesthetics. In: Morgan & Mikhail's Clinical Anesthesiology [Internet]. 5th ed. New York, NY: The McGraw-Hill Companies; 2013 [cited 2017 Aug 13]. Available from: accessanesthesiology.mhmedical.com/content.aspx?aid=57231086

70. Darnobid JA. The Pharmacology of Total Intravenous Anesthesia. Int Anesthesiol Clin. 2015 Apr 1;53(2):13–27.

71. Klompas M, Li L, Szumita P, Kleinman K, Murphy MV. Associations Between Different Sedatives and Ventilator-Associated Events, Length of Stay, and Mortality in Patients Who Were Mechanically Ventilated. Chest. 2016 Jun 1;149(6):1373–9.

72. Upchurch CP, Grijalva CG, Russ S, Collins SP, Semler MW, Rice TW, et al. Comparison of Etomidate and Ketamine for Induction During Rapid Sequence Intubation of Adult Trauma Patients. Ann Emerg Med. 2017 Jan 1;69(1):24–33.e2.

73. Rudolph U, Antkowiak B. Molecular and neuronal substrates for general anaesthetics. Nat Rev Neurosci. 2004 Sep;5(9):709–20.

74. Ritter JM, Rang HP, Flower RJ, Henderson G. Rang & Dale's Pharmacology. 8th ed. Churchill Livingstone; 2015. 776 p.

75. Fritschy J-M, Panzanelli P. GABAA receptors and plasticity of inhibitory neurotransmission in the central nervous system. Eur J Neurosci. 2014 Jun 1;39(11):1845–65.

76. Vogt K. Diversity in GABAergic Signaling. Adv Pharmacol. 2015 Jan 1;73:203–22.

77. Braat S, Kooy RF. The GABAA Receptor as a Therapeutic Target for Neurodevelopmental Disorders. Neuron. 2015 Jun 3;86(5):1119–30.

78. Minami K, Wick MJ, Stern-Bach Y, Dildy-Mayfield JE, Brozowski SJ, Gonzales EL, et al. Sites of Volatile Anesthetic Action on Kainate (Glutamate Receptor 6) Receptors. J Biol Chem. 1998 Apr 3;273(14):8248–55.

79. Grasshoff C, Antkowiak B. Effects of isoflurane and enflurane on GABAA and glycine receptors contribute equally to depressant actions on spinal ventral horn neurones in rats. BJA Br J Anaesth. 2006 Nov 1;97(5):687–94.

80. Iacobucci GJ, Popescu GK. NMDA receptors: linking physiological output to biophysical operation. Nat Rev Neurosci. 2017 Apr;18(4):236–49.

81. Burgos CF, Yévenes GE, Aguayo LG. Structure and Pharmacologic Modulation of Inhibitory Glycine Receptors. Mol Pharmacol. 2016 Sep 1;90(3):318–25.

82. Löscher W, Rogawski MA. How theories evolved concerning the mechanism of action of barbiturates. Epilepsia. 2012 Dec 1;53:12–25.

83. Brodie MJ, Kwan P. Current position of phenobarbital in epilepsy and its future. Epilepsia. 2012 Dec 1;53:40–6.

84. Mo Y, Thomas MC, Karras GE. Barbiturates for the treatment of alcohol withdrawal syndrome: A systematic review of clinical trials. J Crit Care. 2016 Apr 1;32:101–7.

85. Olkkola KT, Ahonen J. Midazolam and Other Benzodiazepines. In: Modern Anesthetics [Internet]. Springer, Berlin, Heidelberg; 2008. p. 335–60. (Handbook of Experimental Pharmacology). Available from: https://link.springer.com/chapter/10.1007/978-3-540-74806-9_16

86. Sigel E, Steinmann ME. Structure, Function, and Modulation of GABAA Receptors. J Biol Chem. 2012 Nov 23;287(48):40224–31.

87. Bergen JM, Smith DC. A review of etomidate for rapid sequence intubation in the emergency department. J Emerg Med. 1997 Mar 1;15(2):221–30.

88. Hohl CM, Kelly-Smith CH, Yeung TC, Sweet DD, Doyle-Waters MM, Schulzer M. The Effect of a Bolus Dose of Etomidate on Cortisol Levels, Mortality, and Health Services Utilization: A Systematic Review. Ann Emerg Med. 2010 Aug 1;56(2):105–113.e5.

89. Drexler B, Jurd R, Rudolph U, Antkowiak B. Distinct actions of etomidate and propofol at β3-containing γ-aminobutyric acid type A receptors. Neuropharmacology. 2009 Sep 1;57(4):446–55.

90. Wagner RL, White PF, Kan PB, Rosenthal MH, Feldman D. Inhibition of Adrenal Steroidogenesis by the Anesthetic Etomidate. N Engl J Med. 1984 May 31;310(22):1415–21.

91. Raines DE. The Pharmacology of Etomidate and Etomidate Derivatives. Int Anesthesiol Clin. 2015 Apr 1;53(2):63–75.

92. Richards G, Schock P, Haefely W. Benzodiazepine receptors: new vistas. Semin Neurosci. 1991 Jun 1;3(3):191–203.

93. Tyler MW, Yourish HB, Ionescu DF, Haggarty SJ. Classics in Chemical Neuroscience: Ketamine. ACS Chem Neurosci. 2017 Jun 21;8(6):1122–34.

94. Zanos P, Moaddel R, Morris PJ, Georgiou P, Fischell J, Elmer GI, et al. NMDAR inhibition-independent antidepressant actions of ketamine metabolites. Nature. 2016 May 26;533(7604):481–6.

95. Zorrilla-Vaca A, Arevalo JJ, Escandón-Vargas K, Soltanifar D, Mirski MA. Infectious Disease Risk Associated with Contaminated Propofol Anesthesia, 1989–20141. Emerg Infect Dis. 2016 Jun;22(6):981–92.

96. Kanto J, Gepts E. Pharmacokinetic Implications for the Clinical Use of Propofol. Clin Pharmacokinet. 1989 Nov 1;17(5):308–26.

97. Kirkpatrick T, Cockshott ID, Douglas EJ, Nimmo WS. Pharmacokinetics of propofol (diprivan) in elderly patients. Br J Anaesth. 1988 Feb;60(2):146–50.

98. Wang H, Tompkins LM. CYP2B6: New Insights into a Historically Overlooked Cytochrome P450 Isozyme. Curr Drug Metab. 2008 Sep;9(7):598–610.

99. Favetta P, Dufresne C, Désage M, Païssé O, Perdrix JP, Boulieu R, et al. Detection of new propofol metabolites in human urine using gas chromatography/mass spectrometry and liquid chromatography/mass spectrometry techniques. Rapid Commun Mass Spectrom RCM. 2000;14(20):1932–6.

100. Favetta P, Degoute CS, Perdrix JP, Dufresne C, Boulieu R, Guitton J. Propofol metabolites in man following propofol induction and maintenance. Br J Anaesth. 2002 May;88(5):653–8.

101. Maas A, Maier C, Michel-Lauter B, Broecker S, Madea B, Hess C. Verification of propofol sulfate as a further human propofol metabolite using LC-ESI-QQQ-MS and LC-ESI-QTOF-MS analysis. Drug Metab Pers Ther. 2017 Mar 1;32(1):67–72.

102. Yip GMS, Chen Z-W, Edge CJ, Smith EH, Dickinson R, Hohenester E, et al. A propofol binding site on mammalian GABAA receptors identified by photolabeling. Nat Chem Biol. 2013 Nov;9(11):715–20.

103. Jayakar SS, Zhou X, Chiara DC, Dostalova Z, Savechenkov PY, Bruzik KS, et al. Multiple Propofol-binding Sites in a γ-Aminobutyric Acid Type A Receptor (GABAAR) Identified Using a Photoreactive Propofol Analog♦. J Biol Chem. 2014 Oct 3;289(40):27456–68.

104. Eaton MM, Germann AL, Arora R, Cao LQ, Gao X, Shin DJ, et al. Multiple Non-Equivalent Interfaces Mediate Direct Activation of GABAA Receptors by Propofol. Curr Neuropharmacol. 2016 Oct;14(7):772–80.

105. Maldifassi MC, Baur R, Sigel E. Functional sites involved in modulation of the GABAA receptor channel by the intravenous anesthetics propofol, etomidate and pentobarbital. Neuropharmacology. 2016 Jun;105:207–14.

106. McCollum JSC, Milligan KR, Dundee JW. The antiemetic action of propofol. Anaesthesia. 1988 Mar 1;43(3):239–40.

107. Cavazzuti M, Porro CA, Barbieri A, Galetti A. Brain and spinal cord metabolic activity during propofol anaesthesia. Br J Anaesth. 1991 Apr;66(4):490–5.

108. Barann M, Dilger JP, Bönisch H, Göthert M, Dybek A, Urban BW. Inhibition of 5-HT3 receptors by propofol: equilibrium and kinetic measurements. Neuropharmacology. 2000 May 1;39(6):1064–74.

109. Barann M, Linden I, Witten S, Urban BW. Molecular Actions of Propofol on Human 5-ht3a Receptors: Enhancement as Well as Inhibition by Closely Related Phenol Derivatives. Anesth Analg. 2008 Mar 1;106(3):846–57.

110. Grattidge P. Patient-controlled sedation using propofol in day surgery. Anaesthesia. 1992 Aug 1;47(8):683–5.

111. Biebuyck JF, Borgeat A, Wilder-Smith OHG, Suter PM. The Nonhypnotic Therapeutic Applications of Propofol. Anesthesiol J Am Soc Anesthesiol. 1994 Mar 1;80(3):642–56.

112. Grouzmann E, Borgeat A, Fathi M, Gaillard RC, Ravussin P. Plasma and cerebrospinal fluid concentration of neuropeptide Y, serotonin, and catecholamines in patients under propofol or isoflurane anesthesia. Can J Physiol Pharmacol. 2000 Feb;78(2):100–7.

113. Hans P, Deby C, Deby-Dupont G, Vrijens B, Albert A, Lamy M. Effect of propofol on in vitro lipid peroxidation induced by different free radical generating systems: a comparison with vitamin E. J Neurosurg Anesthesiol. 1996 Apr;8(2):154–8.

114. Hans P, Deby-Dupont G, Deby C, Pieron F, Verbesselt R, Franssen C, et al. Increase in antioxidant capacity of plasma during propofol anesthesia. J Neurosurg Anesthesiol. 1997 Jul;9(3):234–6.

115. Stratford N, Murphy P. Effect of lipid and propofol on oxidation of haemoglobin by reactive oxygen species. Br J Anaesth. 1997 Mar;78(3):320–2.

116. Stratford N, Murphy P. Antioxidant activity of propofol in blood from anaesthetized patients. Eur J Anaesthesiol. 1998 Mar;15(2):158–60.

117. Thiry J-C, Hans P, Deby-Dupont G, Mouythis-Mickalad A, Bonhomme V, Lamy M. Propofol scavenges reactive oxygen species and inhibits the protein nitration induced by activated polymorphonuclear neutrophils. Eur J Pharmacol. 2004 Sep 19;499(1):29–33.

118. Mikawa K, Akamatsu H, Nishina K, Shiga M, Maekawa N, Obara H, et al. Propofol inhibits human neutrophil functions. Anesth Analg. 1998 Sep;87(3):695–700.

119. Yang S-C, Chung P-J, Ho C-M, Kuo C-Y, Hung M-F, Huang Y-T, et al. Propofol Inhibits Superoxide Production, Elastase Release, and Chemotaxis in Formyl Peptide–Activated Human Neutrophils by Blocking Formyl Peptide Receptor 1. J Immunol. 2013 Jun 15;190(12):6511–9.

120. Murphy K. Janeway's Immunobiology. 8th ed. Garland Science; 2014. 888 p.

121. Inada T, Ueshima H, Shingu K. Intravenous anesthetic propofol suppresses leukotriene production in murine dendritic cells. J Immunotoxicol. 2013 Sep 1;10(3):262–9.

122. Dennis EA, Norris PC. Eicosanoid Storm in Infection and Inflammation. Nat Rev Immunol. 2015 Aug;15(8):511–23.

123. Okuno T, Koutsogiannaki S, Ohba M, Chamberlain M, Bu W, Lin F-Y, et al. Intravenous anesthetic propofol binds to 5-lipoxygenase and attenuates leukotriene B4 production. FASEB J. 2017 Apr 1;31(4):1584–94.

124. Fourcade O, Simon M, Litt L, Samii K, Chap H. Propofol Inhibits Human Platelet Aggregation Induced by Proinflammatory Lipid Mediators. Anesth Analg. 2004 Aug 1;99(2):393–8.

125. Chen R-M, Wu C-H, Chang H-C, Wu G-J, Lin Y-L, Sheu J-R, et al. Propofol Suppresses Macrophage Functions and Modulates Mitochondrial Membrane Potential and Cellular Adenosine Triphosphate Synthesis. Anesthesiol J Am Soc Anesthesiol. 2003 May 1;98(5):1178–85.

126. Shiratsuchi H, Kouatli Y, Yu GX, Marsh HM, Basson MD. Propofol inhibits pressure-stimulated macrophage phagocytosis via the GABAA receptor and dysregulation of p130cas phosphorylation. Am J Physiol - Cell Physiol. 2009 Jun;296(6):C1400–10.

127. Wu G-J, Chen T-L, Chang C-C, Chen R-M. Propofol suppresses tumor necrosis factor-α biosynthesis in lipopolysaccharide-stimulated macrophages possibly through downregulation of nuclear factor-kappa B-mediated toll-like receptor 4 gene expression. Chem Biol Interact. 2009 Aug 14;180(3):465–71.

128. Meng T, Yu J, Lei Z, Wu J, Wang S, Bo Q, et al. Propofol Reduces Lipopolysaccharide-Induced, NADPH Oxidase (NOX2) Mediated TNF-α and IL-6 Production in Macrophages. Clin Dev Immunol [Internet]. 2013 [cited 2017 Aug 11];2013. Available from: http://www.ncbi.nlm.nih.gov/pmc/articles/PMC3859231/

129. Ulbrich F, Eisert L, Buerkle H, Goebel U, Schallner N. Propofol, but not ketamine or midazolam, exerts neuroprotection after ischaemic injury by inhibition of Toll-like receptor 4 and nuclear factor kappa-light-chain-enhancer of activated B-cell signalling: A combined in vitro and animal study. Eur J Anaesthesiol. 2016 Sep 1;33(9):670–80.

130. Fei F, Lee KM, McCarry BE, Bowdish DME. Age-associated metabolic dysregulation in bone marrow-derived macrophages stimulated with lipopolysaccharide. Sci Rep [Internet]. 2016 Mar 4 [cited 2017 Aug 11];6. Available from: http://www.ncbi.nlm.nih.gov/pmc/articles/PMC4778050/

131. Tanaka T, Takabuchi S, Nishi K, Oda S, Wakamatsu T, Daijo H, et al. The intravenous anesthetic propofol inhibits lipopolysaccharide-induced hypoxia-inducible factor 1 activation and suppresses the glucose metabolism in macrophages. J Anesth. 2010 Feb 1;24(1):54–60.

132. Devraj G, Beerlage C, Brüne B, Kempf VAJ. Hypoxia and HIF-1 activation in bacterial infections. Microbes Infect. 2017 Mar 1;19(3):144–56.

133. Lodge KM, Thompson AAR, Chilvers ER, Condliffe AM. Hypoxic regulation of neutrophil function and consequences for Staphylococcus aureus infection. Microbes Infect. 2017 Mar 1;19(3):166–76.

134. Schläpfer M, Piegeler T, Dull RO, Schwartz DE, Mao M, Bonini MG, et al. Propofol increases morbidity and mortality in a rat model of sepsis. Crit Care [Internet]. 2015 [cited 2017 Aug 9];19(1). Available from: http://www.ncbi.nlm.nih.gov/pmc/articles/PMC4344774/

135. Visvabharathy L, Xayarath B, Weinberg G, Shilling RA, Freitag NE. Propofol Increases Host Susceptibility to Microbial Infection by Reducing Subpopulations of Mature Immune Effector Cells at Sites of Infection. PLoS ONE [Internet]. 2015 Sep 18 [cited 2017 Aug 9];10(9). Available from: http://www.ncbi.nlm.nih.gov/pmc/articles/PMC4575148/

136. Visvabharathy L, Freitag NE. Propofol Sedation Exacerbates Kidney Pathology and Dissemination of Bacteria during Staphylococcus aureus Bloodstream Infections. Infect Immun. 2017 Jul 1;85(7):e00097-17.

137. Sydnor ERM, Perl TM. Hospital Epidemiology and Infection Control in Acute-Care Settings. Clin Microbiol Rev. 2011 Jan;24(1):141–73.

138. Yusef D, Shalakhti T, Awad S, Algharaibeh H, Khasawneh W. Clinical characteristics and epidemiology of sepsis in the neonatal intensive care unit in the era of multi-drug resistant organisms: A retrospective review. Pediatr Neonatol [Internet]. 2017 Jun 9 [cited 2017 Aug 9]; Available from: http://www.sciencedirect.com/science/article/pii/S1875957216301577

139. Haley RW, Culver DH, White JW, Morgan WM, Emori TG, Munn VP, et al. The efficacy of infection surveillance and control programs in preventing nosocomial infections in US hospitals. Am J Epidemiol. 1985 Feb;121(2):182–205.

140. Weiner LM, Webb AK, Limbago B, Dudeck MA, Patel J, Kallen AJ, et al. Antimicrobial-Resistant Pathogens Associated With Healthcare-Associated Infections: Summary of Data Reported to the National Healthcare Safety Network at the Centers for Disease Control and Prevention, 2011–2014. Infect Control Amp Hosp Epidemiol. 2016 Nov;37(11):1288–301.

141. Mayr FB, Yende S, Angus DC. Epidemiology of severe sepsis. Virulence. 2014 Jan 1;5(1):4–11.

142. Suarez De La Rica A, Gilsanz F, Maseda E. Epidemiologic trends of sepsis in western countries. Ann Transl Med [Internet]. 2016 Sep [cited 2017 Aug 9];4(17). Available from: http://www.ncbi.nlm.nih.gov/pmc/articles/PMC5050194/

143. Rosenthal VD, Richtmann R, Singh S, Apisarnthanarak A, Kübler A, Viet-Hung N, et al. Surgical site infections, International Nosocomial Infection Control Consortium (INICC) report, data summary of 30 countries, 2005-2010. Infect Control Hosp Epidemiol. 2013 Jun;34(6):597–604.

144. Jawan B, Kao Y-H, Goto S, Pan M-C, Lin Y-C, Hsu L-W, et al. Propofol pretreatment attenuates LPS-induced granulocyte–macrophage colony-stimulating factor production in cultured hepatocytes by suppressing MAPK/ERK activity and NF-κB translocation. Toxicol Appl Pharmacol. 2008 Jun 15;229(3):362–73.

145. Inada T, Kubo K, Shingu K. Promotion of interferon-gamma production by natural killer cells via suppression of murine peritoneal macrophage prostaglandin E2 production using intravenous anesthetic propofol. Int Immunopharmacol. 2010 Oct 1;10(10):1200–8.

146. Inada T, Kubo K, Ueshima H, Shingu K. Intravenous anesthetic propofol suppresses prostaglandin E2 production in murine dendritic cells. J Immunotoxicol. 2011 Dec 1;8(4):359–66.

147. Inada T, Hirota K, Shingu K. Intravenous anesthetic propofol suppresses prostaglandin E2 and cysteinyl leukotriene production and reduces edema formation in arachidonic acid-induced ear inflammation. J Immunotoxicol. 2015 Jul 3;12(3):261–5.

148. Li S, Wang C, Liu N, Liu P. Anti-inflammatory Effects of Propofol on Lipopolysaccharides-Treated Rat Hepatic Kupffer Cells. Cell Biochem Biophys. 2015 Mar 1;71(2):845–50.

149. Zhou C, Zhu Y, Zhao P, Xu C, Zhang M, Huang H, et al. Propofol Inhibits Lipopolysaccharide-induced Inflammatory Responses in Spinal Astrocytes via the Toll-like Receptor 4/myd88-dependent

Nuclear Factor-κb, Extracellular Signal-regulated Protein Kinases1/2, and p38 Mitogen-activated Protein Kinase Pathways. Anesth Analg. 2015 Jun 1;120(6):1361–8.

150. Tasdogan M, Memis D, Sut N, Yuksel M. Results of a pilot study on the effects of propofol and dexmedetomidine on inflammatory responses and intraabdominal pressure in severe sepsis. J Clin Anesth. 2009 Sep;21(6):394–400.

151. Logan LK, Weinstein RA. The Epidemiology of Carbapenem-Resistant Enterobacteriaceae: The Impact and Evolution of a Global Menace. J Infect Dis. 2017 Feb 15;215(suppl_1):S28–36.

152. Rodrigo-Troyano A, Sibila O. The respiratory threat posed by multidrug resistant Gram-negative bacteria. Respirology. :n/a-n/a.

153. Stephenson EH, Moeller RB, York CG, Young HW. Nose-only versus whole-body aerosol exposure for induction of upper respiratory infections of laboratory mice. Am Ind Hyg Assoc J. 1988 Mar;49(3):128–35.

154. Franklin GA, Scott MJ, Patel M, Hoth JJ, Peyton JC, Cheadle WG. A novel model of pneumonia from intraperitoneal injection of bacteria. Am J Surg. 2003 Nov 1;186(5):493–9.

155. Ren X, Lv F, Fang B, Liu S, Lv H, He G, et al. Anesthetic agent propofol inhibits myeloid differentiation factor 88-dependent and independent signaling and mitigates lipopolysaccharide-mediated reactive oxygen species production in human neutrophils in vitro. Eur J Pharmacol. 2014 Dec 5;744:164–72.

156. Borges da Silva H, Fonseca R, Pereira RM, Cassado A dos A, Álvarez JM, D'Império Lima MR. Splenic Macrophage Subsets and Their Function during Blood-Borne Infections. Front Immunol [Internet]. 2015 Sep 22 [cited 2017 Aug 22];6. Available from: http://www.ncbi.nlm.nih.gov/pmc/articles/PMC4585205/

157. Xiong H, Keith JW, Samilo DW, Carter RA, Leiner IM, Pamer EG. Innate lymphocyte/Ly6Chi monocyte crosstalk promotes Klebsiella pneumoniae clearance. Cell. 2016 Apr 21;165(3):679–89.

158. Page AV, Liles WC. Biomarkers of endothelial activation/dysfunction in infectious diseases. Virulence. 2013 Apr 19;4(6):507–16.

159. Arabestani MR, Rastiany S, Kazemi S, Mousavi SM. Conventional, molecular methods and biomarkers molecules in detection of septicemia. Adv Biomed Res. 2015 Jan 1;4(1):120.

160. Kali A, Charles MVP, Seetharam RSK. Hepcidin - A novel biomarker with changing trends. Pharmacogn Rev. 2015;9(17):35–40.

161. Benz F, Roy S, Trautwein C, Roderburg C, Luedde T. Circulating MicroRNAs as Biomarkers for Sepsis. Int J Mol Sci [Internet]. 2016 Jan 9 [cited 2017 Aug 18];17(1). Available from: http://www.ncbi.nlm.nih.gov/pmc/articles/PMC4730322/

162. Aird WC. Phenotypic Heterogeneity of the Endothelium: I. Structure, Function, and Mechanisms. Circ Res. 2007 Feb 2;100(2):158–73.

163. Edgar JDM, Gabriel V, Gallimore JR, McMillan SA, Grant J. A prospective study of the sensitivity, specificity and diagnostic performance of soluble intercellular adhesion molecule 1, highly sensitive C-reactive protein, soluble E-selectin and serum amyloid A in the diagnosis of neonatal infection. BMC Pediatr. 2010 Apr 16;10:22.

164. Whalen MJ, Doughty LA, Carlos TM, Wisniewski SR, Kochanek PM, Carcillo JA. Intercellular adhesion molecule-1 and vascular cell adhesion molecule-1 are increased in the plasma of children with sepsis-induced multiple organ failure. Crit Care Med. 2000 Jul;28(7):2600–7.

165. Jeter CB, Hylin MJ, Hergenroeder GW, Hill JL, Johnson DR, Barrera JA, et al. Biomarkers of Organ Injury. Recent Pat Biomark. 2014;4(2):98–109.

166. Hunter CA, Jones SA. IL-6 as a keystone cytokine in health and disease. Nat Immunol. 2015 May;16(5):448–57.

167. Modur V, Li Y, Zimmerman GA, Prescott SM, McIntyre TM. Retrograde inflammatory signaling from neutrophils to endothelial cells by soluble interleukin-6 receptor alpha. J Clin Invest. 1997 Dec 1;100(11):2752–6.

168. Hurst SM, Wilkinson TS, McLoughlin RM, Jones S, Horiuchi S, Yamamoto N, et al. IL-6 and Its Soluble Receptor Orchestrate a Temporal Switch in the Pattern of Leukocyte Recruitment Seen during Acute Inflammation. Immunity. 2001 Jun 1;14(6):705–14.

169. McLoughlin RM, Hurst SM, Nowell MA, Harris DA, Horiuchi S, Morgan LW, et al. Differential Regulation of Neutrophil-Activating Chemokines by IL-6 and Its Soluble Receptor Isoforms. J Immunol. 2004 May 1;172(9):5676–83.

170. Briso EM, Dienz O, Rincon M. Soluble IL-6R is produced by IL-6R ectodomain shedding in activated CD4 T cells. J Immunol Baltim Md 1950. 2008 Jun 1;180(11):7102–6.

171. Jones GW, McLoughlin RM, Hammond VJ, Parker CR, Williams JD, Malhotra R, et al. Loss of CD4+ T Cell IL-6R Expression during Inflammation Underlines a Role for IL-6 Trans Signaling in the Local Maintenance of Th17 Cells. J Immunol. 2010 Feb 15;184(4):2130–9.

172. Gruys E, Toussaint MJM, Niewold TA, Koopmans SJ. Acute phase reaction and acute phase proteins. J Zhejiang Univ Sci B. 2005 Nov;6(11):1045–56.

173. Li H-X, Liu Z-M, Zhao S-J, Zhang D, Wang S-J, Wang Y-S. Measuring both procalcitonin and C-reactive protein for a diagnosis of sepsis in critically ill patients. J Int Med Res. 2014 Aug 1;42(4):1050–9.

174. Chauhan N, Tiwari S, Jain U. Potential biomarkers for effective screening of neonatal sepsis infections: An overview. Microb Pathog. 2017 Jun 1;107:234–42.

175. Bottazzi B, Inforzato A, Messa M, Barbagallo M, Magrini E, Garlanda C, et al. The pentraxins PTX3 and SAP in innate immunity, regulation of inflammation and tissue remodelling. J Hepatol. 2016 Jun;64(6):1416–27.

176. Chen K-F, Chaou C-H, Jiang J-Y, Yu H-W, Meng Y-H, Tang W-C, et al. Diagnostic Accuracy of Lipopolysaccharide-Binding Protein as Biomarker for Sepsis in Adult Patients: A Systematic Review and Meta-Analysis. PLoS ONE [Internet]. 2016 Apr 7 [cited 2017 Aug 21];11(4). Available from: http://www.ncbi.nlm.nih.gov/pmc/articles/PMC4824361/

177. De Buck M, Gouwy M, Wang JM, Van Snick J, Proost P, Struyf S, et al. The cytokine-serum amyloid A-chemokine network. Cytokine Growth Factor Rev. 2016 Aug 1;30:55–69.

178. Rishi G, Wallace DF, Subramaniam VN. Hepcidin: regulation of the master iron regulator. Biosci Rep [Internet]. 2015 May 19 [cited 2017 Aug 20];35(3). Available from: http://www.ncbi.nlm.nih.gov/pmc/articles/PMC4438303/

179. Bauer M, Press AT, Trauner M. The liver in sepsis: patterns of response and injury. Curr Opin Crit Care. 2013 Apr;19(2):123–7.

180. Davies LC, Jenkins SJ, Allen JE, Taylor PR. Tissue-resident macrophages. Nat Immunol. 2013 Oct;14(10):986–95.

181. Davies LC, Rosas M, Jenkins SJ, Liao C-T, Scurr MJ, Brombacher F, et al. Distinct bone marrow-derived and tissue resident macrophage-lineages proliferate at key stages during inflammation. Nat Commun [Internet]. 2013 [cited 2017 Aug 22];4. Available from: http://www.ncbi.nlm.nih.gov/pmc/articles/PMC3842019/

182. Vasileiou I, Xanthos T, Koudouna E, Perrea D, Klonaris C, Katsargyris A, et al. Propofol: A review of its non-anaesthetic effects. Eur J Pharmacol. 2009 Mar 1;605(1):1–8.

183. Chen R-M, Chen T-G, Chen T-L, Lin L-L, Chang C-C, Chang H-C, et al. Anti-Inflammatory and Antioxidative Effects of Propofol on Lipopolysaccharide-Activated Macrophages. Ann N Y Acad Sci. 2005 May 1;1042(1):262–71.

184. Hsing C-H, Lin M-C, Choi P-C, Huang W-C, Kai J-I, Tsai C-C, et al. Anesthetic Propofol Reduces Endotoxic Inflammation by Inhibiting Reactive Oxygen Species-regulated Akt/IKKβ/NF-κB Signaling. PLoS ONE [Internet]. 2011 Mar 8 [cited 2017 Aug 30];6(3). Available from: http://www.ncbi.nlm.nih.gov/pmc/articles/PMC3050912/

185. Patel SB, Kress JP. Sedation and analgesia in the mechanically ventilated patient. Am J Respir Crit Care Med. 2012 Mar 1;185(5):486–97.

186. Magill SS, Li Q, Gross C, Dudeck M, Allen-Bridson K, Edwards JR. Incidence and Characteristics of Ventilator-Associated Events Reported to the National Healthcare Safety Network in 2014*. Crit Care Med. 2016 Dec;44(12):2154–62.

187. Maroncle N, Balestrino D, Rich C, Forestier C. Identification of Klebsiella pneumoniae Genes Involved in Intestinal Colonization and Adhesion Using Signature-Tagged Mutagenesis. Infect Immun. 2002 Aug;70(8):4729–34.

188. Struve C, Forestier C, Krogfelt KA. Application of a novel multi-screening signature-tagged mutagenesis assay for identification of Klebsiella pneumoniae genes essential in colonization and infection. Microbiology. 2003;149(1):167–76.

189. Lau HY, Clegg S, Moore TA. Identification of Klebsiella Pneumoniae Genes Uniquely Expressed in a Strain Virulent Using a Murine Model of Bacterial Pneumonia. Microb Pathog. 2007 Apr;42(4):148–55.

190. Tu Y-C, Lu M-C, Chiang M-K, Huang S-P, Peng H-L, Chang H-Y, et al. Genetic Requirements for Klebsiella pneumoniae-Induced Liver Abscess in an Oral Infection Model. Infect Immun. 2009 Jul;77(7):2657–71.

191. Bachman MA, Breen P, Deornellas V, Mu Q, Zhao L, Wu W, et al. Genome-Wide Identification of Klebsiella pneumoniae Fitness Genes during Lung Infection. mBio [Internet]. 2015 Jun 9 [cited 2017 Aug 23];6(3). Available from: http://www.ncbi.nlm.nih.gov/pmc/articles/PMC4462621/

192. Goodman AL, McNulty NP, Zhao Y, Leip D, Mitra RD, Lozupone CA, et al. Identifying genetic determinants needed to establish a human gut symbiont in its habitat. Cell Host Microbe. 2009 Sep 17;6(3):279–89.

193. Brooks JF, Gyllborg MC, Cronin DC, Quillin SJ, Mallama CA, Foxall R, et al. Global discovery of colonization determinants in the squid symbiont Vibrio fischeri. Proc Natl Acad Sci U S A. 2014 Dec 2;111(48):17284–9.

194. Goodman AL, Wu M, Gordon JI. Identifying microbial fitness determinants by Insertion Sequencing (INSeq) using genome-wide transposon mutant libraries. Nat Protoc. 2011 Nov 17;6(12):1969–80.

195. Broberg CA, Wu W, Cavalcoli JD, Miller VL, Bachman MA. Complete Genome Sequence of Klebsiella pneumoniae Strain ATCC 43816 KPPR1, a Rifampin-Resistant Mutant Commonly Used in Animal, Genetic, and Molecular Biology Studies. Genome Announc [Internet]. 2014 Sep 25 [cited 2017 Aug 16];2(5). Available from: http://www.ncbi.nlm.nih.gov/pmc/articles/PMC4175196/

196. Huang T-W, Lam I, Chang H-Y, Tsai S-F, Palsson BO, Charusanti P. Capsule deletion via a λ-Red knockout system perturbs biofilm formation and fimbriae expression in Klebsiella pneumoniae MGH 78578. BMC Res Notes. 2014 Jan 8;7:13.

197. Datsenko KA, Wanner BL. One-step inactivation of chromosomal genes in Escherichia coli K-12 using PCR products. Proc Natl Acad Sci U S A. 2000 Jun 6;97(12):6640–5.

198. Baba T, Ara T, Hasegawa M, Takai Y, Okumura Y, Baba M, et al. Construction of Escherichia coli K-12 in-frame, single-gene knockout mutants: the Keio collection. Mol Syst Biol. 2006 Feb 21;2:2006.0008.

199. Le Roux F, Binesse J, Saulnier D, Mazel D. Construction of a Vibrio splendidus Mutant Lacking the Metalloprotease Gene vsm by Use of a Novel Counterselectable Suicide Vector. Appl Environ Microbiol. 2007 Feb;73(3):777–84.

200. Wang N, Ozer EA, Mandel MJ, Hauser AR. Genome-Wide Identification of Acinetobacter baumannii Genes Necessary for Persistence in the Lung. mBio. 2014 Jul 1;5(3):e01163-14.

201. Henderson JC, Zimmerman SM, Crofts AA, Boll JM, Kuhns LG, Herrera CM, et al. The Power of Asymmetry: Architecture and Assembly of the Gram-Negative Outer Membrane Lipid Bilayer. Annu Rev Microbiol. 2016;70(1):255–78.

202. Holtel A, Merrick MJ. The Klebsiella pneumoniae PII protein (glnB gene product) is not absolutely required for nitrogen regulation and is not involved in NifL-mediated nif gene regulation. Mol Gen Genet MGG. 1989 Jun;217(2–3):474–80.

203. Arcondéguy T, van Heeswijk WC, Merrick M. Studies on the roles of GlnK and GlnB in regulating Klebsiella pneumoniae NifL-dependent nitrogen control. FEMS Microbiol Lett. 1999 Nov 1;180(2):263–70.

204. Henry CS, Rotman E, Lathem WW, Tyo KEJ, Hauser AR, Mandel MJ. Generation and Validation of the iKp1289 Metabolic Model for Klebsiella pneumoniae KPPR1. J Infect Dis. 2017 Feb 15;215(suppl_1):S37–43.

205. Ruland J. Return to homeostasis: downregulation of NF-κB responses. Nat Immunol. 2011 Aug;12(8):709–14.

206. Zhang Q, Lenardo MJ, Baltimore D. 30 Years of NF-κB: A Blossoming of Relevance to Human Pathobiology. Cell. 2017 Jan 12;168(1):37–57.

207. Pujari R, Hunte R, Khan WN, Shembade N. A20-mediated negative regulation of canonical NF-κB signaling pathway. Immunol Res. 2013 Dec 1;57(1–3):166–71.

208. Lee EG, Boone DL, Chai S, Libby SL, Chien M, Lodolce JP, et al. Failure to Regulate TNF-Induced NF-κB and Cell Death Responses in A20-Deficient Mice. Science. 2000 Sep 29;289(5488):2350–4.

209. Wertz IE, O'Rourke KM, Zhou H, Eby M, Aravind L, Seshagiri S, et al. De-ubiquitination and ubiquitin ligase domains of A20 downregulate NF-κB signalling. Nature. 2004 Aug 5;430(7000):694–9.

210. Wertz IE, Dixit VM. Signaling to NF-κB: Regulation by Ubiquitination. Cold Spring Harb Perspect Biol [Internet]. 2010 Mar [cited 2017 Aug 28];2(3). Available from: http://www.ncbi.nlm.nih.gov/pmc/articles/PMC2829959/

211. Trompouki E, Hatzivassiliou E, Tsichritzis T, Farmer H, Ashworth A, Mosialos G. CYLD is a deubiquitinating enzyme that negatively regulates NF-κB activation by TNFR family members. Nature. 2003 Aug 14;424(6950):793–6.

212. Kovalenko A, Chable-Bessia C, Cantarella G, Israël A, Wallach D, Courtois G. The tumour suppressor CYLD negatively regulates NF-κB signalling by deubiquitination. Nature. 2003 Aug 14;424(6950):801–5.

213. Kinjyo I, Hanada T, Inagaki-Ohara K, Mori H, Aki D, Ohishi M, et al. SOCS1/JAB Is a Negative Regulator of LPS-Induced Macrophage Activation. Immunity. 2002 Nov 1;17(5):583–91.

214. Liu B, Yang R, Wong KA, Getman C, Stein N, Teitell MA, et al. Negative Regulation of NF-κB Signaling by PIAS1. Mol Cell Biol. 2005 Feb;25(3):1113–23.

215. Maine GN, Mao X, Komarck CM, Burstein E. COMMD1 promotes the ubiquitination of NF-κB subunits through a cullin-containing ubiquitin ligase. EMBO J. 2007 Jan 24;26(2):436–47.

216. Welsby I, Goriely S. Regulation of Interleukin-23 Expression in Health and Disease. In: Regulation of Cytokine Gene Expression in Immunity and Diseases [Internet]. Springer, Dordrecht; 2016. p. 167–89. (Advances in Experimental Medicine and Biology). Available from: https://link.springer.com/chapter/10.1007/978-94-024-0921-5_8

217. Sheikh SZ, Matsuoka K, Kobayashi T, Li F, Rubinas T, Plevy SE. Cutting Edge: IFN-γ Is a Negative Regulator of IL-23 in Murine Macrophages and Experimental Colitis. J Immunol Baltim Md 1950. 2010 Apr 15;184(8):4069–73.

218. Boettcher S, Gerosa RC, Radpour R, Bauer J, Ampenberger F, Heikenwalder M, et al. Endothelial cells translate pathogen signals into G-CSF–driven emergency granulopoiesis. Blood. 2014 Aug 28;124(9):1393–403.

219. Court MH, Duan SX, Hesse LM, Venkatakrishnan K, Greenblatt DJ. Cytochrome P-450 2B6 Is Responsible for Interindividual Variability of Propofol Hydroxylation by Human Liver Microsomes. Anesthesiol J Am Soc Anesthesiol. 2001 Jan 1;94(1):110–9.

220. Honkakoski P, Zelko I, Sueyoshi T, Negishi M. The Nuclear Orphan Receptor CAR-Retinoid X Receptor Heterodimer Activates the Phenobarbital-Responsive Enhancer Module of the CYP2B Gene. Mol Cell Biol. 1998 Oct;18(10):5652–8.

221. Goodwin B, Moore LB, Stoltz CM, McKee DD, Kliewer SA. Regulation of the Human CYP2B6 Gene by the Nuclear Pregnane X Receptor. Mol Pharmacol. 2001 Sep 1;60(3):427–31.

222. Smirlis D, Muangmoonchai R, Edwards M, Phillips IR, Shephard EA. Orphan Receptor Promiscuity in the Induction of Cytochromes P450 by Xenobiotics. J Biol Chem. 2001 Apr 20;276(16):12822–6.

223. van der Poll T, van de Veerdonk FL, Scicluna BP, Netea MG. The immunopathology of sepsis and potential therapeutic targets. Nat Rev Immunol. 2017 Jul;17(7):407–20.

224. Levi M, van der Poll T. Coagulation and sepsis. Thromb Res. 2017 Jan 1;149:38–44.

7. APPENDIX: Identification of *Listeria monocytogenes* genes contributing to oxidative stress resistance under conditions relevant to host infection

7.1. Summary

The Gram positive bacterium *Listeria monocytogenes* survives in environments ranging from the soil to the cytosol of infected host cells. Key to *L. monocytogenes* intracellular survival is the activation of PrfA, a transcriptional regulator that is required for the expression of multiple bacterial virulence factors. Mutations that constitutively activate *prfA* (*prfA** mutations) result in high level expression of multiple bacterial virulence factors as well as the physiological adaptation of *L. monocytogenes* for optimal replication within host cells. Here we demonstrate that *L. monocytogenes prfA** mutants exhibit significantly enhanced resistance to oxidative stress in comparison to wild type strains. Transposon mutagenesis of *L. monocytogenes prfA** strains resulted in the identification of three novel gene targets required for full oxidative stress resistance only in the context of PrfA activation. One gene, *lmo0779*, predicted to encode an uncharacterized protein, and two additional genes known as *cbpA* and *ygbB*, encoding a cyclic-di-AMP binding protein and a 2-C-methyl-D-erythritol 2,4-cyclodiphosphate synthase respectively, contribute to the enhanced oxidative stress resistance of *prfA** strains while exhibiting no significant contribution in wild type *L. monocytogenes*. *ygbB* was unique among the three identified genes in being required for virulence in *prfA** strains. These results indicate that *L. monocytogenes* calls upon specific bacterial factors for stress resistance in the context of PrfA activation and thus under conditions favorable for bacterial replication within infected mammalian cells.

7.2. Introduction

Listeria monocytogenes is a Gram-positive bacterium that is widespread in the outside environment as well as in habitats where survival depends on the organism's ability to mitigate a variety of stresses, including fluctuations in temperature, salinity, and pH (1, 2). One important and medically

relevant habitat occupied by *L. monocytogenes* is the cytosol of infected mammalian cells, where intracellular replication of bacteria occurs within susceptible hosts and can result in devastating disease (3). *L. monocytogenes* is primarily a food-borne pathogen, and to reach its intracellular replication niche the bacteria must survive passage through the gastrointestinal (GI) tract and translocation across the intestinal barrier before reaching additional tissues for replication (4, 5). As a result, *L. monocytogenes* encounters numerous stress conditions that span large variations in pH and osmolarity as well as bacterial exposure to degradative enzymes (such as lysozyme) and reactive oxygen and nitrogen intermediates. Importantly, a number of bacterial gene products associated with stress resistance in *L. monocytogenes* have been identified and linked to successful survival in the environment and to intragastric survival, however less is known regarding how the bacterium manages stresses encountered during systemic infection (2, 6).

Oxidative stress is often considered to represent a significant host defense against pathogen invasion of host cells and tissues (7, 8). Professional phagocytes such as macrophages limit pathogen viability via the oxidative burst delivered following the assembly of the NADPH oxidase complex on the phagosome, however *L. monocytogenes* has been reported to be capable of antagonizing complex assembly (9). In addition to oxidative stress encountered during host infection, *Listeria*, like all aerobes, generates its own sources of oxidative stress via aerobic metabolism and as such has evolved mechanisms to protect itself. Superoxide (O_2^-) and hydrogen peroxide (H_2O_2) are generated during oxidative respiration and *L. monocytogenes* employs superoxide dismutase (SOD) and catalase, respectively, to neutralize these reactive species. Both O_2^- and H_2O_2 can react further with free heavy metals to form the highly potent hydroxyl (OH^-) radical, capable of reacting with most macromolecules (10). Other gene products reported to contribute to *L. monocytogenes* oxidative stress resistance include the metalloregulatory protein PerR and 2-Cys peroxiredoxin (Prx) (11-13).

2518 Recent evidence suggests that *L. monocytogenes* uses redox-responsive transcription factors to
2519 coordinate virulence factor expression within the host, and that the redox state of bacteria within host
2520 cells differs significantly from bacteria grown in broth culture (14, 15). The transition of *L.*
2521 *monocytogenes* from life as a saprophyte to life within host cells is primarily mediated by the virulence
2522 regulator PrfA, which activates the expression of core virulence factors required for growth in response
2523 to increased glutathione levels within the host cell (14). PrfA coordinates virulence factor gene
2524 expression while also modulating *L. monocytogenes* physiology to adapt bacteria to conditions favorable
2525 for intracellular replication (16-19). PrfA activity is maintained at a low basal level in the outside
2526 environment but the protein becomes highly activated upon cytosol access (14, 16-22). Ripio et al (23)
2527 identified a mutation within *prfA* (*prfA**) that resulted in the constitutive activation of PrfA and high
2528 level expression of PrfA-regulated genes in broth grown cultures; since this original description, a
2529 number of other amino acid substitutions have been identified that confer differing levels of PrfA
2530 activation (21, 24-28). The isolation of these various *prfA** mutant strains has enabled detailed
2531 characterization of the effects of PrfA activation on both patterns of *L. monocytogenes* gene expression
2532 and on bacterial physiology (16, 17, 29, 30). The constitutive activation of PrfA increases the
2533 susceptibility of *L. monocytogenes* to selected forms of stress, such as high salinity and low pH, while
2534 simultaneously optimizing growth on host relevant carbon sources (16, 31). As a result of these
2535 physiological changes, *prfA** strains exhibit reduced fitness in comparison to wild type bacteria in broth
2536 culture but are hypervirulent and have a competitive advantage over wild type bacteria in mouse
2537 models of infection (16, 32).
2538 Here we demonstrate that *L. monocytogenes prfA** strains are significantly more resistant to
2539 oxidative stress than wild type strains, a phenotype that may contribute to their competitive advantage
2540 within the infected host. The increased resistance to oxidative stress appears to be due at least in part
2541 to gene products that uniquely contribute to resistance during PrfA activation, with little to no

contribution detected in the absence of PrfA activation. Our results suggest that *L. monocytogenes* relies on specific subsets of gene products for stress resistance in a manner dependent on environmental status, with subsets of gene products contributing to aspects of stress resistance specific to conditions of PrfA activation.

7.3. Materials and Methods

Ethics statement.

This study was carried out in strict accordance with the recommendations in the Guide for the Care and Use of Laboratory Animals of the National Institutes of Health (Protocol number 15–126). Female outbred Swiss Webster mice, 6–8 weeks of age (Envigo, Chicago, IL, USA) were subjected to a 12-hr light/dark cycle with free access to food and water. Animals were carefully monitored twice daily for signs of distress (unkempt appearance, hunched posture, lethargy) and humane endpoints were used in all experiments such that any animal exhibiting severe discomfort, an inability to move around or attain food, water, etc., was euthanized immediately. Euthanasia was carried out via CO_2 inhalation from a bottled source followed by cervical dislocation. Animal suffering and distress was minimized by monitoring the animals as described above and in that tail vein injections were carried out with only brief periods (< 5 minutes) of physical restraint.

Bacterial strains, media, and culture conditions.

L. monocytogenes 10403S (NF-100) (55), 10403S *prfA* L140F [*prfA* actA-gus-neo*, NF-L1166 (24)], and 10403S Δ*prfA* [NF-L890 (56)] were used in this study. All bacterial strains were grown overnight at 37°C with shaking in brain heart infusion broth (BHI) (Difco Laboratories, Detroit, MI, USA). Antibiotic concentrations were used as follows: ampicillin 100 μg ml^{-1}; chloramphenicol 5 ug ml^{-1}; erythromycin 2 μg ml^{-1}; lincomycin, 25 μg ml^{-1}; neomycin 10 μg ml^{-1}; and streptomycin 200 ug ml^{-1}.

Oxidative stress assay.

Strains were grown overnight at 37°C with shaking in BHI broth, and then subcultured by diluting cultures 1:20 into fresh BHI broth the following day and grown to mid-log phase. Optical density (OD 600 nm absorbance) for each strain was adjusted to 0.2. Hydrogen peroxide (Sigma-Aldrich, St. Louis, MO, USA) was diluted in fresh BHI broth to create a 1 molar working solution. In a 1.5 ml microcentrifuge tube, 890 µl of culture was mixed with 110 µl of BHI + 1 M H_2O_2 and incubated at room temperature for two hours. Viable bacteria were enumerated by serial dilution in 1X sterile phosphate buffered saline (PBS), plated on LB agar, and incubated at 37°C overnight.

Construction of a random Mariner transposon insertion library.

*L. monocytogenes prfA** strain (NF-L1166) was made electrocompetent as previously described (57). *E. coli* (NF-E1130) containing the Mariner transposase driven by the *B. subtilis mrgA* promoter on pMC38 (58) was grown on BHI agar containing 5 µg ml^{-1} chloramphenicol overnight and then grown in LB broth. Plasmid pMC38 was purified using the Qiagen Plasmid Midi Kit (Qiagen, Frederick, MD, USA). Plasmid pMC38 was introduced into electrocompetent *L. monocytogenes* 10403S *prfA** using a chilled 1-mm electroporation cuvette (BioRad, Hercules, CA, USA) and pulsed at 10 kV/cm, 400 Ω, and 25 µF. Cells were immediately resuspended in 1 ml fresh BHI broth containing 500 mM sucrose and incubated statically at 30°C for 1.5 hours. Transformants were selected on BHI agar containing 2 µg ml^{-1} erythromycin. Two independent transformations were carried out to generate two separate independent libraries. Transformants were then grown in fresh BHI broth overnight at 30°C while shaking. Cultures were diluted 1:200 in fresh BHI broth and grown with shaking at 30°C for one hour, then shifted to 40°C with shaking for an additional six hours until the OD_{600nm} registered between 0.3 and 0.5. Cultures were then plated on BHI agar + 2 µg ml^{-1} erythromycin with the remainder frozen in 1 ml aliquots with 20% sterile glycerol.

Screening of transposon libraries.

Frozen library aliquots were thawed and plated on BHI agar containing 2 ug ml^{-1} erythromycin and 10 ug ml^{-1} neomycin (to select for PrfA activation as measured by *actA-gus-neo* expression) and grown overnight at 37°C. Individual colonies were picked into 96 well plates containing 200 µl BHI broth and grown overnight at 37°C without shaking. The following day, optical densities were measured and 10 µl of each isolate culture was transferred in duplicate to a new 96 well plate containing 190 µl of BHI broth with 40 mM H_2O_2. Cultures were grown for 48 hours at 37°C statically and assessed for growth. Isolates failing to grow were retested under the same conditions before being verified individually.

Phage transduction.

Susceptible mutants were grown overnight at 37°C without shaking in 2 ml BHI + 2 µg ml^{-1} erythromycin + 10 µg ml^{-1} neomycin and then subcultured 1:10 in 2 ml fresh BHI broth. Cultures were grown for 3 hours at 30°C with shaking. In sterile 12x75 mm culture tubes, *Listeria* mutant cultures were mixed with phage in several ratios from 1:1 to 100:1 and incubated at room temperature statically for 40 minutes. Three ml of liquid LB soft agar (0.75% agar, 10 mM $CaCl_2$, 10 mM $MgSO_4$) was added to each tube, mixed, and then poured over a pre-warmed LB plate. Plates were grown overnight at room temperature. Two ml of TM buffer (10 mM Tris-HCl pH 7.5, 10 mM $MgSO_4$) were added to the plate with confluent plaques for each mutant. After 20 minutes, the soft agar with TM buffer was scraped into a 15 ml centrifuge tube (Denville Scientific, South Plainfield, NJ, USA) with a flame sterilized scoop and centrifuged at 8,000 rpm for 15 minutes. Supernatant was collected into a sterile microcentrifuge tube and 1/5 volume of chloroform was added. The solution was incubated at room temperature with rocking for 30 minutes. The recovered phage suspensions were incubated with either the 10403S or NF-L1166 (*prfA**) strains for the recovery of transductants containing the selected transposon insertion as follows: *Listeria* strains for phage transduction were grown overnight at 37°C with shaking, subcultured 1:40 in fresh BHI the following day, and grown at 30°C shaking to an OD of ~0.19. In separate tubes, 200 µl of *Listeria* were mixed with 100 µl of the phage library, plus 10 mM $CaCl_2$ and 10 mM $MgSO_4$, and

incubated at room temperature for 40 minutes with gentle shaking every 10 minutes. Each tube was then supplemented with 200 µl fresh BHI and incubated at 37°C with shaking for two hours. The cultures were plated on BHI + 2 µg ml^{-1} erythromycin plates and grown overnight at 37°C. Finally, each transductant was confirmed for the transposon encoded erythromycin resistance by streaking each colony on BHI + 25 µg ml^{-1} lincomycin plates.

Inverse PCR to identify transposon insertion sites.

Genomic DNA of sensitive mutants was isolated with GenElute Bacterial DNA Genomic DNA kit (Sigma-Aldrich). Genomic DNA was restriction digested with DpnI (New England Biolabs, Ipswich, MA, USA) according to the manufacturer's instructions. Digests were ligated with T4 DNA ligase (New England Biolabs) overnight at 16°C. Ligated loops were PCR amplified with primers p255-1 and Marq255, gel purified on a 0.8% TAE agarose gel with QIAquick Gel Extraction kit (Qiagen), and then Sanger sequenced with primer TnSeq (Table 1).

Complementation of LMRG_00235 (*lmo0553* or *cbpB*), LMRG_00467 (*lmo0779*), & *LMRG_02671* (*lmo0236* or *ygbB*).

Each gene was PCR amplified from the 10403S genome using primers listed in Table 1, restriction digested with BamHI overnight at 16°C, and then CIP treated for 1 hour at 37°C. The digested fragment was ligated into plasmid pPL2 (59) and sequence verified. The constructs were electroporated into *E. coli* SM10 cells and subsequently mated into *L. monocytogenes prfA** to generate *prfA* cpbB::tnHimar1*, *prfA* lmo0779::tnHimar1*, or *prfA* ygbB::tnHimar1* and selected for on BHI agar containing 200 ug ml^{-1} streptomycin and 5 ug ml^{-1} chloramphenicol.

Animal infections.

All animal procedures were approved by the University of Illinois at Chicago Animal Care Committee and were conducted in the Biological Resources Laboratory. $1x10^4$ colony forming units of each strain were injected via tail vein into 6- to 8-week old Swiss Webster mice (Envigo) as previously

described (60). After 72 hours, mice were sacrificed, livers and spleens isolated, homogenized, and plated on BHI agar for enumeration of bacterial burdens in each organ.

Statistical analyses.

In vivo infection assays were tested for significance using the nonparametric Mann-Whitney U test. All statistical tests were performed using Prism (GraphPad, La Jolla, CA).

Table 7.1: Strains, plasmids, and primers.

Strain	Feature(s)	Reference
NF-100	10403S parent strain	(55)
NF-1166	10403S *prfA L140F actA-gus-neo-plcB* (*prfA** strain)	(18)
NF-890	10403S Δ*prfA*	(27)
NF-4239	*prfA* ygbB*::tnHimar1	This Study
NF-4238	10403S *ygbB*::tnHimar1	This Study
NF-4241	*prfA* cbpA*::tnHimar1	This Study
NF-4240	10403S *cbpA*::tnHimar1	This Study
NF-4242	*prfA* lmo0779*::tnHimar1	This Study
NF-4241	10403S *lmo0779*::tnHimar1	This Study
NF-4245	*prfA* ygbB*::tnHimar1 + pPL2*(ygbB)*	This Study
NF-4247	*prfA* cbpA*::tnHimar1 + pPL2*(cbpA)*	This Study
NF-4249	*prfA* lmo0779*::tnHimar1 + pPL2(*lmo0779)*	This Study
Plasmid		
pPL2	Single copy integration vector	(59)
pPL2-*ygbB*	*ygbB* complementation vector	This Study
pPL2-*cbpA*	*cbpA* complementation vector	This Study
pPL2-*lmo0779*	*lmo0779* complementation vector	This Study
Primer		
p255-1	5’-TCT TTT AGC AAA CCC GTA TTC CAC G-3’	This Study
Marq255	5’-CAG TAC AAT CTG CTC TGA TGC CGC ATA GTT-3’	(58)
TnSeq	5’-ACA ATA AGG ATA AAT TTG AAT ACT AGT CTC GAG TGG GG-3’	This Study
*ygbB*_BamHI_F2	5’-CAC GGG ATC CTT GAG CGA ATT CCT TGT CCT-3’	This Study
*ygbB*_BamHI_R3	5’-CAG CGG ATC CGT ACA CGC ACT CGT TTT GT-3’	This Study
*cbpA*_BamHI_F1	5’-CGG GAT CCT CATTTT CAA GCT GTT TCA-3’	This Study
*cbpA*_BamHI_R2	5’-GCG GAT CCC GTT CTA CAC TTC CAC CAC CA-3’	This Study
*lmo0779*_BamHI_F2	5’-CGG GAT CCG GAA GTA AGC GTG GCG TTT-3’	This Study
*lmo0779*_BamHI_R2	5’-GCG GAT CCT TTT GTT AAC CAA CCG TGT C-3’	This Study

7.4. Results

Activation of PrfA via *prfA confers increased resistance of *L. monocytogenes* to oxidative stress.** During the course of host infection, *L. monocytogenes* is anticipated to encounter multiple exposures to oxidative stress (11, 15, 33). Given that activation of the central virulence regulator PrfA has been shown to increase bacterial fitness during host infection (16), we sought to determine whether constitutively activated *prfA** strains exhibited any changes in resistance to oxidative stress in comparison to wild type bacteria. An assay designed to assess killing by peroxide exposure *in vitro* was used to compare the oxidative stress resistance of wild type, *prfA*,* and *ΔprfA* strains. Strains were incubated in BHI medium containing 110 mM H_2O_2 and aliquots were removed at 30, 60, 90 and 120 minutes to determine bacterial viability by plating for colony forming units on LB agar. *L. monocytogenes prfA** strains were significantly more resistant to H_2O_2 exposure than wild type or *ΔprfA* strains, with up to 90% of bacteria remaining viable after two hours of exposure to H_2O_2 (Fig. 7.1A). In contrast, no viable CFU were observed following 90 minutes of peroxide exposure for wild type cells, and the *ΔprfA* mutant was even more susceptible with no viable colonies recovered after one hour. Resistance to peroxide exposure was influenced by culture density, such that wild type 10403S required a nearly two-fold greater cell density in the initial inoculum to withstand peroxide exposure than did the *prfA** mutant (Fig. 7.1B). These data indicate that activation of PrfA results in an enhancement in the ability of *L. monocytogenes* to survive exposure to oxidative stress.

Identification of transposon insertion mutations that reduce the resistance of *L. monocytogenes prfA strains to oxidative stress *in vitro*.** The ability of *prfA** strains to better withstand exposure to H_2O_2 suggested that PrfA activation influenced the expression of gene products contributing to oxidative stress resistance. We therefore sought to identify gene products that contribute to bacterial survival following H_2O_2 exposure by screening for transposon insertions mutants with reduced oxidative stress

resistance in the *prfA** background (Fig. 7.2). Mariner transposon random insertion libraries were constructed in *L. monocytogenes prfA** strains containing transcriptional fusions of *gus* and *neo* to the PrfA-dependent *actA* gene (*actA-gus-neo*) (24). The *actA-gus-neo* fusion allows selection of PrfA* activity based on increased expression of *gus*-encoded β-glucuronidase activity and *neo*-encoded neomycin resistance. Individual transposon insertion mutants were isolated on BHI plates containing 2 ug ml^{-1} erythromycin to select for the transposon insertion and 10 ug ml^{-1} neomycin to select for the retention of PrfA* activity. Isolated mutants were then inoculated into BHI medium with 10 ug ml^{-1} neomycin in 96 well plates and grown statically at 37°C overnight, then sub-cultured into BHI and neomycin and 40mM H_2O_2 and grown at 37°C for 48 hours. Transposon insertion mutants that failed to replicate in the presence of H_2O_2 were selected and retested to confirm increased sensitivity to H_2O_2 while maintaining PrfA* activity as assessed by neomycin resistance and blue colony color on GUS indicator plates.

Twenty-five mutants with increased sensitivity to hydrogen peroxide *in vitro* were identified after screening more than 7,500 transposon insertion mutant colonies. After the elimination of candidate mutants that exhibited growth defects in BHI broth with no H_2O_2 selection, the selected mutants were evaluated for sensitivity to 110mM H_2O_2 in BHI in comparison to wild type and *prfA** strains. A spectrum of mutant sensitivity to H_2O_2 was observed with 9 mutants demonstrating a 3-log or greater reduction in viable CFUs at 2 hours (Fig. 7.3). Three representative mutants were chosen for further analyses.

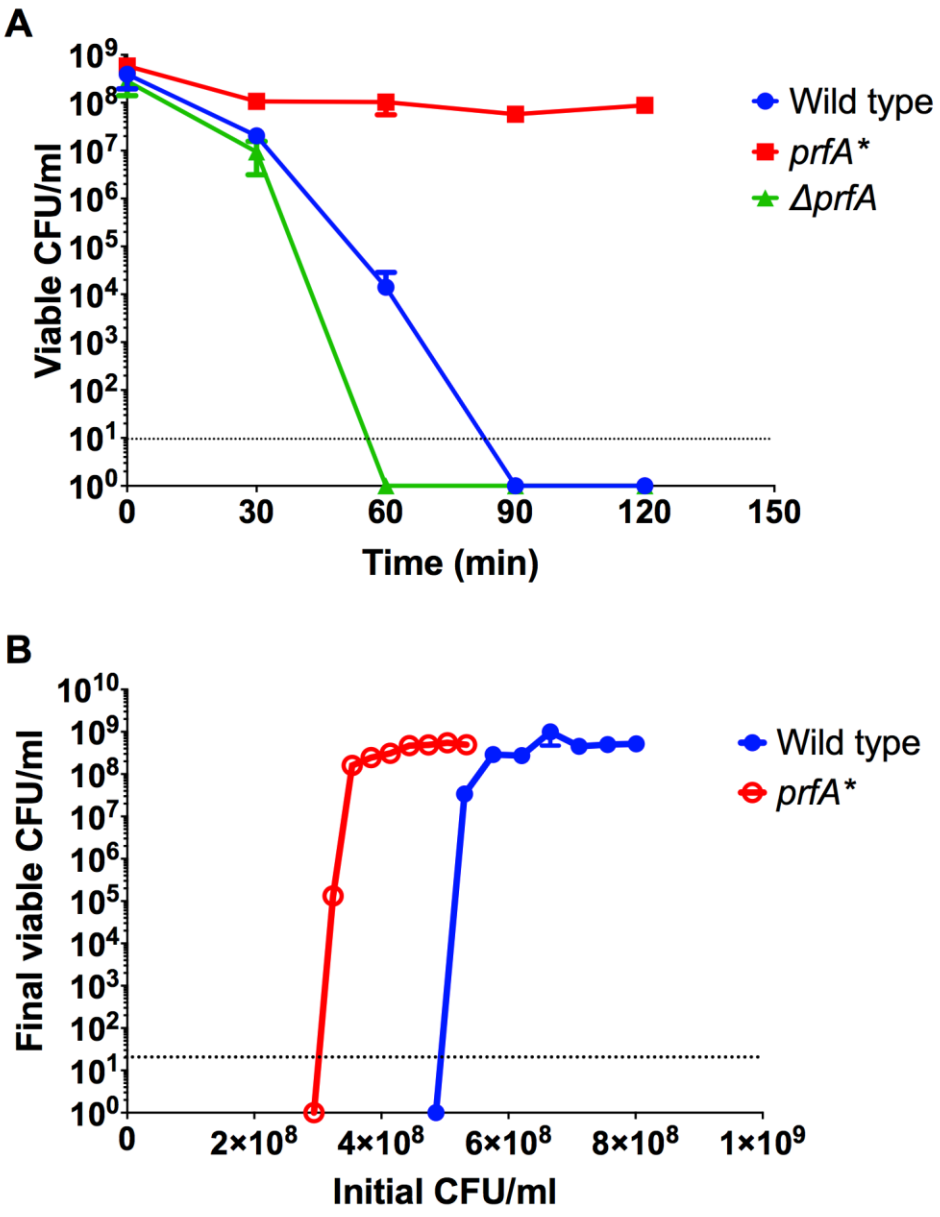

Figure 7.1. A *prfA strain is more resistant to H_2O_2-mediated killing in vitro.** Strains were grown to mid-log phase and adjusted to an OD of 0.2. 890 µl of culture was transferred to a 1.5 ml microcentrifuge tube and combined with 110 µl of freshly diluted 1M H_2O_2 solution in BHI. Tubes were incubated statically for two hours at room temperature and plated on LB agar for viable bacteria at 30 minute intervals (**A**) or after two hours (**B**). Data is representative of four independent experiments.

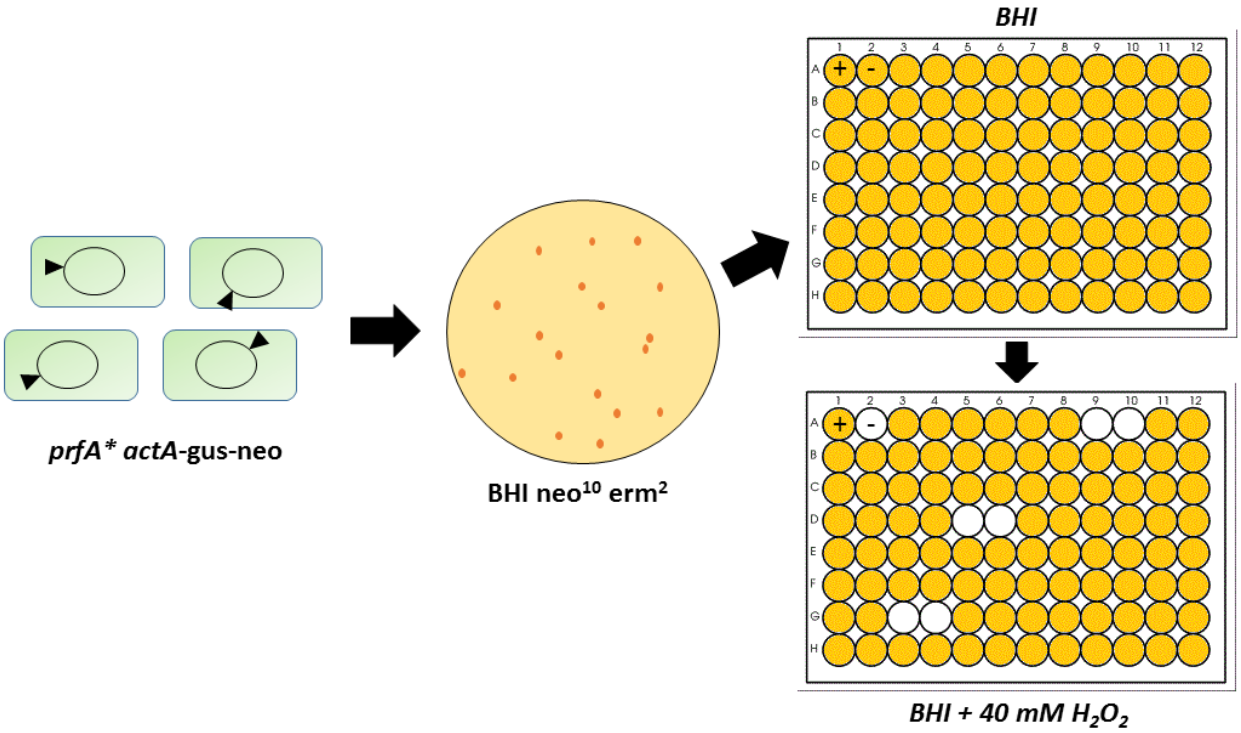

Figure 7.2. Screening of *L. monocytogenes prfA transposon insertion mutant libraries for increased sensitivity to hydrogen peroxide.** Two independently generated *prfA** transposon libraries were generated and randomly screened for increased sensitivity to 40 mM H_2O_2 in BHI medium. Individual mutants were picked into 200 µl BHI medium in 96-well plates and grown at 37°C statically overnight. The following day ODs were recorded and 10 µl of each culture was transferred in duplicate to new 96-well plates containing 190 µl of 40 mM H_2O_2 in BHI. These plates were grown statically at 37°C for 48 hours and mutants that failed to grow were rescreened for susceptibility. Transposon insertion sites were determined with inverse PCR and Sanger sequencing.

Identification of three genes associated with *prfA-dependent resistance to oxidative stress.**

Transposon insertion sites were identified within three selected mutants (Fig. 7.3). Two mutants contained insertion within predicted open reading frames: *LMRG_00235* (or *lmo0553*, using EGDe notation*)* and *LMRG_02671 (lmo0236)*, and in the immediate upstream region and predicted promoter region shared by LMRG_00467 (*lmo0779)* and LMRG_00468 (*lmo0780*) (Fig. 7.4A). *lmo0236*, also known as *ygbB*, encodes the enzyme 2-C-methyl-D-erythritol 2,4-cyclodiphosphate synthase (MEcPP synthase), part of the alternative 2-C-methyl-D-erythritol 4-phosphate (MEP) pathway for isoprenoid synthesis in bacteria (34). The MEP pathway has been associated with *L. monocytogenes* bile resistance (35) and has been reported to be required for full bacterial virulence in a mouse model of systemic infection (34). The functions of the *lmo0553* and *lmo0779/lmo0780* predicted gene products are not known, however the *lmo0553* gene product, also known as CbpA*,* has been identified as a binding receptor for the signaling molecule cyclic-di-AMP (c-di-AMP), associated with *L. monocytogenes* metabolism and cell wall synthesis (36, 37). Structural predictions using the Phyre2 protein fold prediction server (38) predicted that CbpA may function as a cytoplasmic transporter with potential magnesium and/or cobalt efflux function, while the *lmo0779* gene product is predicted to be membrane bound with a C-terminal cytoplasmic domain with potential nitrite/sulfite reductase activity and the *lmo0780* gene product may have DNA binding activity. All three transposon insertion mutants demonstrated a marked increase in sensitivity to H_2O_2 in the context of *prfA** (Fig. 7.4B-D) while exhibiting similar growth in BHI medium (Fig. 7.4E). The phenotype of each individual transposon insertion was confirmed following transduction into a clean *prfA* actA-gus-neo* genetic background. In addition, to assess the insertion mutant phenotypes in the absence of PrfA activation, each mutant was also transduced into the 10403S parent strain. All of the transposon insertions were found to recapitulate the original H_2O_2 sensitive phenotype when introduced back into *prfA** (Fig. 7.5A-C). Interestingly, none of the transposon insertions

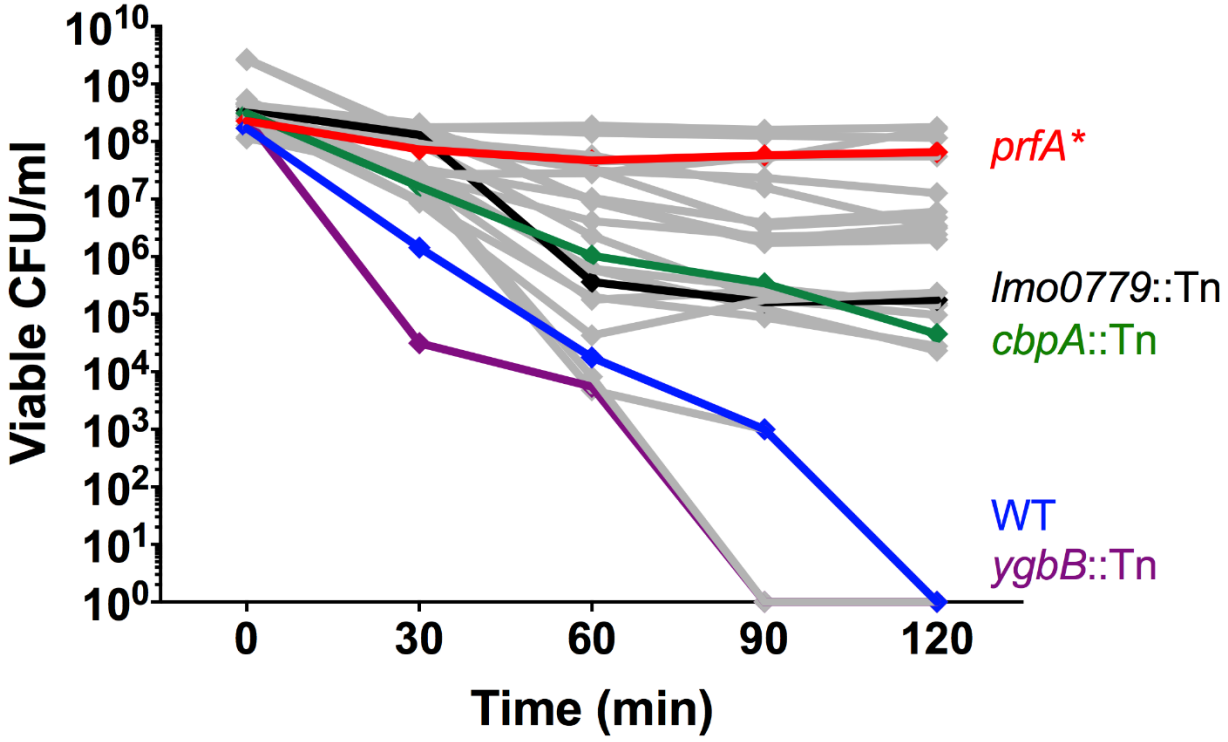

2728

2729 **Figure 7.3. H_2O_2 sensitivity profiles of candidate mutants.** Strains were grown to mid-log phase and

2730 incubated at room temperature with 110 mM H_2O_2 for two hours. Samples were taken every 30

2731 minutes and plated on BHI agar to enumerate viable CFUs.

increased wild type sensitivity to H_2O_2, indicating that the enhanced sensitivity to oxidative stress was only observed in the context of PrfA activation. Complementation of mutant phenotypes was achieved via the introduction of the wild type copy of each gene (*lmo0779* for the promoter insertion), confirming the role of each in enhancing *prfA** sensitivity to oxidative stress (Fig. 7.5A-C).

The *ygbB* gene product is required for *L. monocytogenes prfA virulence in mice.** Resistance of *L. monocytogenes* to oxidative stress is predicted to contribute to bacterial viability during host infection (11, 15, 33, 39, 40). We have previously demonstrated that *prfA** strains are hypervirulent in mouse models of infection (16), therefore we sought to determine how the transposon insertions that increase the sensitivity of *prfA** strains to oxidative stress might potentially impact bacterial virulence. Female 6-8 week old Swiss Webster mice were infected via tail vein injection with either *prfA** or the transposon insertions mutants in the *prfA** background. Strains containing insertions within *cbpA* or *lmo0779* exhibited no significant defects in virulence *in vivo* as assessed by the measurement of bacterial burdens in target organs at 72 hours post infection (Fig. 7.6). In contrast, strains containing the transposon insertion within *ygbB* exhibited severe virulence defects with approximately 1000-fold reductions in bacterial burdens in both liver and spleen in comparison to *prfA** strains. While *ygbB* is a component of the MEP pathway for isoprenoid synthesis and this pathway has been previously associated with *L. monocytogenes* virulence, the virulence defect observed for *prfA** strains lacking *ygbB* (1000-fold) appears larger than that observed for loss of MEP in wild type strains (10-100-fold defect) (34). These results confirm a critical role for the *ygbB* gene product during host infection, and suggest that some of its function may relate to oxidative stress resistance.

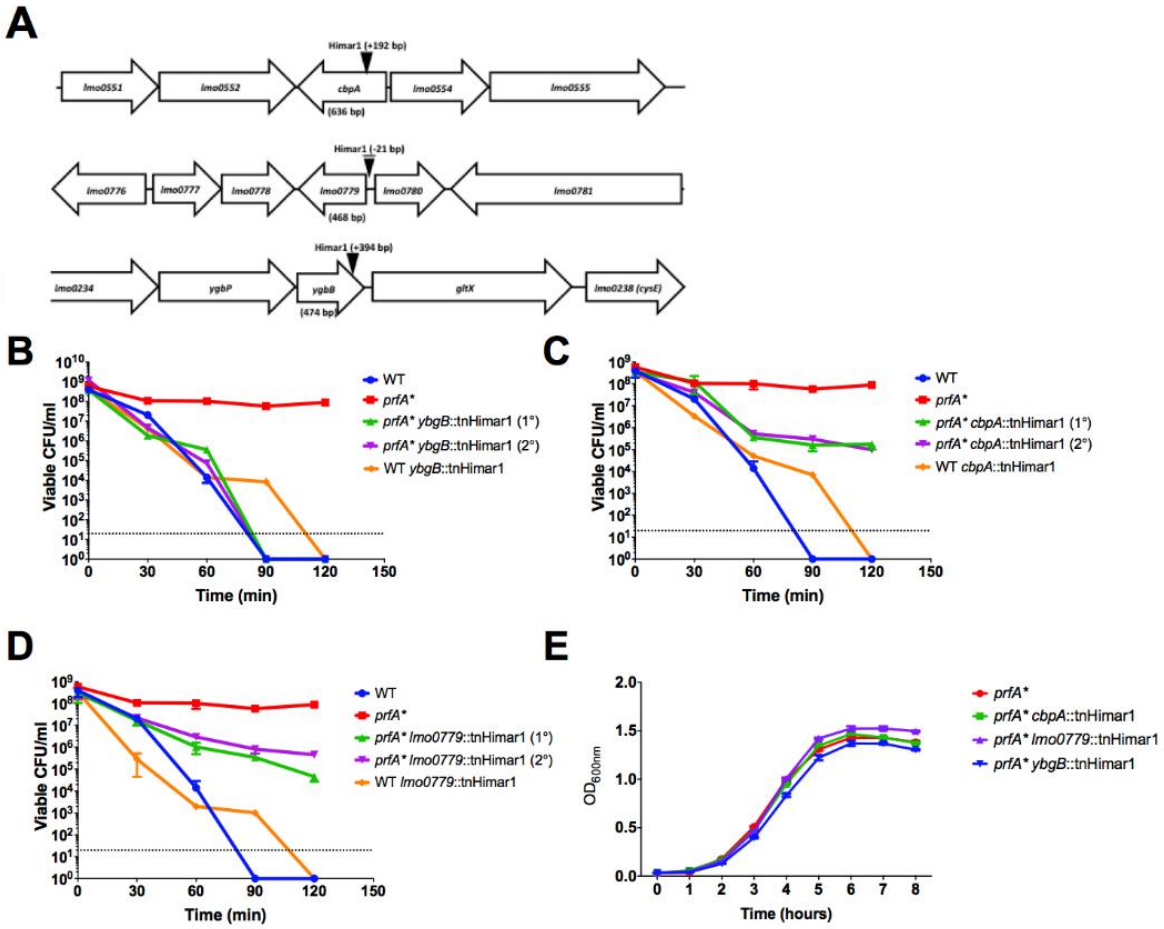

Figure 7.4. Phage transduction to introduce transposon insertions into clean genetic backgrounds and exclude second site mutations. (A) Location of each transposon insertion. Transposon insertions in *cbpA* (B), *lmo0779* (C), and *ygbB* (D) are moved into both 10403S and *prfA** background strains as described in Material and Methods. Strains were tested for peroxide sensitivity by incubation in BHI containing 110 mM H_2O_2 over two hours. Viable CFUs were enumerated at the indicated time points by plating on BHI agar. Standard growth curves in BHI at 37°C with shaking were performed (E). The data is representative of three independent experiments.

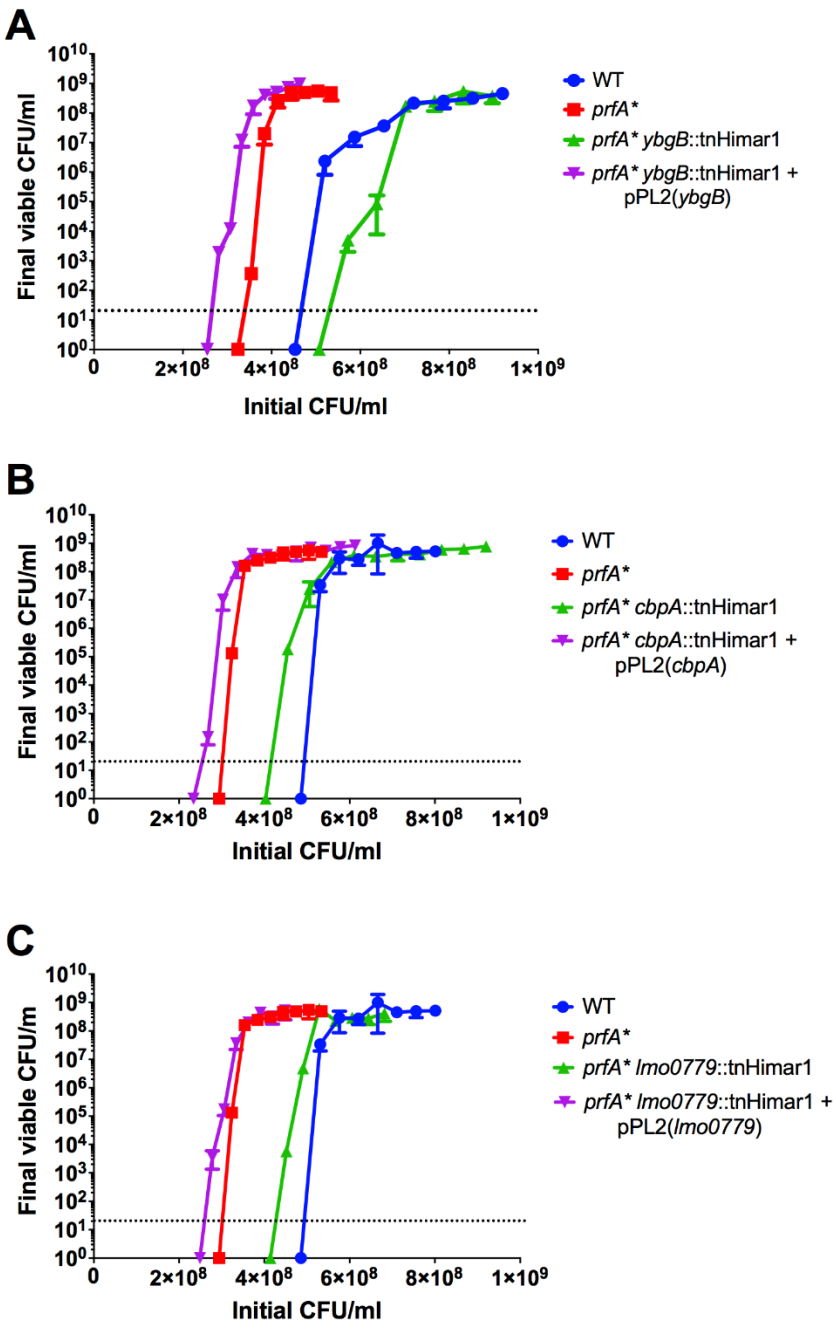

Figure 7.5. Gene complementation restores oxidative stress resistance to transposon insertion mutants *in vitro*. Transduced transposon mutants were complemented in single copy as described in Materials and Methods. The transposon insertion mutants and the complemented strains were incubated statically at room temperature for 2 hours and viable CFU were enumerated via plating on LB agar. Data are representative of three independent experiments.

7.5. DISCUSSION

The activation of the *L. monocytogenes* virulence regulator PrfA is central to the ability of this bacterium to transition from a saprophyte into an intracellular pathogen within mammalian hosts (1, 21). PrfA is required for the expression of multiple gene products that promote bacterial invasion of host cells, replication within the cytosol, and spread to adjacent cells during infection (19). The characterization of constitutively activated *prfA** mutants has revealed the scope and breadth of this regulator's influence on virulence factor expression, bacterial metabolism, and adaptation to periods of nutrient starvation (16, 17, 23-25, 27, 28, 30, 32, 41). Here we demonstrate that PrfA activation adds an additional facet to *L. monocytogenes* survival by conferring increased resistance to oxidative stress. This enhanced resistance relies on gene products whose activity was most notable under conditions of PrfA activation as loss of these products in wild type strains resulted in no significant changes in peroxide resistance. It thus appears that specific gene products uniquely contribute to *L. monocytogenes* stress resistance under conditions of PrfA activation, suggesting therefore that these products may contribute to bacterial life within infected host cells.

L. monocytogenes resistance to oxidative stress was dependent on bacterial density for both wild type and *prfA** strains (Fig. 7.1B). Approximately 40% fewer *prfA** bacteria were required to survive peroxide challenge in comparison to wild type bacteria, suggesting that *prfA** strains are better able to tolerate exposure to specific concentrations of reactive oxygen species. The basis for this resistance is not known, but *prfA** strains have been shown to exhibit altered surface properties leading to bacterial aggregation, a situation that may increase local concentrations of bacteria and perhaps limit the exposure of certain members of the population to oxygen radicals.

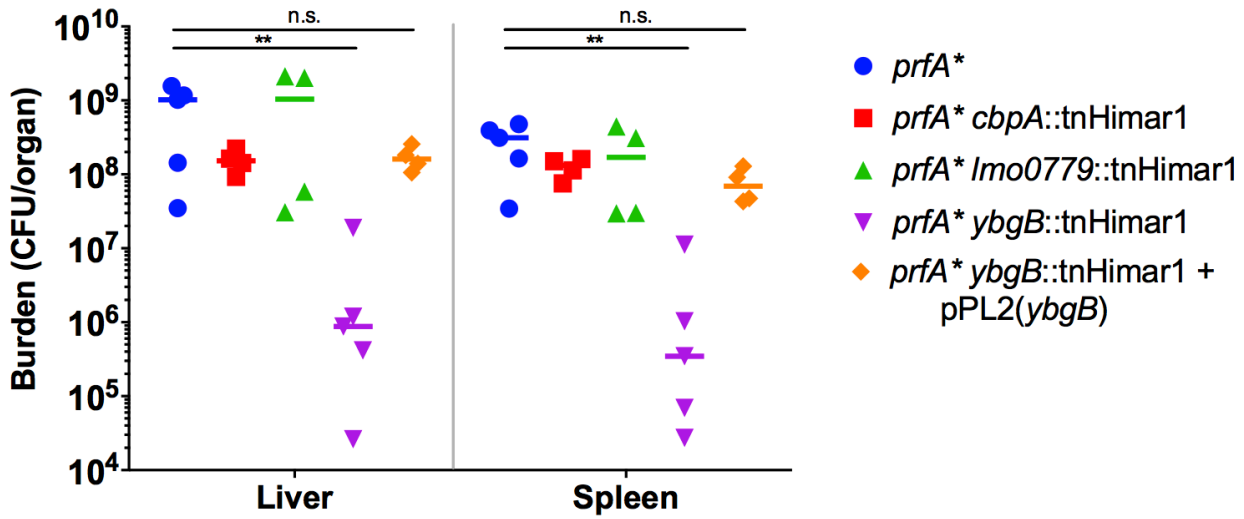

2791

2792 **Figure 7.6. YbgB is critical for virulence in PrfA* strains.** Six-to-eight week old female Swiss Webster

2793 mice were infected via tail vein injection with $1x10^4$ CFU of either *prfA** or each *prfA** transposon

2794 insertion mutant as indicated. Burdens were assessed 72 hours post-infection. Data are representative

2795 of two independent experiments.

2796

We identified the sites of transposon insertion for three selected mutants that demonstrated increased sensitivity to peroxide exposure, implicating the gene products of *lmo0779*, *cbpA,* and *ygbB* in oxidative stress resistance under conditions of PrfA activation. None of these three gene products have been previously implicated in oxidative stress resistance, most likely because none of the gene products appear to contribute to the oxidative stress resistance of wild type strains. The insertion of the transposon in the 5' upstream region of *lmo0779* has the potential to also influence the expression of the divergently transcribed gene *lmo0780*, however complementation studies indicated that the introduction of a wild type copy of *lmo0779* was sufficient to restore resistance to *prfA** levels. The predicted *lmo0779* gene product has no known homologues, however structural predictions using Phyre2 (38) suggest that Lmo0779 is a putative membrane protein that may feature a cytosolic C-terminal nitrite- or sulfite-reductase domain, making it likely to be a metal binding enzyme important for nitrogen or sulfur assimilation, respectively. Lmo0779 has a single cysteine residue, and it's possible that this membrane protein may be part of a signal relay that coordinates oxidative stress resistance. While highly conserved among *Listeria* species with >80% identity among sequenced isolates, *lmo0779* gene product homologs are not found among other bacteria.

The *cbpA* gene product was recently identified as a *L. monocytogenes* high affinity cyclic-di-AMP (c-di-AMP) receptor protein (42). C-di-AMP has been shown to regulate *L. monocytogenes* metabolism, resistance to cell wall targeting antibiotics, and osmoregulation (36). In other bacteria, it has been linked to ion transport and cell wall homeostasis [*Staphylococcus aureus* (43, 44)], DNA damage sensing and biofilm formation [*Bacillus subtilis* (45, 46)], and membrane lipid homeostasis [*Mycobacterium smegmatis* (47)]. Oxidative stress may therefore represent yet another physiological condition that uses c-di-AMP signaling to coordinate bacterial resistance, however in the case of *L. monocytogenes* that coordination appears most relevant under conditions of PrfA activation.

The *ybgB* gene product has also been associated with bacterial metabolism as it encodes the fifth of seven enzymes in the non-mevalonate (MEP) pathway of isoprenoid biosynthesis (34). *L. monocytogenes* is exceptional among pathogens in possessing both the classical and non-mevalonate pathways for the end product isopentenyl pyrophosphate (IPP), which is essential for growth and survival (48). Isoprenoids and their biosynthetic pathways have only recently begun to be appreciated in bacteria (49, 50) and their derivatives have been implicated in oxidative stress resistance (51). Ostrovsky et al (51) reported the accumulation of a MEP pathway intermediate, 2-C-methyl-D-erythritol-2,4-cyclopyrophosphate (MEC or MEcPP) in response to benzylviologen-induced oxidative stress, and stress-resistant mutants accumulated more MEC than sensitive strains. YbgB is the enzyme that generates MEC (34), thus it is possible that the reduction in *L. monocytogenes* resistance to peroxide is due to a lack of MEC accumulation resulting from the loss of YbgB. The MEP pathway has been previously shown to be required for *L. monocytogenes* virulence in mice (34) and the current study confirms an association of the MEP pathway with oxidative stress and with virulence; whether these phenotypes are linked or distinct from one another remains to be determined.

Perhaps notable is the absence of insertions detected within the gene encoding for catalase (*kat*), an enzyme associated with detoxifying peroxide (8). Nine mutants isolated from the screen that exhibited the greatest levels of peroxide sensitivity were examined by PCR amplification for insertions within *kat*, however no *kat*-specific insertion mutants were detected within this population and all mutants had confirmed catalase activity (D.R. Mains and N.E. Freitag, unpublished data). Catalase activity has been reported to be associated with resistance of *L. monocytogenes* to hydrogen peroxide exposure (52) however *kat* gene expression appears to be downregulated in intracellular *L. monocytogenes* (53). In addition, the loss of catalase does not appear to affect *L. monocytogenes* virulence in mouse models of infection and catalase-negative strains have been isolated from human

infections (54). These findings strongly suggest that bacterial factors other than catalase may be the primary mediators of oxidative stress resistance during PrfA activation within host cells.

Taken together, our results reveal yet another facet of *L. monocytogenes* physiology that is influenced by the central virulence regulator PrfA, that being enhanced bacterial resistance to oxidative stress under conditions of PrfA activation. Given the recent evidence suggests that *L. monocytogenes* uses redox-responsive transcription factors to coordinate virulence factor expression within the host, and that PrfA itself binds a reducing agent (14, 15), it would appear that this bacterium is well positioned for both redox sensing and survival during the course of host infection.

Acknowledgements

The authors would like to thank Lavanya Visvabharathy for initial observations leading to this study and Grischa Chen and John-Demian Sauer for assistance and advice with inverse PCR protocols. Members of the Freitag lab and the UIC Positive Thinking group provided valuable feedback and discussion.

Funding Information

This work was supported by NIH grant R01 AI041816-18A1 to NEF. Its contents are solely the responsibility of the authors and do not necessarily represent the official views of the funding source. The funders had no role in study design, data collection and analysis, decision to publish, or preparation of the manuscript.

7.6. Literature Cited

1. **Freitag NE, Port GC, Miner MD**. 2009. *Listeria monocytogenes* - from saprophyte to intracellular pathogen. Nat Rev Microbiol 7:623-8.

2. **NicAogain K, O'Byrne CP**. 2016. The Role of Stress and Stress Adaptations in Determining the Fate of the Bacterial Pathogen *Listeria monocytogenes* in the Food Chain. Front Microbiol 7:1865.

3. **Swaminathan B, Gerner-Smidt P**. 2007. The epidemiology of human listeriosis. Microbes Infect 9:1236-43.

4. **Czuprynski CJ**. 2005. *Listeria monocytogenes*: silage, sandwiches and science. Anim Health Res Rev 6:211-7.

5. **Lecuit M**. 2005. Understanding how *Listeria monocytogenes* targets and crosses host barriers. Clin Microbiol Infect 11:430-6.

6. **Gahan CG, Hill C**. 2005. Gastrointestinal phase of *Listeria monocytogenes* infection. J Appl Microbiol 98:1345-53.

7. **Slauch JM**. 2011. How does the oxidative burst of macrophages kill bacteria? Still an open question. Mol Microbiol 80:580-3.

8. **Staerck C, Gastebois A, Vandeputte P, Calenda A, Larcher G, Gillmann L, Papon N, Bouchara JP, Fleury MJJ**. 2017. Microbial antioxidant defense enzymes. Microb Pathog 110:56-65.

9. **Lam GY, Fattouh R, Muise AM, Grinstein S, Higgins DE, Brumell JH**. 2011. Listeriolysin O suppresses phospholipase C-mediated activation of the microbicidal NADPH oxidase to promote *Listeria monocytogenes* infection. Cell Host Microbe 10:627-34.

10. **Fu H, Yuan J, Gao H**. 2015. Microbial oxidative stress response: Novel insights from environmental facultative anaerobic bacteria. Arch Biochem Biophys 584:28-35.

11. **Dons LE, Mosa A, Rottenberg ME, Rosenkrantz JT, Kristensson K, Olsen JE**. 2014. Role of the *Listeria monocytogenes* 2-Cys peroxiredoxin homologue in protection against oxidative and nitrosative stress and in virulence. Pathog Dis 70:70-4.

12. **Kim KP, Hahm BK, Bhunia AK**. 2007. The 2-cys peroxiredoxin-deficient *Listeria monocytogenes* displays impaired growth and survival in the presence of hydrogen peroxide in vitro but not in mouse organs. Curr Microbiol 54:382-7.

13. **Rea R, Hill C, Gahan CG**. 2005. *Listeria monocytogenes* PerR mutants display a small-colony phenotype, increased sensitivity to hydrogen peroxide, and significantly reduced murine virulence. Appl Environ Microbiol 71:8314-22.

14. **Reniere ML, Whiteley AT, Hamilton KL, John SM, Lauer P, Brennan RG, Portnoy DA**. 2015. Glutathione activates virulence gene expression of an intracellular pathogen. Nature 517:170-3.

15. **Whiteley AT, Ruhland BR, Edrozo MB, Reniere ML**. 2017. A Redox-Responsive Transcription Factor Is Critical for Pathogenesis and Aerobic Growth of *Listeria monocytogenes.* Infect Immun 85.

16. **Bruno JC, Jr., Freitag NE**. 2010. Constitutive activation of PrfA tilts the balance of *Listeria monocytogenes* fitness towards life within the host versus environmental survival. PLoS One 5:e15138.

17. **Bruno JC, Freitag NE**. 2011. *Listeria monocytogenes* adapts to long term stationary phase survival without compromising bacterial virulence. FEMS Microbiol Lett in press.

18. **Port GC, Freitag NE**. 2007. Identification of novel *Listeria monocytogenes* secreted virulence factors following mutational activation of the central virulence regulator, PrfA. Infect Immun 75:5886-97.

19. **Scortti M, Monzo HJ, Lacharme-Lora L, Lewis DA, Vazquez-Boland JA**. 2007. The PrfA virulence regulon. Microbes Infect 9:1196-207.

20. **Shetron-Rama LM, Marquis H, Bouwer HGA, Freitag NE**. 2002. Intracellular induction of *Listeria monocytogenes actA* expression. Infect Immun 70:1087 - 1096.

21. **Xayarath B, Freitag NE**. 2012. Optimizing the balance between host and environmental survival skills: lessons learned from *Listeria monocytogenes*. Future Microbiol 7:839-52.

22. **Xayarath B, Volz KW, Smart JI, Freitag NE**. 2011. Probing the role of protein surface charge in the activation of PrfA, the central regulator of *Listeria monocytogenes* pathogenesis. PLoS One 6:e23502.

23. **Ripio M-T, Dominguez-Bernal G, Lara M, Suarez M, Vazquez-Boland J-A**. 1997. A Gly145Ser substitution in the transcriptional activator PrfA causes constitutive overexpression of virulence factors in *Listeria monocytogenes*. J Bacteriol 179:1533-1540.

24. **Miner MD, Port GC, Freitag NE**. 2008. Functional impact of mutational activation on the *Listeria monocytogenes* central virulence regulator PrfA. Microbiology 154:3579-89.

25. **Shetron-Rama LM, Mueller K, Bravo JM, Bouwer HG, Way SS, Freitag NE**. 2003. Isolation of *Listeria monocytogenes* mutants with high-level in vitro expression of host cytosol-induced gene products. Mol Microbiol 48:1537-51.

26. **Vega Y, Rauch M, Banfield MJ, Ermolaeva S, Scortti M, Goebel W, Vazquez-Boland JA**. 2004. New *Listeria monocytogenes prfA** mutants, transcriptional properties of PrfA* proteins and structure-function of the virulence regulator PrfA. Mol Microbiol 52:1553-65.

27. **Wong KK, Freitag NE**. 2004. A novel mutation within the central *Listeria monocytogenes* *r*egulator PrfA that results in constitutive expression of virulence gene products. J Bacteriol 186:6265-76.

28. **Xayarath B, Smart JI, Mueller KJ, Freitag NE**. 2011. A novel C-terminal mutation resulting in constitutive activation of the *Listeria monocytogenes* central virulence regulatory factor PrfA. Microbiology in press.

29. **Deshayes C, Bielecka MK, Cain RJ, Scortti M, de las Heras A, Pietras Z, Luisi BF, Nunez Miguel R, Vazquez-Boland JA**. 2012. Allosteric mutants show that PrfA activation is dispensable for

vacuole escape but required for efficient spread and *Listeria* survival in vivo. Mol Microbiol 85:461-77.

30. **Vasanthakrishnan RB, de Las Heras A, Scortti M, Deshayes C, Colegrave N, Vazquez-Boland JA**. 2015. PrfA regulation offsets the cost of *Listeria* virulence outside the host. Environ Microbiol 17:4566-79.

31. **Chico-Calero I, Suarez M, Gonzalez-Zorn B, Scortti M, Slaghuis J, Goebel W, European Listeria Genome Consortium T, Vazquez-Boland JA**. 2002. Hpt, a bacterial homolog of the microsomal glucose- 6-phosphate translocase, mediates rapid intracellular proliferation in *Listeria*. Proc Natl Acad Sci U S A 99:431-6.

32. **Mueller KJ, Freitag NE**. 2005. Pleiotropic enhancement of bacterial pathogenesis resulting from the constitutive activation of the *Listeria monocytogenes* regulatory factor PrfA. Infect Immun 73:1917-26.

33. **Myers JT, Tsang AW, Swanson JA**. 2003. Localized reactive oxygen and nitrogen intermediates inhibit escape of *Listeria monocytogenes* from vacuoles in activated macrophages. J Immunol 171:5447-53.

34. **Begley M, Bron PA, Heuston S, Casey PG, Englert N, Wiesner J, Jomaa H, Gahan CG, Hill C**. 2008. Analysis of the isoprenoid biosynthesis pathways in *Listeria monocytogenes* reveals a role for the alternative 2-C-methyl-D-erythritol 4-phosphate pathway in murine infection. Infect Immun 76:5392-401.

35. **Begley M, Gahan CG, Hill C**. 2002. Bile stress response in *Listeria monocytogenes* LO28: adaptation, cross-protection, and identification of genetic loci involved in bile resistance. Appl Environ Microbiol 68:6005-12.

36. **Whiteley AT, Garelis NE, Peterson BN, Choi PH, Tong L, Woodward JJ, Portnoy DA**. 2017. c-di-AMP modulates *Listeria monocytogenes* central metabolism to regulate growth, antibiotic resistance and osmoregulation. Mol Microbiol 104:212-233.

37. **Woodward JJ, Iavarone AT, Portnoy DA**. 2010. c-di-AMP secreted by intracellular *Listeria monocytogenes* activates a host type I interferon response. Science 328:1703-5.

38. **Kelley LA, Mezulis S, Yates CM, Wass MN, Sternberg MJ**. 2015. The Phyre2 web portal for protein modeling, prediction and analysis. Nat Protoc 10:845-58.

39. **Camejo A, Buchrieser C, Couve E, Carvalho F, Reis O, Ferreira P, Sousa S, Cossart P, Cabanes D**. 2009. In vivo transcriptional profiling of *Listeria monocytogenes* and mutagenesis identify new virulence factors involved in infection. PLoS Pathog 5:e1000449.

40. **Olsen KN, Larsen MH, Gahan CG, Kallipolitis B, Wolf XA, Rea R, Hill C, Ingmer H**. 2005. The Dps-like protein Fri of *Listeria monocytogenes* promotes stress tolerance and intracellular multiplication in macrophage-like cells. Microbiology 151:925-33.

41. **Scortti M, Lacharme-Lora L, Wagner M, Chico-Calero I, Losito P, Vazquez-Boland JA**. 2006. Coexpression of virulence and fosfomycin susceptibility in *Listeria*: molecular basis of an antimicrobial in vitro-in vivo paradox. Nat Med 12:515-7.

42. **Sureka K, Choi PH, Precit M, Delince M, Pensinger D, Huynh TN, Jurado AR, Goo YA, Sadilek M, Iavarone AT, Sauer JD, Tong L, Woodward JJ**. 2014. The cyclic dinucleotide c-di-AMP is an allosteric regulator of metabolic enzyme function. Cell 158:1389-1401.

43. **Corrigan RM, Campeotto I, Jeganathan T, Roelofs KG, Lee VT, Grundling A**. 2013. Systematic identification of conserved bacterial c-di-AMP receptor proteins. Proc Natl Acad Sci U S A 110:9084-9.

44. **Corrigan RM, Grundling A**. 2013. Cyclic di-AMP: another second messenger enters the fray. Nat Rev Microbiol 11:513-24.

45. **Bejerano-Sagie M, Oppenheimer-Shaanan Y, Berlatzky I, Rouvinski A, Meyerovich M, Ben-Yehuda S**. 2006. A checkpoint protein that scans the chromosome for damage at the start of sporulation in *Bacillus subtilis.* Cell 125:679-90.

46. **Witte G, Hartung S, Buttner K, Hopfner KP**. 2008. Structural biochemistry of a bacterial checkpoint protein reveals diadenylate cyclase activity regulated by DNA recombination intermediates. Mol Cell 30:167-78.

47. **Zhang L, Li W, He ZG**. 2013. DarR, a TetR-like transcriptional factor, is a cyclic di-AMP-responsive repressor in *Mycobacterium smegmatis.* J Biol Chem 288:3085-96.

48. **Begley M, Gahan CG, Kollas AK, Hintz M, Hill C, Jomaa H, Eberl M**. 2004. The interplay between classical and alternative isoprenoid biosynthesis controls gammadelta T cell bioactivity of Listeria monocytogenes. FEBS Lett 561:99-104.

49. **Cane DE, Ikeda H**. 2012. Exploration and mining of the bacterial terpenome. Acc Chem Res 45:463-72.

50. **Heuston S, Begley M, Gahan CG, Hill C**. 2012. Isoprenoid biosynthesis in bacterial pathogens. Microbiology 158:1389-401.

51. **Ostrovsky D, Diomina G, Lysak E, Matveeva E, Ogrel O, Trutko S**. 1998. Effect of oxidative stress on the biosynthesis of 2-C-methyl-D-erythritol-2,4-cyclopyrophosphate and isoprenoids by several bacterial strains. Arch Microbiol 171:69-72.

52. **Boura M, Keating C, Royet K, Paudyal R, O'Donoghue B, O'Byrne CP, Karatzas KA**. 2016. Loss of SigB in *Listeria monocytogenes* Strains EGD-e and 10403S Confers Hyperresistance to Hydrogen Peroxide in Stationary Phase under Aerobic Conditions. Appl Environ Microbiol 82:4584-91.

53. **Chatterjee SS, Hossain H, Otten S, Kuenne C, Kuchmina K, Machata S, Domann E, Chakraborty T, Hain T**. 2006. Intracellular gene expression profile of *Listeria monocytogenes.* Infect Immun 74:1323-38.

54. **Leblond-Francillard M, Gaillard JL, Berche P**. 1989. Loss of catalase activity in Tn1545-induced mutants does not reduce growth of *Listeria monocytogenes* in vivo. Infect Immun 57:2569-73.

55. **Bishop DK, Hinrichs DJ**. 1987. Adoptive transfer of immunity to *Listeria monocytogenes*: The influence of in vitro stimulation on lymphocyte subset requirements. J Immunol 139:2005-2009.

56. **Miner MD, Port GC, Bouwer HG, Chang JC, Freitag NE**. 2008. A novel prfA mutation that promotes *Listeria monocytogenes* cytosol entry but reduces bacterial spread and cytotoxicity. Microb Pathog 45:273-81.

57. **Monk IR, Gahan CG, Hill C**. 2008. Tools for functional postgenomic analysis of listeria monocytogenes. Appl Environ Microbiol 74:3921-34.

58. **Cao M, Bitar AP, Marquis H**. 2007. A mariner-based transposition system for *Listeria monocytogenes*. Appl Environ Microbiol 73:2758-61.

59. **Lauer P, Chow MY, Loessner MJ, Portnoy DA, Calendar R**. 2002. Construction, characterization, and use of two *Listeria monocytogenes* site-specific phage integration vectors. J Bacteriol 184:4177-86.

60. **Alonzo F, 3rd, Port GC, Cao M, Freitag NE**. 2009. The posttranslocation chaperone PrsA2 contributes to multiple facets of *Listeria monocytogenes* pathogenesis. Infect Immun 77:2612-23.

8. Vita

David R. Mains

11676 Aileron Court, Inver Grove Heights, MN 55077 | (651) 343-5832 | dmains2@uic.edu

Educational Background

University of Illinois at Chicago — August 2012 - Present
Chicago, IL
Ph.D. Microbiology & Immunology; Expected graduation September 2017

University of Minnesota — September 2004 – December 2007
Minneapolis, MN
B.S. Microbiology, GPA 3.09; Graduated 2007

Research Experience

Graduate Student — August 2012 - Present
University of Illinois at Chicago, Chicago, IL
Mentor: Nancy Freitag, Ph.D.
Projects: **(1)** Identification of *Listeria monocytogenes* genes contributing to oxidative stress resistance; **(2)** Exploring the immunomodulation caused by the general anesthetic propofol in a mouse model of *Klebsiella pneumoniae* lung infection; **(3)** Investigating how sedative choice impacts *K. pneumoniae* virulence determinants *in vivo*.

Quality Assurance Analyst — November 2010 – August 2012
3M Company, St. Paul, MN
Project: Quality Assurance for the 3M Molecular Detection System™ for the Department of Food Safety.

Laboratory Technician — November 2008 – September 2010
Cargill, Inc., Minnetonka, MN

Research Associate — May 2006 – July 2009
University of Minnesota – Twin Cities Campus
Mentor: Steven Juhn, M.D.
Project: A novel combination treatment for the resolution of *Streptococcal* otitis media.

Publications

Mains DR, Gantner B, and Freitag NE. Propofol sedation potentiates a hyper inflammatory response during Klebsiella pneumoniae lung infection (Working title). Manuscript in preparation.

Mains DR, Rotman ER, Kocher AA, Freitag NE, Mandel MJ. Propofol exacerbates *Klebsiella pneumoniae* lung pathogenesis and dissemination (Working title). Manuscript in preparation.

Mains DR and Freitag NE. 2017. Identification of *Listeria monocytogenes* genes contributing to oxidative stress resistance under conditions relevant to host infection. mSphere, in revision.

Juhn SK, Jung MK, Hoffman MD, Drew BR, Preciado DA, Sausen NJ, Jung TT, Kim BH, Park SY, Lin J, Ondrey FG, **Mains DR**, Huang T. The role of inflammatory mediators in the pathogenesis of otitis media and sequelae. *Clin Exp Otorhinolaryngol*. 2008 Sep;1(3): 117-38.

Meetings Attended

- 60th Annual Wind River Conference on Prokaryotic Biology, Estes Park, CO. June 2016.
- 13th Annual Chicago Biomedical Consortium Symposium, Chicago, IL. October 2015.
- 22nd Annual Midwest Microbial Pathogenesis Conference, Indianapolis, IN. August 2015.
- 5th Annual International Conference on Gram-Positive Pathogens, Omaha, NE. October 2014.
- 21st Annual Midwest Microbial Pathogenesis Conference, Chicago, IL. August 2014.
- 20th Annual Midwest Microbial Pathogenesis Conference, Columbus, OH. August 2013.

Presentations and Abstracts

Mains DR and Freitag NE. The common anesthetic propofol increases the pathological severity of *Klebsiella pneumoniae* lung infections. 60th Annual Wind River Conference on Prokaryotic Biology, Estes Park, CO, June 2016. *Oral presentation*.

Rotman E, **Mains DR**, Freitag NE, Mandel M. *Klebsiella* pathogenesis in propofol-immunosuppressed mice. 13th Annual Chicago Biomedical Consortium Symposium, Chicago, IL, October 2015. *Poster presentation*.

Mains DR and Freitag NE. Identification of *Listeria monocytogenes* genes contributing to oxidative stress resistance. 5th Annual International Conference on Gram-Positive Pathogens, Omaha, NE, October 2014. *Poster presentation*.

Mains DR and Freitag NE. Identification of *Listeria monocytogenes* genes contributing to oxidative stress resistance. 21st Annual Midwest Microbial Pathogenesis Conference, Chicago, IL, August 2014. *Poster presentation*.

Committees

2016-2017 – Graduate Student Counsel, Department of Microbiology and Immunology, University of Illinois at Chicago

Honors and Awards

2016 Travel Award, 60th Annual Wind River Conference on Prokaryotic Biology, Estes Park, CO.
2015 UIC Center for Clinical and Translational Science Pre-doctoral Education for Clinical and Translational Scientists (PECTS) Fellowship
2014 Travel Award, 5th Annual International Conference on Gram-Positive Pathogens, Omaha, NE.